Delft University of Technology

Master Thesis

Geotechnical aspects of the Blue Piling Installation Technique

Design of a measurement plan and elaboration of results for prototype hammer on life size piles in Maasvlakte 2

Author:
Charlotte Stokman (4580273)

Supervisor:
Prof. Dr. Ir. K.G. Gavin
TU Delft, Geotechnical Engineering

Thesis Committee:
Dr. Ir. C. Mai Van
TU Delft, Hydraulic Engineering

Dr. Ir. J. van Wijk
IQIP

in partial fulfilment of the requirements for the degree of

Master of Science
in Civil Engineering

at the Delft University of Technology

May 23, 2023

Sponsors:

Abstract

The energy market is growing and noise regulations for offshore foundation pile installation grow stricter. New initiatives arise to comply with the ongoing developments in the field, such as the BLUE Piling Technology under development by IQIP. Its features are presented as reduced underwater noise levels during installation up to 20 decibel, which is attributed to the lower pile wall vibrations caused during driving. The quasi-static pile movement caused by the Blue Piling hammer causes installation phenomena different than those encountered for conventional (dynamic) driving. This thesis aims to design a field test, identifying the most important differences in geotechnical aspects between a prototype Blue Piling hammer and a conventional driving hammer, S-30 Hydrohammer, IQIP. By analyzing data obtained from total and pore pressure transducers during driving, a difference in drainage conditions, stress magnitude around pile tip due to plugging and difference in friction fatigue are identified. Water pressure data shows an increase in the stationary phase of the blow for Blue Piling whereas water pressures generated by conventional driving hammer quickly equalize. Radial stress magnitude near pile tip grows a factor 2-3 larger for Blue Piling installation, where plugging is significant. Lastly, radial stresses developed at higher distance from the pile tip are a factor 2-4 higher for Blue Piling installations. This is appointed to less cycling indicating less friction fatigue. The results show that the Blue Piling hammer creates a response between pile and soil that is very different from conventional driving hammer, and is more similar to rapid loading conditions or jacked installations. This brings advantages such as lower vibrations and noise emission. To be able to scale the test results to larger monopiles, the contribution of pile plugging needs to be further investigated since larger monopiles may not encounter plugging leading to different stress magnitudes around pile tip.

Preface

While writing my thesis, I am working as an intern with IQIP in Sliedrecht, the Netherlands. In the preparation phase towards the experiments executed on Maasvlakte 2 I have been in close contact with the Bluepiling Team and throughout with the Geotechnical team.

I want to thank Prof. Dr. Ir. K.G. Gavin, Dr. Ir. C. Van Mai and Dr. Ir. J. van Wijk for embarking on this journey with me and for the support and their support throughout the process. First of all Ken, for your flexibility and sharing of knowledge, Cong for your feedback and enthousiasm every time I would come by for an update meeting and on the Maasvlakte and Jort, for your daily supervision, willingness to answer any questions any time, sympathy, understanding and creativity throughout the process. Dr. Ir. M.A. Cabrera for your help with the noise processing. Also everybody attending the Blue Piling update meeting towards the end phase of the thesis; the gathering has been of great value in the data processing phase.

Within IQIP I would like to thank the following people. Jaap Houbolt for leading the project team and having a fierce but fair attitude towards the plans brought forward. Wilbert Coumans for keeping me in the loop in the pile design and other practical and technical details for the in-situ tests. Leon Martens for his involvement in the preparatory phase such as getting the Simulink model to run again. Everybody during the Maasvlakte tests for their willingness to accept any request I might have, their patience and laughs. Specifically Leon Martens together with Erik van Deursen for doing anything in their power to make the Blue Piling hammer work and making sure all the measurements can be done. Rick van der Drift for managing the site perfectly. The guys from Boekestein, Edwin specficially for letting me use his microwave every day. Nico from van 't Hek, for letting me use the tool container as control room and his kitchen skills. Ofcourse Arjan Roest, for teaching me how to install strain gauges onto the pile, being at the ready for questions and cooperation at all times and doing a thorough job in the data processing. All my colleagues in the Geotech team, for sharing their geotechnical insights but also their personal experiences and walk and coffee breaks together in Sliedrecht and later in Delft.

All my friends in Delft and outside, for accompanying me in the coffee breaks, on walks and their willingness to listen to me telling them enthusiastically about my pile tests and the Maasvlakte, even if it's not in their field of expertise. My family, for their support throughout these turbulent times, my new housemates for giving me a renewed home - we miss you Pietro, Bente for accompanying me on the water and hearing me out when I need to, and Alberto, without your company, support and smiles I would not have come this far.

Contents

1 Introduction **8**
1.1 Background . . . 8
1.2 Aim . . . 10
1.3 Thesis Outline . . . 10
1.4 Scope of work . . . 10

2 Literature Research **12**
2.1 Installation Phenomena . . . 12
2.1.1 Drainage conditions and resistance . . . 12
2.1.2 Plugging Effect . . . 13
2.1.3 Friction fatigue . . . 18
2.1.4 Set-up . . . 18
2.2 Smith's model for Modelling Driving Resistance . . . 20
2.2.1 1D Wave equation . . . 20
2.2.2 Pile model . . . 21
2.2.3 Soil model . . . 21
2.2.4 Hammer model . . . 24

3 Site Investigation **25**
3.1 Site History . . . 25
3.2 Water level investigation . . . 26
3.3 Cone Penetration Test analysis . . . 26

4 Experiment Design **29**
4.1 Pile Design and Hydrohammer selection . . . 29
4.1.1 Input Parameters - GRLWeap . . . 30
4.1.2 Methodology . . . 30
4.1.3 Results . . . 31
4.1.4 Revisiting GRLWeap after Maasvlakte tests . . . 34
4.2 Measurement devices . . . 36

5 Execution of the Maasvlakte field tests **43**
5.1 Experiment lay-out . . . 43
5.2 Methodology . . . 45
5.3 Procedural Adjustments in the field . . . 46

6 Data Obtained **48**
6.1 During installation - Blow investigation . . . 48
6.2 During Installation - Radial Soil Pressure, Water Pressure and IFR . . . 52
6.3 Plug Heights . . . 54
6.4 During driving stop - Total and pore stress equalization . . . 55
6.5 Acceleration . . . 58
6.6 Field study stand pipes . . . 59

7 Conclusion **61**

8 Recommendations **62**

References **63**

A Supplement to Literature Study **67**
A.1 Soil Mechanics . . . 67
A.1.1 Particle packing . . . 67
A.1.2 Stress-strain behaviour of sand . . . 68
A.1.3 Soil in compression . . . 69
A.1.4 Mobilization of resistance . . . 69
A.2 Installation Phenomena . . . 70
A.2.1 Plugging . . . 70

A.3 Modelling . . . 72
A.3.1 Blue Piling Hammer - Simulink . . . 72
A.3.2 ICP - Static Soil Resistance Model . . . 74

B Site Investigation **75**
B.1 Water table . . . 75
B.1.1 Desk study water tables . . . 75
B.2 CPT comparison . . . 76
B.3 Soil profile S14 . . . 77
B.4 Relative densities . . . 79

C Experiment Design **80**
C.1 Supplement: Pile Design - GRLWeap . . . 80
C.2 GRLWeap SRD Input . . . 82
C.2.1 Revisiting Pile design after Maasvlakte tests . . . 83
C.3 Supplement: Transducer design . . . 87
C.3.1 Information Strain Gauge configuration . . . 87

D Experiment Execution **89**

E Data Processing **90**
E.1 Time and pile penetration . . . 90
E.2 Retrieving Soil and Pore Pressures . . . 90
E.3 Noise filtering . . . 91
E.4 Fourier Transform - Frequency Amplitude space . . . 92

F Data Obtained **94**
F.1 Driving stops . . . 94
F.1.1 Table Overview . . . 94
F.1.2 Visualization . . . 96
F.2 During installation - Blow investigation . . . 97
F.2.1 Depth horizon 1.5 meters . . . 97
F.2.2 Depth horizon 4 meters . . . 100
F.2.3 Depth horizon 5 meters . . . 102
F.3 Accelerations . . . 106
F.4 Strains . . . 107
F.4.1 Hydrohammer Installation . . . 107
F.4.2 Blue Piling Installation . . . 109

List of Figures

1 Blue Piling Concept (Martens, 2020) . . . 8
2 Comparison of Blue Piling vs. Hydrohammer blow (IQIP, 2021) . . . 9
3 Comparison of IQIP hammer energy, (IQIP, 2021) . . . 9
4 Incremental filling ratio defined (M.F. Randolph & Gourvenec, 2011) . . . 13
5 Open-ended pile failure mechanisms, (M.F. Randolph & Gourvenec, 2011) . . . 14
6 Arching principle (Karlowskis, 2014) and soil deformation indicating passive arching (S.G. Paikowsky et al., 1989) . . . 15
7 Plugging criterion as stated by (Jardine, 2005) . . . 16
8 Stress wave through pile during driving . . . 17
9 Mechanism of Friction Fatigue as described by (White et al., 2002) . . . 18
10 Stress wave travelling down pile, (M.F. Randolph, 2003) . . . 20
11 Schematization of the pile-soil model for Simulink and Weap, (Martens, 2019) . . . 21
12 Load-deformation characteristics for soil spring, (E. Smith, 1960) . . . 23
13 Schematization of the hammer model for Weap, (Dynamics, 2010) . . . 24
14 Noordzee sea floor elevations around the Maasvlakte . . . 25
15 Available CPT locations, (vd Straaten, 2022) . . . 26
16 CPT's taken by Ingenieursbureau Rotterdam from west to east on the Maasvlakte site . . . 27

17 Soil Profile S14 - Classification of soil profile based on (Robertson, 2010) . . . 28
18 Pile dimensions and cross-section . . . 29
19 Blowcounts obtained for (a) S70 - Safety Factor and Energy adjustments, (b) S30 . . . 31
20 Blowcounts obtained for S-30 and BP Hammer . . . 33
21 Virtual stroke comparison HH2 and HH3 during respective pile installation . . . 34
22 Blowcount measurements vs. Blowcount (GRLWeap) prediction . . . 35
23 PDA (a) Receiver connected to module on 0° and 180° (b) Full bridge strain module with accelerometer 36
24 Schematic of pile and measurement devices . . . 37
25 Foil Strain Gauge, (Meijer, 2010) . . . 38
26 Strain gauges installed under U profile (a) Quarter bridge set-up (Roest, A.) (b) Full bridge module . 39
27 Accelerometer on Full bridge module . . . 39
28 Laser displacement measurement installed on (a) the Blue Piling hammer (b) the S-30 Hydrohammer 40
29 (a) KPE-PB Miniature Pore Pressure gauge, (Athen Sensors, 2022) (b) PDB-PB Miniature Pressure Transducer, (Tokyo Measuring Instruments Lab, 2022)(c) Lay-out in-situ . . . 41
30 (a) Measuring the pile plug with respect to ground level (b) Used device (Tecso, n.d.) . . . 41
31 Installation locations . . . 43
32 Test set-up of (a) Blue Piling Hammer (b) Hydro Hammer and (c) Vibratory driver . . . 44
33 (a) Hole burnt in the pile around 9 meter (from pile tip) mark (b) Performing plugging measurement from aerial work platform . . . 47
34 Illustration of (a) Characteristic BP blow with negative dip, peak value, gradual decrease towards plateau and second narrow plateau value (b) A build-up to negative pore pressures. . . . 48
35 Illustration of (a) Characteristic BP blow without negative dip, but with peak value, gradual decrease towards plateau and second narrow plateau value (b) A strong build-up in pore pressures in 'stationairy phase' of blow in sand while hydrostratic pressure is around 45 kPa . . . 49
36 Illustration of (a) BP blow with sharp decrease and reach into plateau value (b) Weak response of the pore pressure with hydrostatic pressure being equal to around 20 kPa. . . . 49
37 Illustration of (a) BP blow above groundwater table showing no strong dip (b) Pore pressure sensor showing no excitation . . . 49
38 Illustration of (a) Characteristic HH blow with strong peak, strong dip into negative pressures, oscillating plateau of around 0.2 seconds and 'stationairy' phase plateau dependent on blow rate (b) Typical pore pressure response, dip for time of blow and quick recovery into plateau value . . . 50
39 Illustration of (a) HH blow with strong peak, strong negative peak and non-distinct oscillatory plateau equal to 0.2 seconds (b) Typical pore pressure response, dip for time of blow and quick recovery into plateau value. . . . 51
40 Illustration of (a) Characteristic HH blow (b) Feable response to to blows in pore water pressure measurements, hydrostatic pressure being around 30 kPa . . . 51
41 (a) CPT Profile S14 (b) HH3 - Radial Soil Pressures (c) HH3 - Pore Pressures (d) HH2 - IFR ratios obtained in driving stops . . . 52
42 (a) CPT Profile S14 (b) BP3 - Radial Soil Pressures (c) BP3 - Pore Pressures (d) BP4 - IFR ratios obtained in driving stops . . . 53
43 BP5 - IFR . . . 54
44 HH3 - Driving stops indicated over depth of pile tip and sensor levels next to CPT S14 . . . 55
45 BP3 - Driving stops indicated over depth of pile tip and sensor levels next to CPT S14 . . . 57
46 HH3 - LVL 5 - L/D = 0.4 - Accelerations . . . 58
47 BP4 - LVL 5 - L/D = 0.4 - Accelerations . . . 59
70figure.caption.70
49 Schematization of the pile-soil model, (Martens, 2019) . . . 73
50 B37A0113 Grondwaterstand . . . 75
51 B37A0113 Peilbuis 001 (Dinoloket, n.d.) . . . 75
52 B37A0113 Peilbuis 002 (Dinoloket, n.d.) . . . 75
53 Soil Profile S14 - Cone resistance found in-situ compared to (a) minimum and maximum (b) mean . 77
54 Soil Profile S14 - Sleeve friction found in-situ compared to (a) minimum and maximum (b) mean . . 78
55 Relative Density as found by Lunne . . . 79
56 S-70 hammer half energy - Blowcounts obtained for different Pile Geometries . . . 81
57 Input Parameters Weap calculated according to Alm Hamre, 2001 . . . 82
58 Virtual stroke comparison HH2 and HH3 during respective pile installation . . . 84
59 HH2 - Comparison of In-situ data with GRLWeap prediction (original vs. adjusted 'virtual' stroke (VS)) 85

60 HH3 - (a) Comparison of In-situ data with GRLWeap prediction (original vs. adjusted 'virtual' stroke (VS)) (b) Parametric study, effect of adjusting C.O.R. and Efficiency (Eff) . . . 85
61 HH3 - Enthru research, comparing EMX and result virtual stroke from Weap . . . 86
62 Wheatstone Bridge configuration . . . 87
63 Full bridge strain module - AAA battery for scale . . . 87
64 Maasvlakte 2 - Locatie In-situ test . . . 89
65 Location with respect to the Site Investigation done for the Stress Wave Conference 2022 . . . 89
66 HH3 - Soil Pressure . . . 92
67 BP3 - Soil Pressure . . . 92
68 HH3 - Pore Pressure . . . 92
69 BP2 - Pore Pressure . . . 92
70 HH3 . . . 92
71 BP2 . . . 92
72 HH3 . . . 93
73 BP4 . . . 93
74 HH1 Start driving 16/1 14:20:50 . . . 96
75 BP1 position file not available . . . 96
76 HH2 position file not available, based on soil pressures . . . 96
77 BP2 . . . 96
78 HH3 . . . 96
79 BP3 . . . 96
80 BP4 . . . 96
81 . . . 97
82 . . . 97
83 . . . 98
84 . . . 98
85 . . . 99
86 . . . 99
87 . . . 100
88 . . . 100
89 . . . 101
90 . . . 101
91 . . . 102
92 . . . 102
93 . . . 103
94 . . . 103
95 . . . 104
96 . . . 104
97 . . . 105
98 . . . 105
99 HH3 - LVL 3 - L/D = 4.1 - Accelerations . . . 106
100 BP4 - LVL 3 - L/D = 4.1 - Accelerations . . . 106
101 HH3 - LVL 5 - L/D = 0.4 - Strain . . . 107
102 HH3 - LVL 4 - L/D = 2.3 - Strain . . . 107
103 HH3 - LVL 3 - L/D = 4.1 - Strain . . . 108
104 HH3 - LVL 2 - L/D = 5.9 - Strain . . . 108
105 HH3 - LVL 1 - L/D = 7.8 - Strain . . . 109
106 BP4 - LVL 5 - L/D = 0.4 - Strain . . . 109
107 BP4 - LVL 4 - L/D = 2.3 - Strain . . . 110
108 BP4 - LVL 3 - L/D = 4.1 - Strain . . . 110
109 BP4 - LVL 3 - L/D = 4.1 - Strain . . . 111
110 BP4 - LVL 2 - L/D = 5.9 - Strain . . . 111
111 BP4 - LVL 1 - L/D = 7.8 - Strain . . . 112

List of Tables

1 First iteration Pile Geometry . . . 31
2 Further iteration Pile Geometry . . . 32
3 Performed installations during the Maasvlakte in-situ tests . . . 45
4 Standpipe nr. 34, Loc 100 - Observed Water levels Maasvlakte 2 . . . 59
5 Standpipe nr. 1041, Loc 100 NWZ - Observed Water levels Maasvlakte 2 . . . 60
6 Unnamed Standpipe (located between nr. 34 and nr. 1040) - Observed Water levels Maasvlakte 2 . . . 60
7 Standpipe nr. 1040, Loc 100 NWZ - Observed Water levels Maasvlakte 2 . . . 60
8 Relative density, (Barnes, 1995) . . . 67
9 Relative density according to Lunne . . . 68
10 Composition hammer weight S-30 . . . 80
11 Composition hammer weight S-70 . . . 80
12 Further iteration Pile Geometry . . . 81
13 Taken from 'Soil Sensor Calibration Data.xls' by Arjan Roest, IQIP . . . 88
14 Taken from 'Logbook.xls', tab Sensor Offset Correction by Arjan Roest, IQIP . . . 88
15 Driving stops for HH1 . . . 94
16 Driving stops for HH2 . . . 94
17 Driving stops for HH3 . . . 94
18 Driving stops for HH5 - *Dataset not available for processing* . . . 94
19 Driving stops for BP1 - *Dataset not available for processing* . . . 95
20 Driving stops for BP2 . . . 95
21 Driving stops for BP3 . . . 95
22 Driving stops for BP4 . . . 95
23 Driving stops for BP5 - *Dataset not available for processing* . . . 95

1 Introduction

1.1 Background

The energy market is growing and water depths for installation of wind turbines are increasing. This calls for the installation of larger and taller monopiles for wind turbines which make the installation of these foundations offshore considerably challenging. In combination with ever stricter noise regulations for offshore foundation pile installation, new initiatives arise to comply with the ongoing developments in the field. One such initiative is the BLUE Piling Technology developed by Jasper Winkes and his Bluepiling team. The company IQIP has seen its potential and has incorporated the BLUE Piling team in a coalition to be able to further develop the technology and bring it to the market (Innovators, 2019).

Concept 2018 - Fistuca
A previous version of the Blue Piling technology was developed under the former company name Fistuca. For this 2018 version, a large water column is used to generate a driving force. Inside the steel tube which is closed at the bottom, sea water is pushed upwards by a gas mixture combusting in a reservoir at the bottom. Due to the present water mass, flue gasses are kept from expanding, causing a downward force pulse to lift the water mass. When the water falls down again, A second downward force pulse is produced. This process can be repeated until the desired installation depth of the pile is reached. A gradual force build-up is obtained since pulse duration is increased by a factor of 20, low tension stress is created which in turn results in a lower noise emission.

Concept 2020 - IQIP
Since the Blue Piling project team has merged with IQIP, the Blue Piling Technology has undergone changes from its previous Fistuca 2008 Concept. The 2020 version is referred to as the Blue Piling hydraulic concept. The mass of a water filled tank remains key to the design, but now the base construction is equipped with a pneumatic damper system which transfers the piling loads towards the mono pile. The final design would encompass the following.

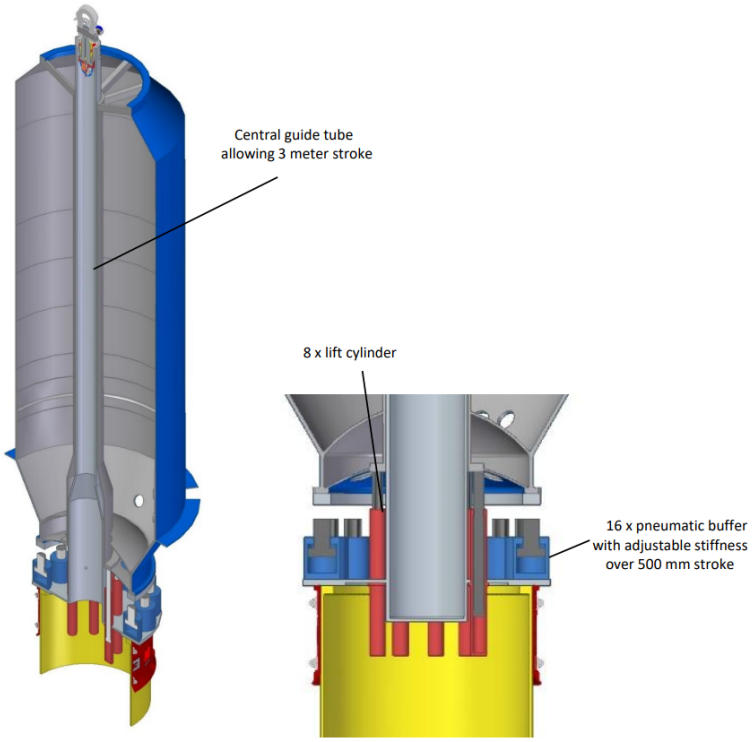

Figure 1: Blue Piling Concept (Martens, 2020)

The water compartment tank of 2000 m^3 is filled with sea water and follows the central guide tube when moving up and down. Any lateral loads such as wind and inclined loads will be guided to the base construction by the guide tube. The hammer is lifted to the required lift height and dropped down onto pneumatic buffer. The buffer volume is nitrogen which is pressurized due to displacement of the piston, after the hammer (fully or partially filled with water)

has fallen. Since the mass falls on a deceleration device, contact during hammer blow will be longer (/ 200 ms), delivered forces can be higher, as well as the energy levels. This makes the process of installation fully controllable (Martens, 2020). The largest hammer currently in production with IQIP is the IQ6 Hydrohammer. For this hammer, the minimum energy delivered equals 275 kJ. At 100% energy, 5500 kJ can be delivered and the absolute maximum energy at 120% equals 6600 kJ. The pulse duration of a Hydrohammer is between 8-12 ms, meaning there is a significant difference in blow character as displayed in the following figure. Note the energy levels are different (IQIP, 2021).

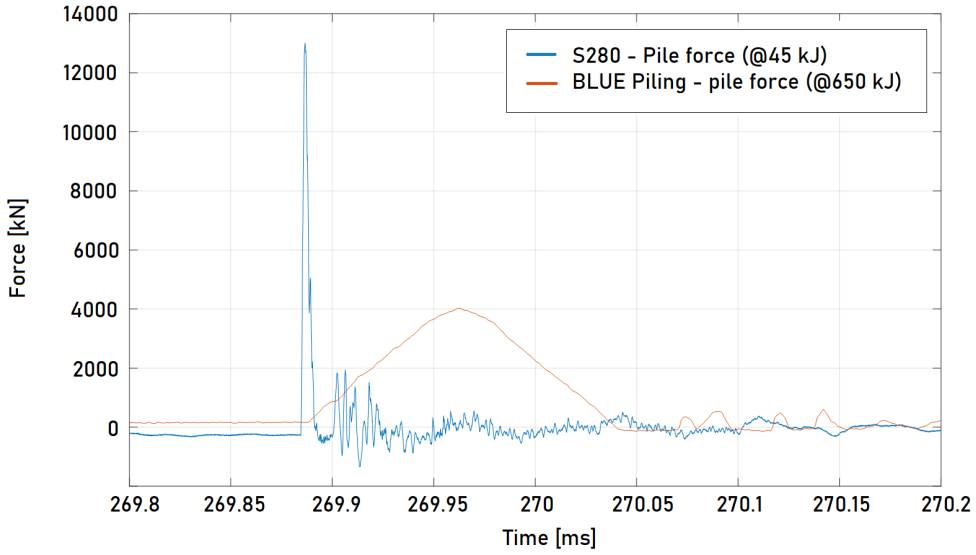

Figure 2: Comparison of Blue Piling vs. Hydrohammer blow (IQIP, 2021)

The figure below shows a comparison of the potential delivered energy of the Blue Piling hammer compared to other IQIP hammers, used for the installation of monopiles for different windfarms constructed over the last years.

Wind farm	Horns Rev	Gunfleets sands	Westermost rough	Hornsea II	Future?		
					S-5500 with 8 m sleeve	S-5500 with 8 m sleeve & Pulse	BLUE Piling
Hammer energy	600 kJ	1400 kJ	2000 kJ	4000 kJ	5500 kJ	5500 kJ	>70.000 kJ
Impact Force	60 MN	110 MN	190 MN	350 MN	450 MN	350 MN	330 MN
Overall weight	165 tons	310 tons	525 tons	775 tons	965 tons	1075 tons	1200 tons startup ±3000 tons full energy

Figure 3: Comparison of IQIP hammer energy, (IQIP, 2021)

The IQIP Blue Piling technology today is marketed as the next generation in pile driving. Its features are presented as reduced underwater noise levels during installation up to 20 decibel, which is attributed to the lower pile wall vibrations caused during driving. In addition to this, unlimited ranges of pile size and weights that can be installed (IQIP, 2022). Installation operation cost are a large part of the total cost of an offshore wind farm. This means

that with increasing energy levels while maintaining a handleable weight, the Blue Piling may be a good contender in future monopile installations offshore.

1.2 Aim

Before the concept can be widely deployed for commercial use, a solid performance of a prototype hammer in test phase is necessary and its behaviour needs to be understood on a mechanical and geotechnical level. This research project serves to get a better understanding of the geotechnical aspects that are involved with installation of open-ended monopiles using Blue Piling Technology on Maasvlakte 2. The goal is to design an experiment which after execution provides understanding of the soil response to driving and to find the main differences compared to conventional driving. The main research question is:

"In which geotechnical aspects is Blue Piling Installation different from conventional driving using a Hydrohammer?

Subquestions are established to be able to answer the main research question are the following.

"What previous findings are relevant to consider with respect to geotechnical analysis of the Blue hammer blow?"

"Which installation phenomena are relevant to quantify and compare between the Blue Hammer, conventional and vibratory driving?"

"Based on Site investigation data, relevant comparison to mono piles and material availability, what is the suitable pile design to achieve around 10 meters of penetration during pile tests on Maasvlakte 2 for all installation methods?"

"Which measurement devices are needed in the experiment set-up to adequately quantify the relevant installation phenomena during open-ended pile installation on Maasvlakte 2?"

"How are the life size pile installations executed on Maasvlakte 2?"

1.3 Thesis Outline

Chapter 2 elaborates on the literature research done in preparations of the measurement device plan. Installation phenomena are elaborated and Smith's model for Modelling driving resistance is explored in preparation for pile design. Chapter 3 elaborates on the Site Investigation done which serves as input for the simulations done for pile design. Chapter 4 elaborates on Experiment design, showing the process of GRLWeap simulations and the pile geometry as end result. In this chapter also the measurement devices plan is elaborated. Chapter 5 shows the execution of the Maasvlakte field test, experiment layout, methodology and procedural adjustments made on-site. Chapter 6 shows the data obtained.

1.4 Scope of work

The main deliverable of this thesis is the design of the experiment using the prototype Blue Hammer on the Maasvlakte in November 2022. In preparation of the experiments, GRLWeap simulations are performed to establish a feasible pile geometry based on the available site investigation data. After establishing the pile geometry, a plan for the measurement devices should be delivered which aims to measure the deemed relevant geotechnical aspects of pile installation, determined by literature study. A part of the data obtained will be visualized and partly interpreted, with special attention for the total radial pressures and water pressures.

- The test pile designed for installation at Maasvlakte 2 is installed using a Vibratory hammer. Vibratory installation is thus mentioned in the preparatory investigation and in the experiment set-up, but further elaboration in theory and data is not performed due to time constraints.
- The available data is only elaborated for HH3 and BP3 or BP4, depending on availability of data.
- No real data processing is performed in Python. The moving mean is displayed with the original data to give the reader a better idea of data development.

- The Pile Driving Analaysis (PDA) which is part of the measurement devices designed on the pile to investigate development of resistance during driving is not completed. The development of resistance during driving is thus not further elaborated.
- Set-up is a relevant geotechnical aspect to consider as it will differ when compared between conventional driving and Blue Piling. Due to unavailability of the dataset, this phenomenon will not be further elaborated in this thesis.
- It is to be noted that the installation effects will be mainly focused on installation in (silty) sand. This is the material that is mainly present at the Maasvlakte site that is investigated. Theoretical details of partially saturated soils are not considered. Additionally, long term time effects in soil compression are not considered such as creep.
- A future goal is to build a GRLWeap implementation of the Blue Piling hammer. Building a representative GRLWeap model of the Blue Piling hammer is out of scope of this thesis.

2 Literature Research

2.1 Installation Phenomena

During driving, a stress-wave travels down the pile. Simultaneously, radial waves are generated in the soil, generating energy in the form of shear waves leading to displacements, velocities and accelerations in the soil. Installation methods with different loading duration, energy rates and frequency of loading lead to characteristically different stress waves through a foundation pile during installation. This leads to different soil response in terms of drainage conditions, mobilization of resistance, likelihood of plugging, friction fatigue and set-up. The following installation methods are researched to be able to compare to the results obtained by driving using the Blue Piling technique.

1. **Conventional Driving**

   For conventional driving, hydraulic hammers are used (steam and diesel hammers in the past). Piles are driven by the blows delivered from a ram weight onto the anvil that is located on top of the pile. High rates of shear strain and a slip zone will form when the soil starts to slip along the pile. Because of the propagation of stress wave through the pile, large differences in stresses, velocities and displacements are generated along the pile. Parts are under compression, parts are under tension and this again fluctuates with time.

2. **Stat-namic load pile testing**

   Statnamic load pile testing is also known as rapid load testing. The aim of rapid load testing is to reach target loads some time after installation of the pile that is to be tested. During this process, settlements are measured over time which can be used to derive velocity and accelerations. A fuel is burned up in a combustion chamber that is loaded onto the pile. Due to controlled venting of the gas inside the combustion chamber, a reaction mass is pressurized and accelerated which results in a 100 ms loading time of the pile. This duration of the blow indicate behaviour of the pile in a quasi static way. Relative loading durations t_r between 5 and 500 [-] are considered as rapid loading conditions (on Rapid Pile Load Test Methosd, 1998). Blue Piling Installations falls towards the lower bound of this range found in previous research performed by Beuckelaers, (2018). As a consequence, rate dependency of soil resistance and inertia of the pile body must be considered, but stress wave phenomena may be neglected (Hölscher et al., 2012).

3. **Jacked installation**

   In pile jacking, hydraulic jacks are used to press piles into the ground. An advantage of jack piling when compared to vibrating and drop hammers is that the process brings about less noise and vibration due to the quasi-static loading operation during driving. This makes the technique suitable for use in areas sensitive to noise and vibration. The jacking procedure essentially loads the pile until full static capacity, proof-testing the pile during installation (Yang, Tham, Lee, & Yu, 2006). Jacking is compared to Blue Piling technique seen as previous research has proven the Blue Piling blow to cause a rigid body movement, similar to push-in methods (Beuckelaers, 2018).

4. **Vibratory driving** Vibratory driving is performed using a hydraulic apparatus gripped to the top of the element to be driven. The frequency chosen for the vibration block partially liquifies the soil, causing the pile to be able to penetrate into the soil.

2.1.1 Drainage conditions and resistance

For conventional driving in sand, free draining conditions are likely. Any excess pore pressures dissipate before the end of installation. While the pile tip advances through the soil, particles are displaced radially which increases the stress levels, comparable to values of in-situ cone resistance (q_c). Past the pile tip, along the shaft the stresses drop again since vertical penetration is not acting directly on the sand. These reduced stress levels are comparable to the measured values of sleeve friction (f_s) measured prior to installation (M. F. Randolph & Gourvenec, 2011).

Rate effects is a manner of describing the effects of loading rate on pile behaviour, relevant for Stat-namic loading. In sand, the rate effect is visible in the generation of pore water pressures. Drainage conditions may thus differ based on loading rates exerted while pile driving in sand. In clay, an increase in strength can be observed with rate of loading, leading to the rate effect being a constitutive soil property. Dry granular material behaves differently from saturated granular material. Loose sands will contract during loading, whereas dense sands will dilate. Development of pore pressures during contraction may lead to a decrease of soil strength whereas the negative pore pressures during dilation may lead to an increase of strength. Relative density, loading rate and permeability of the penetrated material play an important role (Hölscher et al., 2012).

Jackson, White, Bolton, and Nagayama (2008) has performed pile jacking field tests using the ' press-in' method at a site consisting of sand and underlying silt. Installation shaft and base resistances are found to be less than predicted by standard medium-term axial capacity methods based on CPT data. This is appointed to rate-dependent partially-drained installation behaviour, which is quantified using pore pressure measurements taken on the pile. Three pore pressure measurement devices are installed; at the pile tip (u1), 325 mm from the pile tip (u2) and 725 mm (u3) from the pile tip. During the jacking procedure, pore pressures measured by the first transducer are higher than the ones measured at u2 and u3. This reflects the dissipation of pore pressures and the unloading that occurs when the soil passes around the based and moves along the shaft. The higher excess pore pressures measured in the silt are attributed to the slower possible rate of dissipation in the material. Excess pore pressures induced under undrained or partially drained response may lead to a decrease in encountered resistance during installation due to reduction of effective stresses around the pile (Jackson et al., 2008).
Vibratory hammering in turn has a large effect on the effective soil stresses since soil in place is liquefied. The sand is brought into a loose configuration by the induced vibrations and then contracts which transfers load from the soil skeleton to the pore water causing a significant increase in pore water pressure. In cohesive soils there may be no resistance losses in installation while in cohesionless soils, shaft resistance losses up to 95% and base resistance losses of up to 50% may take place (Dynamics, 2010).

Both for Jacking and Stat-namic loading, rate effects play a role, characterized by the development in pore water pressures in sand and silty material. Based on the reference techniques, rate affects are likely encountered during Blue Piling Installation.

2.1.2 Plugging Effect

Definition of plugging
The Internal Friction Ratio (IFR) describes the degree of plugging in tubular piles. The IFR can be found during pile installation and is defined as follows.

$$IFR = \frac{\delta h_p}{\delta L} \tag{1}$$

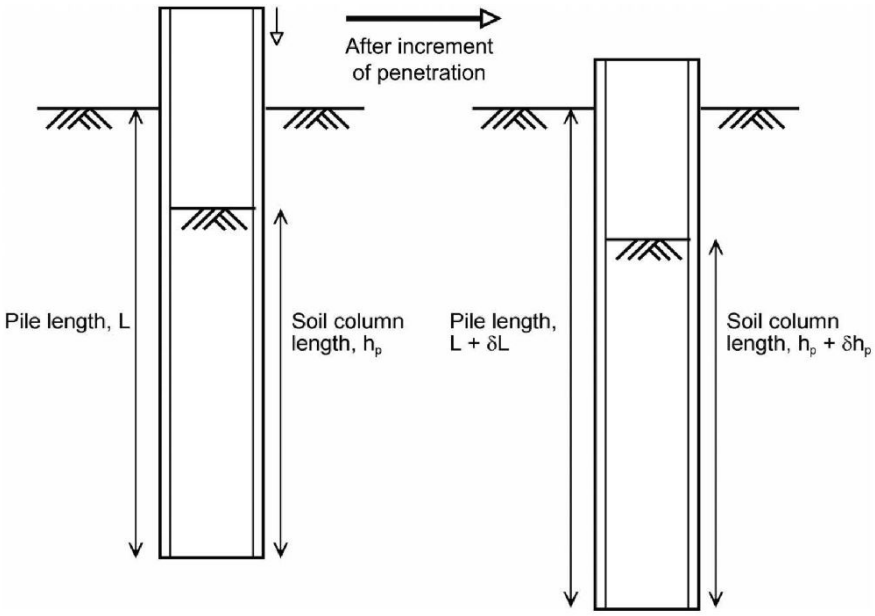

Figure 4: Incremental filling ratio defined (M.F. Randolph & Gourvenec, 2011)

The expression describes the increment of internal core length (δh_p) per change in pile penetration (δL). At the start of the process of pile driving, the pile may start unplugged, meaning the soil level inside the tubular pile remains at initial ground level. The increase in pile penetration then equals the increase in plug length, leading to IFR = 1, fully coring. When the soil plug starts moving downward with the pile, causing the length of the soil plug to become smaller than the penetration depth, partial plugging takes place. Plugged conditions are reached when sufficient frictional

resistance is mobilized inside the pile, preventing soil from pertruding into the pile. The penetration characteristics of an open-ended pile are then comparable to those of a closed-ended pile (S. G. Paikowsky, Whitman, & Baligh, 1989), but are not completely the same (Jardine, 2005). Plugging is affected by factors such as pile diameter, depth of penetration, installation method (Dean & Deokiesingh, 2013), internal friction angle (Saathoff et al., 2005) and relative density (Jardine, 2005) as will be further elaborated below.

Plugging is related to an increase in pile driving resistance. To avoid pile plugging and to aid pile driving, a driving shoe is often deployed near the pile tip. This thickened wall acts as a reinforcement and reduces driving resistance along the pile shaft in hard soils to allow easier penetration of the pile. The benefits apply mainly for higher penetration ratios (Byrne, 1995). No driving shoe is implemented on the pile used for experiments in this thesis.

Plugging under static loading

A pile plugs under static loading, not taking into account inertial effect, when the internal skin friction ($Q_{sf,internal}$) that develops is higher than the base resistance on the soil plug ($Q_{bf-plug}$) deducted by the plug weight (W_p) seen as the latter is a driving component and decreases resistance against plugging (M. F. Randolph & Gourvenec, 2011).

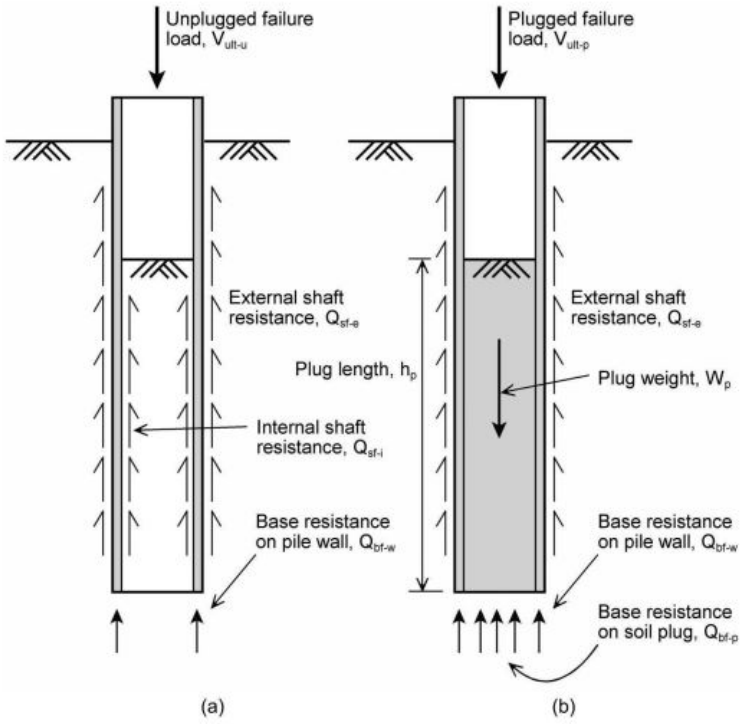

Figure 5: Open-ended pile failure mechanisms, (M.F. Randolph & Gourvenec, 2011)

Whether or not a pile plugs under static loading, largely determines the axial capacity of a pile. There is a component for i) internal skin friction and ii) base resistance developed under the annular area of the pile base.

i) The contribution of the internal skin friction becomes most relevant when arching mechanisms form in the internal soil column and plugging occurs. The original theory for behaviour of soil settlement in a laterally confined space was covered in Janssen, 1895 in the Silo approach which considers active arching. The name comes from load transferring mechanisms mobilized in actual silos. S. G. Paikowsky et al., (1989) uses the theory as a base to study soil plug behaviour under static loads, acknowledging the model lacks to describe the plug-pile interaction. An adjusted version of the model describes the formation of concave soil formations at the pile toe level as passive arching, since with the pile moving downwards, the soil is being pushed upwards and a supporting arch forms made of grain contact in the direction of major principal stress. The arches transfer axial stress acting on the internal soil column to the pile walls, which increases internal shaft friction. On micro level this is appointed to the movement and rotation of sand grains to the most stable position as a response to the major principle stress applied. The long axes of the particles arrange perpendicularly to the direction of the maximum principal stresses to form the arrangement, which increases contact and can transfer increasing axial stress, see Figure 6. High angle of friction (ϕ) and strong dilation in dense sands at internal pile interface aid the development of arching mechanisms, correlating to high values of relative density

(D_r) (Jardine, 2005). As pile diameters increase, these arching mechanisms cannot be sustained and thus likelihood plugging decreases. For a fully plugged pile no resistance can be retrieved from the internal skin friction.

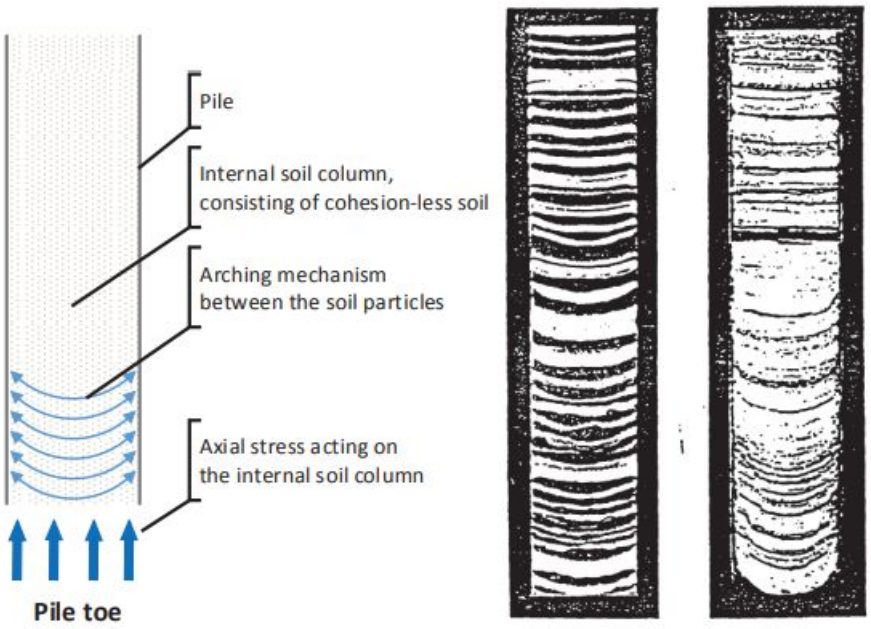

Figure 6: Arching principle (Karlowskis, 2014) and soil deformation indicating passive arching (S.G. Paikowsky et al., 1989)

ii) When the inner soil column is locked into the pile, the full end-bearing resistance acts over the total base of the open pile, increasing static bearing capacity (I. Smith, To, & Willson, 1986) and approaching characteristics of an equivalent closed-ended pile. When partially plugged, contribution of the base resistance is compromised compared to a closed-ended equivalent pile. This is firstly, due to local settlement being required to establish an arching effect and secondly, due to a non-similar degree of pre-stressing and pre-stiffening experienced by the soil beneath the soil plug with respect to a close ended pile (Jardine, 2005).

Two formulations are given by Jardine (2005) based on empirical data that formulate the critical diameter under which a pile will plug under static loading. The database consisted of piles with varying internal diameter between 0.05 - 1.9 meters. If either of the formulations is fulfilled, a rigid basal plug may form.

$$D_{inner} < 0.02(D_r - 30) \tag{2}$$

where:

D_r = Relative Density [%]
0.02 = Empirical parameter [m/%]
30 = Empirical parameter [m], both based on the relation visualized in Figure 7

$$\frac{D_{inner}}{d_{CPT}} < 0.083\frac{q_c}{p_a} \tag{3}$$

where:

D_r = Relative Density [%]
d_{CPT} = Diameter of cone Penetrometer [m]
q_c = Measured cone resistance [kPa]
p_a = Atmospheric Pressure = 100 kPa
0.083 = Empirical parameter [-]

The following figure displays the corresponding graph.

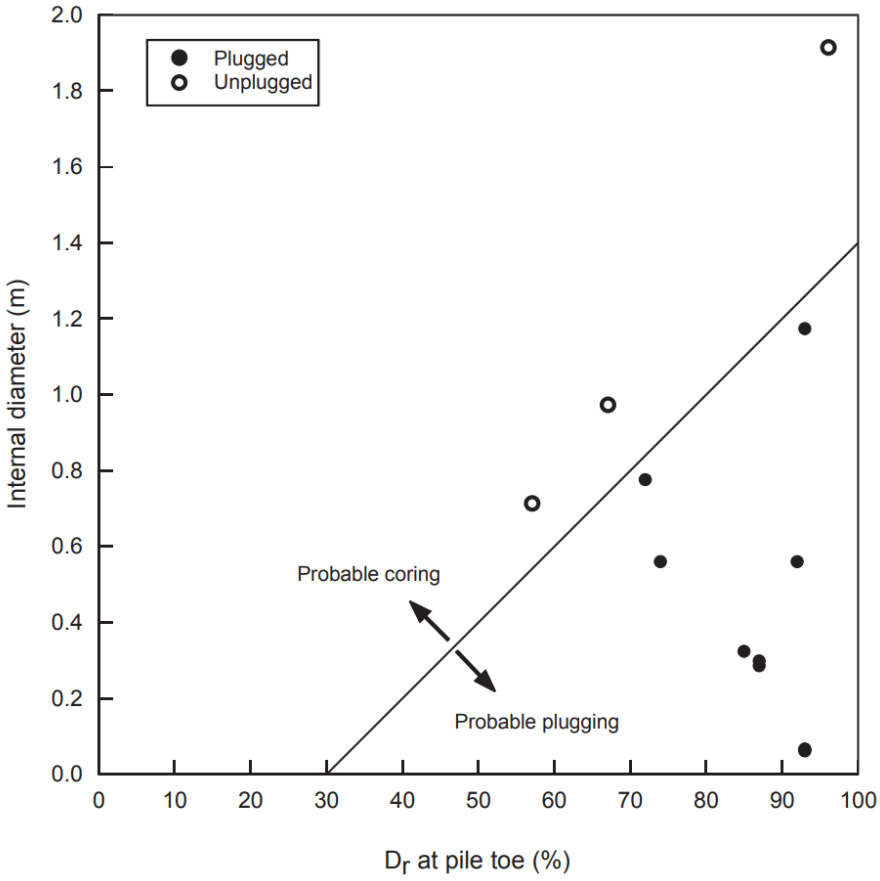

Figure 7: Plugging criterion as stated by (Jardine, 2005)

Also Kodsy and Iskander, (2022) have researched the influence of pile dimensions on plugging phenomena. Datasets of 74 load test on pipe piles and their geotechnical profiles were investigated. Based on the estimated total capacity with respect to the measured capacity, an estimation was made whether the pile had been plugged. Validation was performed for two other datasets and similar accuracy was reached. Piles smaller than 0.5 meter in diameter have a high likelihood of being plugged, whereas piles with diameter higher than 0.9 meters have a likelihood of being unplugged.

Plugging during driving

During conventional pile driving, plugging rarely occurs due to the inertia of the soil column creating an additional component of resistance in the process, resulting in slip along the steel-soil interface (M. Randolph & Deeks, 1992). Other authors support this such as Schneider and Harmon (2010) who have incorporated in their pile driveability model based on the UWA-05 method that inertial effects during driving mean that soil plug remains at or near the sea bed level during installation. However, piles may still plug during driving. Especially when pile tip passes from strong to weak material. The internal shaft resistance will then outweigh the base resistance as defined by the relation before, allowing the plug to move downwards with the pile.

Dean and Deokiesingh (2013) have proposed a new objectively calculable criterion to establish whether a pile plugs during the driving process. A shock wavefront analysis is combined with a simplified impact analysis to establish the plugging criteria. The criteria is based on the consideration that the shaft friction between soil and pile will largely be mobilized before the time the wave front reaches the pile tip. As a result, end-bearing is not yet available to the wave, so that the plugging criterion during driving cannot be the same as the one noted for static loading. During travelling of the wave down the pile annulus, friction develops in the steel-soil interface. Stress waves travel into the soil with velocity characterized by the shear wave velocity. For a strong soil, a waveform like drawn in Figure 48 may be expected.

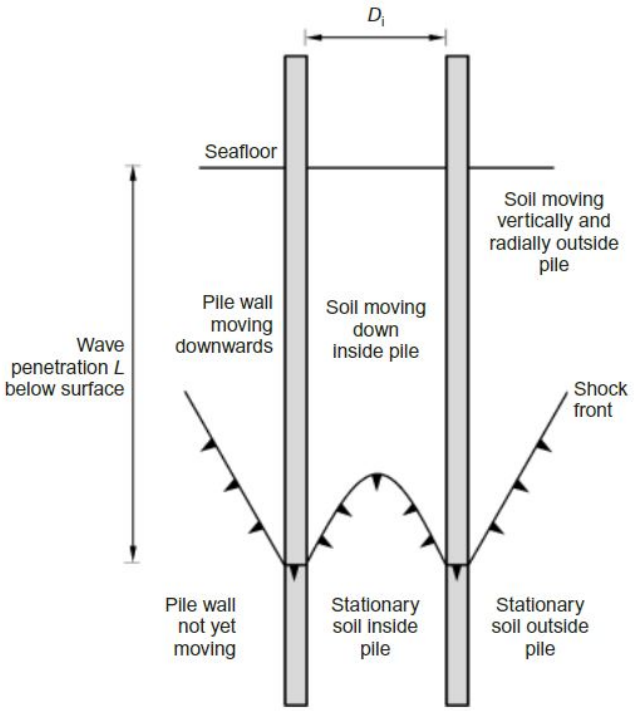

Figure 8: Stress wave through pile during driving

From equation 20 it can be inferred that plugging is less likely in weaker soils, heavier soils and in hammer-pile configurations that manage to convey impulse to generate a larger material velocity behind the shock front. It is concluded that plugging is more likely for long piles of small diameter.

Murthy, Robinson, and Rajagopal (2021) has performed calibration chamber tests of open-ended pipe piles in sandy soils and found that the incremental filling ratio (IFR) during driving decreases with pile penetration, indicating plugging behaviour, and IFR increases with hammer energy, indicating coring behaviour. This is in agreement with formulation 20.

De Nicola and Randolph, (1997) have performed model pile tests in the geotechnical centrifuge to compare open and sleeve-ended (also called a driving shoe) piles in sand using both driving and jacking driving configurations. By driving into silica flour of varying densities the relative density is varied. For jacking, the plug length decreased with increasing relative density and adopting a driving shoe increased coring behaviour significantly. For conventional driving, the presence of a driving shoe worked counterproductive seen as soil column heights were found lower than those of internally flush piles, attributed to the reduced entry area by application of a driving shoe. Additionally, driven piles had higher soil columns with increasing density of soil because of higher bearing resistance of the dense soil in place. A greater volume of soil was able to enter the pile. This indicates that in the absence of dynamic effects, high normal stresses can be locked into the soil plug, encouraging plugging. Stresses increase internally for dense soil conditions due to dilation.

For jacked piles, plugging during driving and loading increases axial capacity, as was amongst others reported by Lehane and Gavin (2001). The found base response of the jacked piles installed was much stiffer than that of similar piles driven in a coring mode.

Liu, Zhang, Yu, and Xie (2012) has performed comprehensive field tests to study behaviour of plugged open-ended concrete piles jacked in silt. The outer diameter of the piles used for installation appointed to 500 mm with a wall thickness of 110 mm. The piles were jacked to a depth of 15 meter and a follower was adopted to draw the pile to its final depth of 22 meters. Complementary laboratory tests were performed which showed compaction in the investigated soil plug and an increase in strength with time. In addition to this it was found that the formation of the plug is generally in accordance with the already present strata. The soil in the shear zone along the inner pipe wall mainly comes from the upper layer of soil strata which is appointed to the soil-arching behaviour during pile penetration.

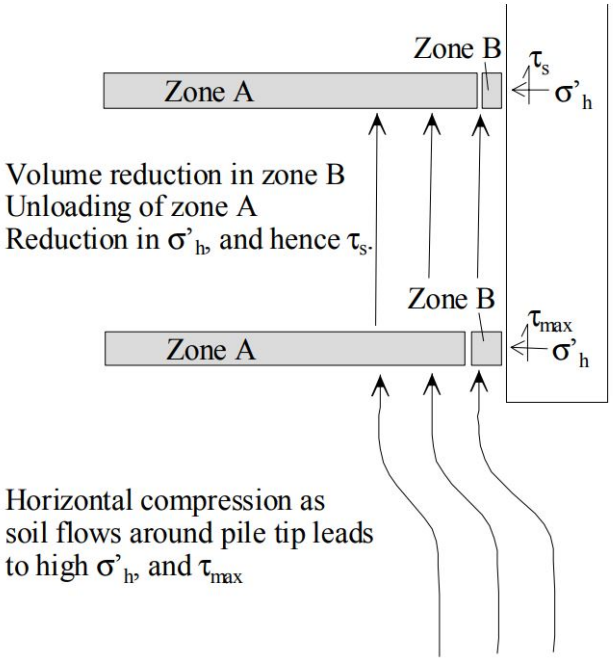

Figure 9: Mechanism of Friction Fatigue as described by (White et al., 2002)

For vibro installation, a continuous cyclic motion is adopted. During this process, soil in and around the pile is compacted. Numerical simulations performed by Henke, show this brings about a large decrease in radial stresses. Because horizontal stresses are decreased inside the pile, formation of a soil plug is not possible (Henke & Grabe, 2013).

2.1.3 Friction fatigue

Heerema, (1978) described friction fatigue for clay, as the reduction in skin friction in clay with increasing distance behind the pile tip. D. White and Bolton, in (2002) describe the process as follows. Before passage of the pile, at a certain soil horizon, the particle is at rest. As the pile moves closer, the particle moves outward with respect to the pile, generated by migrating fines through soil crushing and repacking of sand grains. This increases horizontal stresses due to the resulting lateral compression. The zone near the pile contracts with continued shearing. Contraction is possible in sand since the permeability of sand is high enough for a change in volume to occur. In the surrounding soil cylinder, relaxation can now occur which causes a reduction in horizontal stress acting on the pile shaft. As h increases along pile shaft, vertical effective stress decreases which in turn results in decreasing available shaft resistance.
As researched by D. J. White and Lehane (2004) using centrifuge test data, cyclic loading imposed during pile installation is presented as the primary mechanism controlling friction fatigue. It is caused by contraction of narrow shear zone at the interface between soil and shaft. Under more cyclic shearing and loading, the contraction at the interface becomes more significant. This is why D. J. White and Bolton, (2004) also argue the importance of reduced cyclic installation methods such as jacking. Radial effective stresses were found to vary significantly by number of cycles applied during installation. Friction fatigue is noted as more affected by cyclic loading than the upward distance (h) along the shaft.
Yang, Tham, Lee, Chan, and Yu, (2006) has found that at a given depth, jacked piles tend to show a shaft resistance that is higher than for a driven pile at the same soil horizon. Friction fatigue is appointed as the cause for the observation. The aim of the research has been to investigate similarities and differences in behaviour between installation techniques. A comprehensive field study was performed on H-piles driven and jacked into the ground. Piles of length 32 to 55 meters were installed in material similar to silty sand and load tested.

2.1.4 Set-up

Pile set-up is described by the gain in shaft capacity of a pile that takes place some time after installation. During installation, there is a development of circumferential arching mechanisms which limits radial stresses acting on the pile shaft. Creep tends to break down these arching stresses, which allow increasing radial stresses to develop which

yield a gain in shaft capacity. Dilation due to ageing in sand may yield a similar response and add to the set-up. Chow, Jardine, Brucy, and Nauroy, (1998) have found an increase in shaft capacity of 85% reached between 6 months to five years after installation of pipe piles in dense marine sand.

Lim and Lehane, (2014) have compared capacity of jacked and driven installed piles. It was found that set-up is the gain in shaft capacity of a pile as a result of disturbance brought about during installation (p. 482). It was found that the shaft capacity of normally driven piles, which were subjected to a comparably large number of blows compared to jacking, is much lower on short and medium term after installation. However, shaft capacity of driven piles showed to exceed maximum capacity for jacked piles within a few months. This leads to the conclusion set-up is more of a recovery process than just a capacity gain.

This Chapter gives an overview of installation effects relevant to consider during pile installation. during the Maasvlakte tests. Drainage conditions, plugging and friction fatigue affect the driving resistance, while set-up may affect mainly long-term capacity.

2.2 Smith's model for Modelling Driving Resistance

In this thesis, the finite-difference software used for drivability performance of the Hydrohammer used for Conventional Driving is GRLWEAP 2010. The analysis software can simulate the response of a pile to pile driving equipment and is based on the wave equation and Smith's model. Inputs consist of a part for soil, pile and hammer. Soil inputs consist of the soil site investigation parameters, SRD model (Alm and Hamre, (2001)) and damping quake factors. Pile inputs consist of geometry and material. Lastly, hammer input consists of a hammer model, cushion and helmet parameters, drop heights coefficient of restitution (C.O.R.) and efficiency. Using the wave equation, GRLWEAP can give as an output the blowcounts, driving time and (dynamic) installation stresses based on the 1D-Wave equation (Dynamics, 2010). For the Blue Piling hammer, a Simulink model has been created by the Blue Piling Team, based on Newton's second Law, to solve for the applied forces with the input of the velocities and masses of all relevant hammer parts and yield also blowcounts, driving time and energy levels reached by the prototype Blue Piling hammer. The model for pile and soil are based on Smith's model and are built the same as in GRLWeap. For additional elaboration will be referred to Appendix A.3 and for the details and equations will be referred to (Martens, 2019), (Ligthart, 2019) and (Hessels, 2020).

2.2.1 1D Wave equation

The one-dimensional wave equation can be used to describe the propagation of driving energy along a foundation pile as proposed by E. Smith in (1960). Before this time, rigid body mechanics were at the base of so called 'pile driving formulas' used in analyses. The 1D wave equation is based on Newton's Law containing both a parameter for mass and acceleration in the left part of the following equation.

$$\rho\left(\frac{\delta^2 w}{\delta t^2}\right) = E\left(\frac{\delta^2 w}{\delta z^2}\right) \tag{4}$$

rewritten as

$$\left(\frac{\delta^2 w}{\delta t^2}\right) = c^2\left(\frac{\delta^2 w}{\delta z^2}\right) \tag{5}$$

where:

w = Displacement $[m]$
z = Downward coordinate $[m]$
t = Time $[s]$
ρ = Mass density $[kg/m^3]$
E = Elastic modulus $[mPa]$
$c = \sqrt{E/\rho}$ = Wave speed $[m/s]$

w in this case represents a particle of the pile moving down at a certain speed and z is the downward coordinate. The solution of the equation is the superposition of an upward and downward waves travelling at wave speed (c). The other parameters are described as noted above. The upward and downward travelling waves are caused by mobilization of both shaft and toe resistance travelling up and downwards at the same time. A schematic display can be found in the following figure.

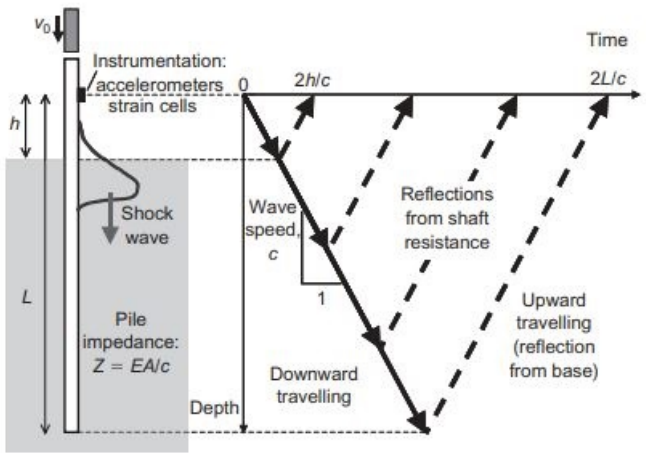

Figure 10: Stress wave travelling down pile, (M.F. Randolph, 2003)

Drivability analyses and axial capacity estimations require appropriate soil models to simulate load transfer along pile shaft and to the base of a pile. Soil is a continuum, but one-dimensional models may be equipped so that the soil layers along the shaft act on the pile and independently from their neighbouring layers. At the pile base any interaction with the lowest soil element on the pile shaft is ignored and the integrated response of the semi-infinite half-space below the pile tip is represented. Smith's model uses an assembly of mass elements, (non-linear) springs, plastic sliders and dashpots. The parameters of the system are found empirically by fitting to measured responses to find suitable parameters which connect to the fundamental soil properties.

2.2.2 Pile model

The pile is modelled as a discretized lumped masses connected by springs. Each pile segment is appointed their on weight which are connected by springs without weight. The damping of the internal material is linear. The following figure displays the implementation into GRLWeap and Simulink that is used.

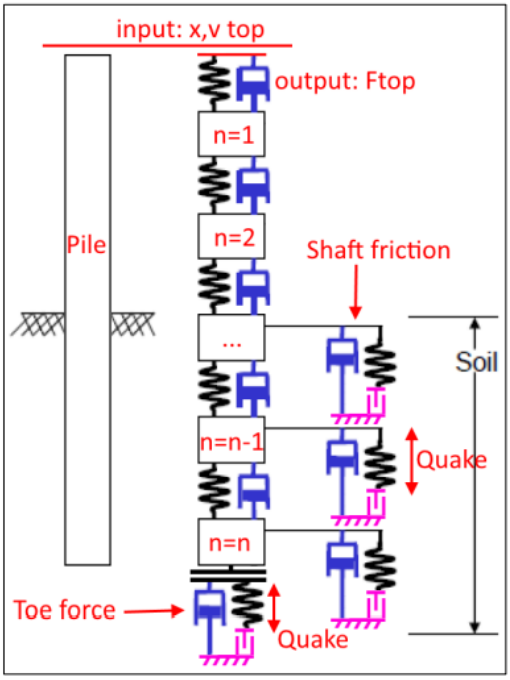

Figure 11: Schematization of the pile-soil model for Simulink and Weap, (Martens, 2019)

2.2.3 Soil model

Total driving resistance models consist for the largest part of a static resistance part which is supplemented by a damping contribution, described by the following formulation (Alm, Bye, & Kvalstad, 1989):

$$R_d = R_s + D \tag{6}$$

where:

R_d = Dynamic resistance during driving
R_s = Static resistance during driving (SRD)
D = Damping component

Static resistance during driving (SRD)
The static resistance (R_s) is modelled as a linear elastic-plastic system. The soil spring is elastic, its stiffness defined as the ratio of the maximum static resistance and the maximum elastic deformation, also described as quake (Q) in $[mm]$. This value is the maximum elastic deformation, after which the local pile displacement may cause slip between pile and soil (M. Randolph & Deeks, 1992). Physically it is the rebound of the pile after being subjected to the hammer push, the expansion and contraction of the elastic spring between pile segment and fixed soil segment around the pile. A plastic slider in series with the spring represents the limiting shaft friction.

During driving, it is calculated in a similar manner as the static capacity of a friction pile. It differs from the static capacity profile since an updated toe resistance is considered with every driving increment instead of a constant base resistance, aswell as a cumulative increase in shaft capacity with increasing pile penetration. Different methods have been presented by (Toolan, Fox, & BP, 1977), (Semple & Gemeinhardt, 1981) and (Stevens, Wiltsie, & Turton, 1982) which for long piles, generally predict resistance on the conservative side and has been largely calibrated empirically on CPT and end resistance qc values lower than 30 MPa. The first time the friction fatigue concept was introduced was by (Heerema, 1978) which has been updated by (van Zandwijk, van Dijk, Voeten, & Heerema, 1983) for non-linear damping, but are not suitable for easy use in common wave equation programs. An alternative was presented by Alm et al. in (1989), based on back calculations of driving records from the North Sea, also including friction fatigue concepts. The static resistance of the proposed model was updated in Alm and Hamre, (2001) and is elaborated below. The database used to calibrate the model consists of data from 18 installations performed on 16 locations consisting of a variety of North Sea Soils: dense sands to highly over-consolidated clay layers at sea depth between 70 and 170 meters. The piles installed are between 1.83 to 2.74 meters diameter and were installed by hydraulic underwater hammers. For further information about the database will be referred to the original paper.

Alm and Hamre

For sand, initial friction is taken as the basic static friction formulation. This is input for the unit shaft resistance (f_{si}) before driving.

$$f_{si} = K * \sigma'_v * \tan\delta \tag{7}$$

Here, the lateral stress coefficient (K) is directly linked to the cone resistance.

$$K = 0.0132 * \frac{q_c}{\sigma'_v} * \frac{\sigma'_v}{p_a}^{0.13} \tag{8}$$

where:

f_{si} = Initial pile side friction [kPa]
K = Lateral stress coefficient or horizontal stress ratio after driving (-)
σ'_v = Effective overburden pressure [kPa]
ϕ = Constant volume friction angle [degrees]
q_c = Cone tip resistance (corrected for pore water effects if applicable) [kPa]
p_a = Reference pressure = 100 kPa

Shape factor for degradation (k) then gives a relation suitable for both clays and sand as follows.

$$k = \frac{q_c/\sigma'^{0.5}_v}{80} \tag{9}$$

In clays, unit tip resistance is taken as 60% of the total cone resistance while for sand the following formula is used to find optimum correlation.

$$q_{tip} = 0.15 * q_c * \frac{q_c}{\sigma'_v}^{0.2} \tag{10}$$

With increasing sand density, the unit tip resistance will increase. Noted is that the value of tip resistance will be lower than the q_c value directly. This is lower than for usual bearing capacity relations, which is likely due to the effect of wedged pile tips in which the actual tip area is reduced to almost half of the original. In predictions for SRD, still the full pile tip area should be used in combination with the formulation above.

Dynamic resistance during driving

The dynamic resistance during driving equals the static resistance to driving, extended by a damping term as can be seen in Equation 6. This is due to the inertial effects and increased capacity due to viscous rate effects. The Smith type formulation is given by the following expression, with slightly different values used for shaft and tip as elaborated below.

$$D = R_s \cdot J_{Smith} \cdot v \tag{11}$$

where:

$J_{Smith} = J_s$ or J_p= Smith damping factor for side or tip, respectively $[s/m]$
v = Pile segment velocity $[m/s]$
R_s = Static resistance during driving (SRD)

Damping (D) coefficients model the viscous behaviour of the soil, modelled by a quasi-linear dashpot in parallel with the elasto-plastic spring/slider configuration. The damping term leads to additional soil resistance, thus reduction of displacement per blow.

In the case of Smith's model, the dynamic soil resistance and the velocity are assumed to have a linear relationship. The value of the side damping coefficient (J_s) and tip damping coefficient (J_p) have been proposed by Smith based on matching of pile response to load testing results for pile diameters of typically 300 mm: Q = 2.54 mm, J_s = 0.164 s/m and J_p = 0.492 s/m which are widely accepted for pile drivability analyses.

The following figure displays the load-deformation characteristic assumed by Smith. On the left side, the damping effects are not included, both loading and unloading are displayed. The response for compressive loading is given on the positive side of the axis while for loading in tension the negative side is reserved. Q is quantified and the ultimate ground resistance quantified by R_u displays the load at which the soil spring behaves only plastically (E. Smith, 1960).

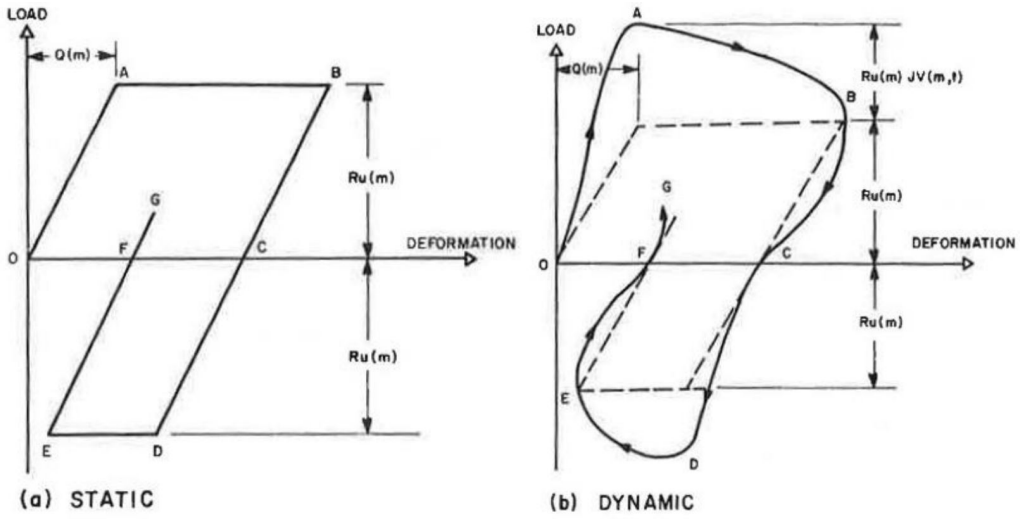

Figure 12: Load-deformation characteristics for soil spring, (E. Smith, 1960)

2.2.4 Hammer model

The hammer system considered by Smith exists of a ram with initial velocity given by the pile driving system, a cap block, a pile cap and a cushion block on top of the pile inside it's supporting medium. Configurations may differ seen as cushions may not be deployed or an anvil may be added between ram and cap block. Total assembly weight is an input parameter.

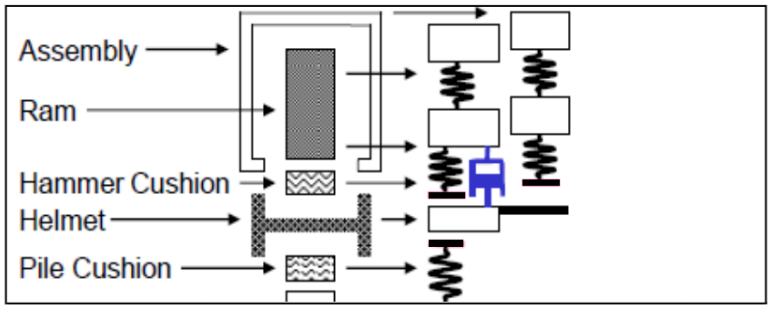

Figure 13: Schematization of the hammer model for Weap, (Dynamics, 2010)

The Simulink for the Blue Piling hammer has carefully been composed by the Blue Piling Team. The hammer input consists of the hammer stiffness, water and air cap. A part for the cilinders is considered since there are two cylinders present in the system, both relevant in consideration namely the main buffer cylinder and the lift cylinder. The sleeve is finally implemented as a single mass without stiffness.

3 Site Investigation

The following section elaborates on the Site investigation information that is available for the site. Based on a relevant profile chosen, the preliminary pile dimensions will be established and driving resistances are simulated in both Simulink and GRLWeap modellation for a first drivability analysis.

3.1 Site History

The Maasvlakte is a man-made extension of the port of Rotterdam at the mouth of the river Maas. In 1960, initiatives were started to commence its construction, which were mainly driven by increasing frequency of use of the harbour and increasing ship sizes. This first extension of the Maasvlakte, called Maasvlakte 1 was finished in 1969. At the end of the 20st century, a second extension was initiated due to constant need for increase in capacity for large scale harbour-activities. Its construction was finished in 2013 (of Rotterdam, n.d.-a).

Figure 14 shows the current configuration of Maasvlakte 1 and Maasvlakte 2. Before construction of Maasvlakte 2, the Noordzee reached to a depth of 17 meters. This can approximately be traced back from the current sea depths even though these are being continuously maintained with dredging activities (nautical charts, 2022). To be able to reach to a height of 5 meters above sea level as present nowadays, sand was dredged from the North Sea, nearby water bodies and port fairways and deposited in place.

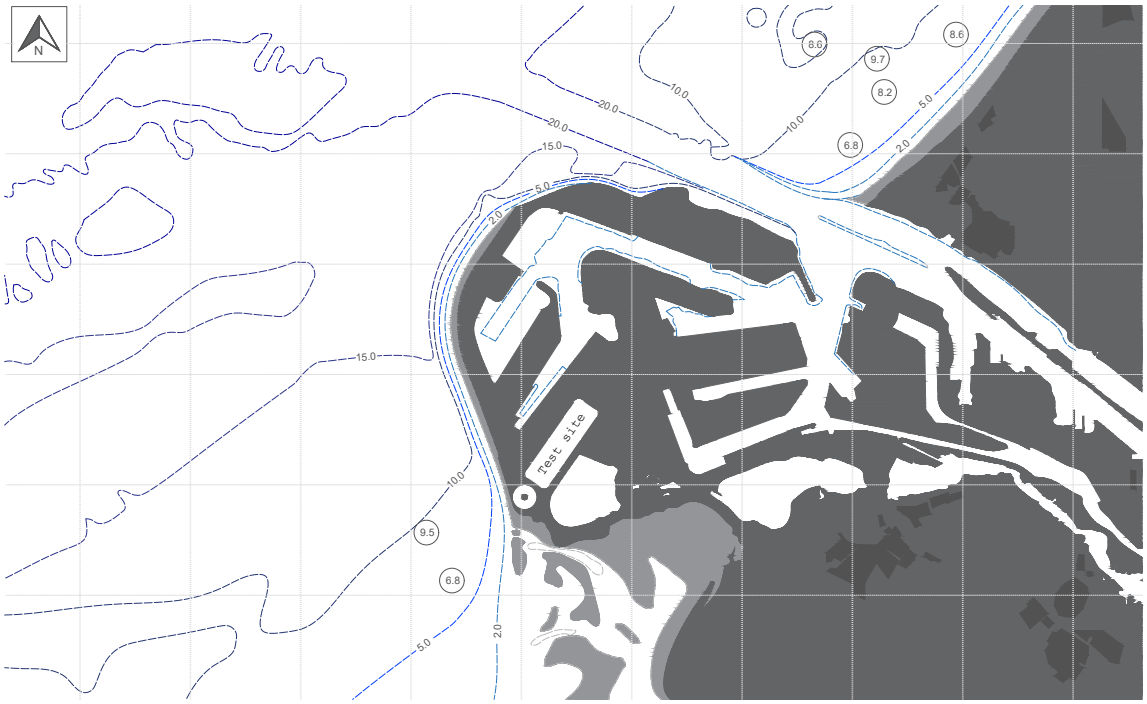

Figure 14: Noordzee sea floor elevations around the Maasvlakte

Site investigation performed by BAM on Kade 5.3 and 5.4. in 2010 in the Prinses Amaliahaven on Maasvlakte 2 confirm that the top $+5$ m until -10 m NAP exists of dense to loose sand, dumped in place. Between -10 and -15 to -24 m NAP the Bligh Bank formation is found, consisting of sand rich in shells which were deposited in high energy marine environments, reworked by waves and tides in the period of placement (Rijsdijk et al., 2005). Soil layers beneath are appointed to the Banjaard, Nieuwkoop, Elbow and Krefentheije formations respectively (van Paassen, 2010).

The top layer of deposited sand was found to contain a silt content of less than 5%. Three degrees of sand compositions are found for values of R_n, where R_n indicates: Loose (0 - 33%), medium dense (33- 66%) and dense ($>33\%$) according to NEN 6740 [32] tabel 1.. Appendix B.4 shows the relative density values obtained and their classification in-situ.

3.2 Water level investigation

Groundwater monitoring data from Dinoloket is mostly available right after the construction of the Maasvlakte 1 onwards; between 1970 and 1986. Taken alongside the Europaweg, the most westward ground water monitoring tables inside the dike show that for the shallow standpipe *001* installed around +0.4m NAP, the water level fluctuates between $+1.9$ and -0.5 m with respect to NAP between 1970 and 1986. Stand pipe *002* installed to a depth of -4.7 m NAP display a more stable fluctuation after 1972, where the water level now fluctuates between $+0.7$ m NAP and 0 m NAP until 1986. A biyearly trend can be spotted, showing a peak in summer and winter as can be seen in Appendix B.1 (DINOloket, n.d.).

Water heights as measured in the Amaliahaven by Rijkswaterstaat show a fluctuation between $+2$ m and -0.5 m NAP in the month of October. The fluctuation is caused by the tides, which reaches two peaks per day (Rijkswaterstaat, n.d.). Water level fluctuations caused by tides and weather are continuously measured by the Port of Rotterdam around the port area. Around the northern mouth of the harbour, Papegaaiebek, water levels fluctuate between $+1.5$ m NAP and -0.5 m NAP (of Rotterdam, n.d.-b).

Based on the available water level investigation, a stationary water level between 0 and $+0.5$ m NAP is assumed as average value, as relevant for the preliminary calculations. The effect of tidal effects may be considered in the top sand layer.

3.3 Cone Penetration Test analysis

The CPT site investigation on site Maasvlakte was conducted by three parties: Fugro (S1-S12), Ingenieursbureau Rotterdam (S13-S22) and Van der Straaten Geotechniek B.V. (S23-S32).

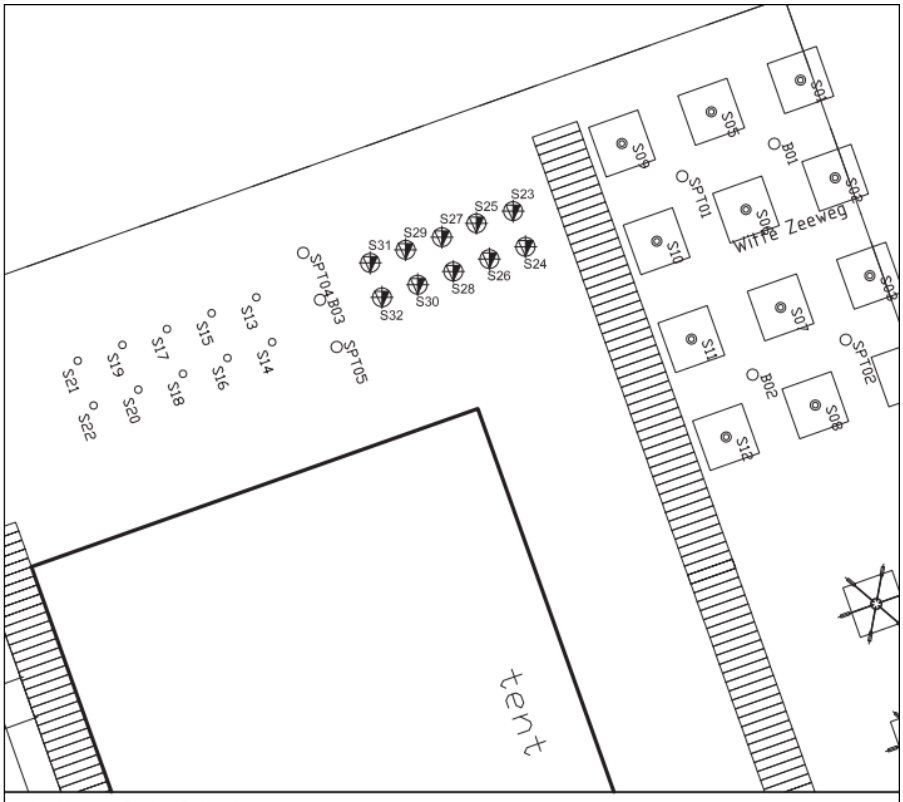

Figure 15: Available CPT locations, (vd Straaten, 2022)

From the Site Investigation, the homogeneity of the site is assessed from east to west. What can be seen is that there is a spread of around 2000 kPa for the cone resistances measured and a spread of 50 kPa for the sleeve friction measured.

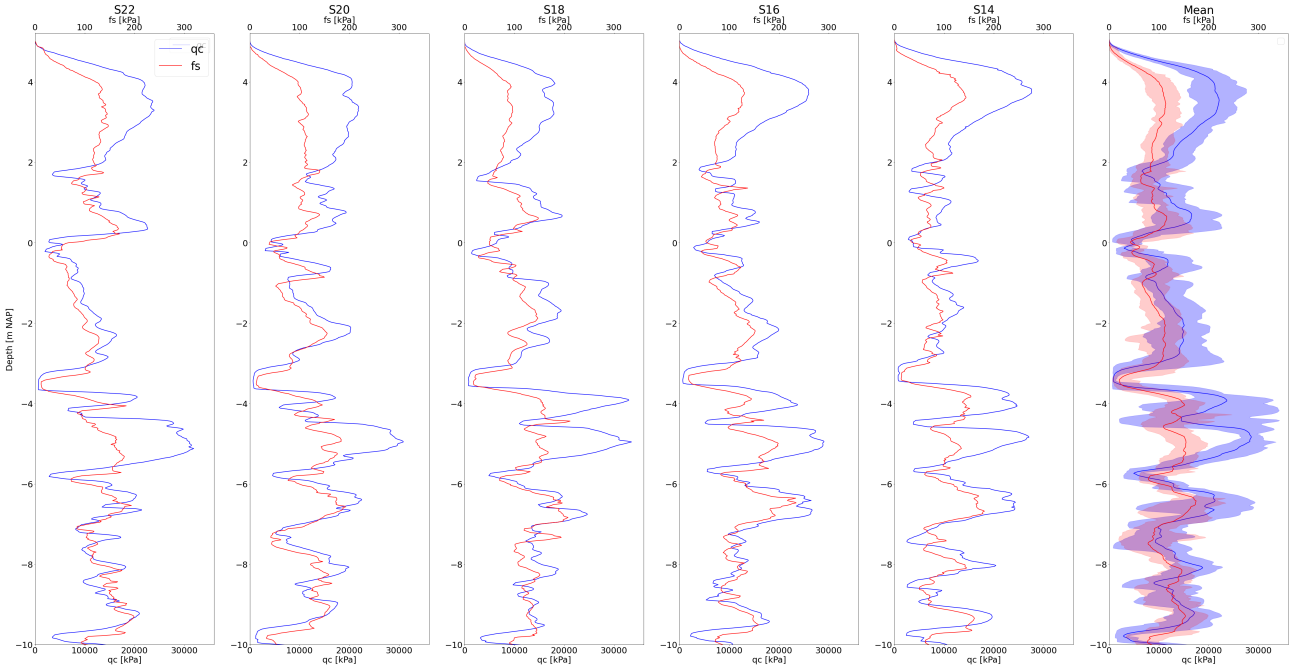

Figure 16: CPT's taken by Ingenieursbureau Rotterdam from west to east on the Maasvlakte site

The interval between $+5$; -20 meters is selected for elaboration seen as larger depths are outside the scale of piles potentially used for the project. The materials found in-situ consist of sand: slightly silty, silty, gravelly and clay: slightly silty, silty / Silt. The CPTs that indicate the most potential for high shaft and base resistance are taken by Fugro (S1 and S3). Additionally, S14 from Municipality Rotterdam Engineering Firm shows high shaft and base resistance potential. The CPT was taken on the other side of the perimeter, see Figure 15. See Appendix B.2 for the comparative values of cone resistance.

For assessing potential driving difficulties such as in-sufficient self-penetration and refusal, consideration of upper bound soil strength is necessary (M. F. Randolph & Gourvenec, 2011). For soil profile S14, the maximum value of site data is reached for the [5m ; 3m] depth interval, as found by both Ingenieursbureau Rotterdam and Van der Straaten Geotechniek B.V. The first design calculations using profile S14 can thus be justified. A margin of 25% is taken over the found cone resistance and sleeve friction to find an upper bound in calculations. These values are displayed relative to the maximum values as found on site in Appendix B, Figure 53 and 54.

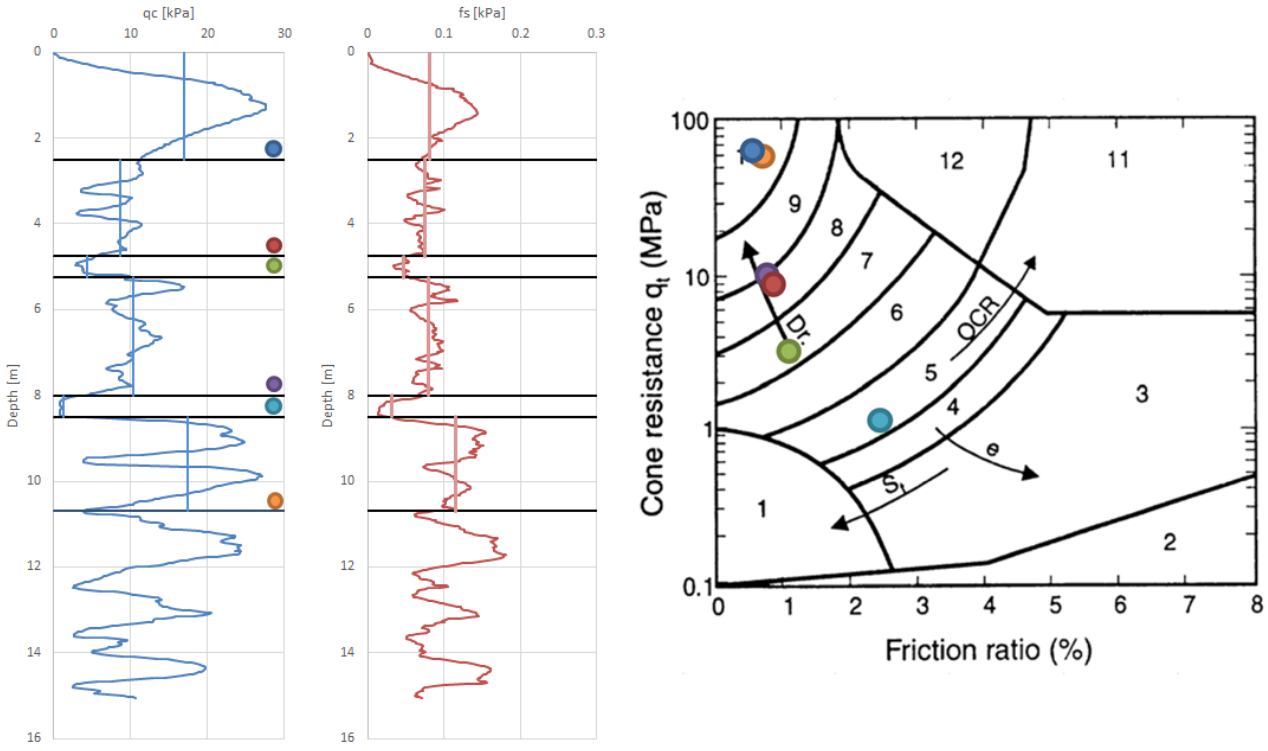

Figure 17: Soil Profile S14 - Classification of soil profile based on (Robertson, 2010)

From the Site investigation desk study, it is found that the top meters of soil which will be used for pile installation are man-made indicating it is relatively homogeneous. The water level on the Maasvlakte will on average lie around 0 m NAP and from the CPT information is is taken that the site mainly consists of silty to gravelly sand. To make sure that the pile can be driven to depth, CPT S14 is chosen for the first design calculations with a factor of 1.25 to consider the upper bound.

4 Experiment Design

4.1 Pile Design and Hydrohammer selection

In order to design the pile used for the experiment on the Maasvlakte, design calculations are performed as drivabilities GRLWeap using a conventional hydro-hammer in the in-situ soil conditions. The prerequisites are; to maintain a relevant comparison to mono piles (L/D-ratio = 4-10) (M. F. Randolph & Gourvenec, 2011), possible comparison between Hydrohammer and Blue Piling installation (thus acquiring penetration depths) and availability of the material. This resulted in the following pile design: pile length equal to 11.9 meters, diameter equal to 1.22 meters and thickness equal to 20 mm, as visualized in Figure 18. The U-profile serves as housing for the measurement devices, placed at 0°, 90°, 180° and 270° along the pile circumference. Further elaboration about the measurement devices is found in Chapter 4.2. For more drawings in details will be referred to '9000281801-B Test pile.pdf' as found in the IQIP repository.

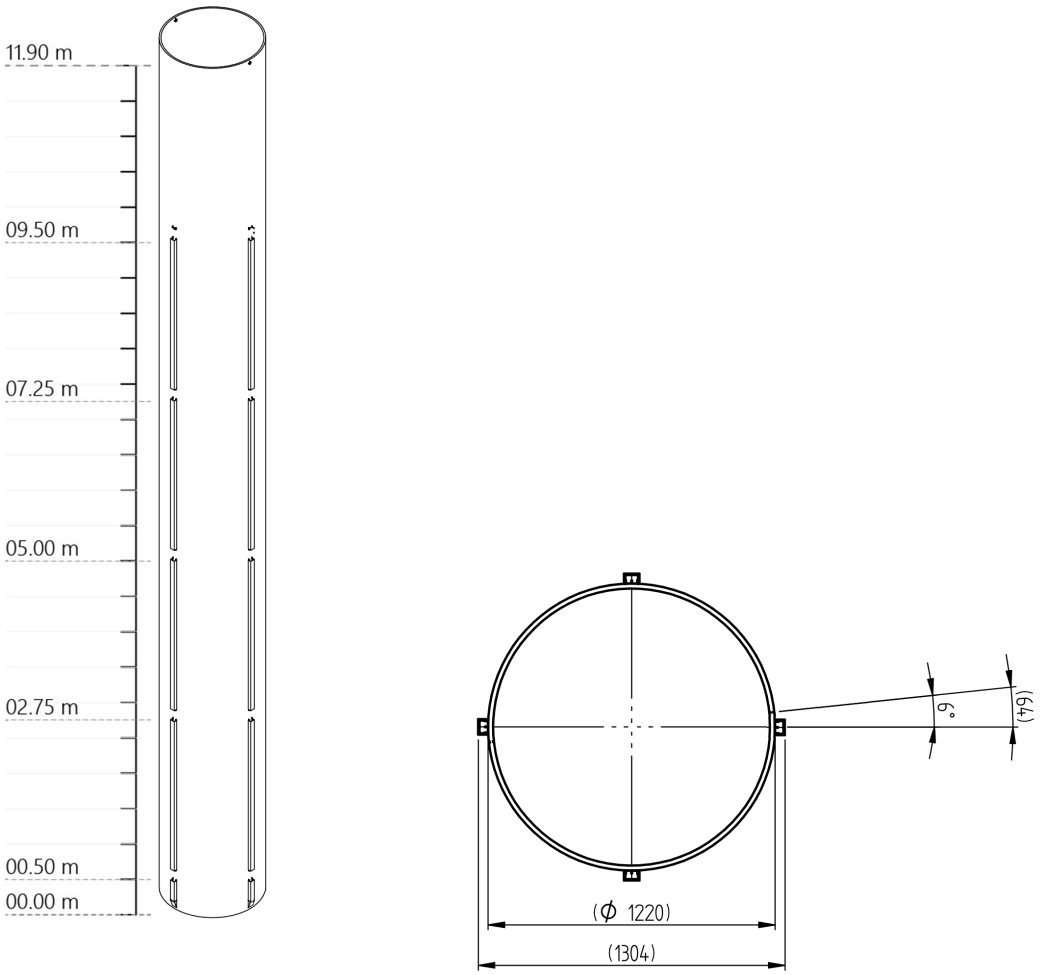

Figure 18: Pile dimensions and cross-section

The diameter used for the pile has not been adjusted from the first iteration value picked. The main reason for this is that the prototype hammer is already built for this diameter of pile, streamlining the preparation process of the experiment. From Simulink simulations performed by Leon Martens of the Blue Piling Team, the pile is expected to reach to a depth of 9 meters before refusal using the Prototype Blue Hammer. Consequently, the Hydrohammer should be driven to a similar depth, which makes the L/D-ratio equal to 7.4. The additional pile length allows for the use of the available anvil of 1.5 meter height without application of a follower. Pile thickness is 21 mm along the full length of the pile. Implementation of a driving shoe in GRLWeap drivability only increases the base resistance, leading to higher blowcounts. Seen as plugging is unlikely for pile diameters around 1.22 meter as found in Chapter 2.1.2, no driving shoe is implemented. For Soil input, profile S14 as found in Chapter 3 is investigated.

4.1.1 Input Parameters - GRLWeap

In the following section, the process of obtaining pile and hammer configuration from the available site investigation is elaborated. The following parameters are input parameters that are constant throughout the drivabilities performed.

Hammer parameters		
Efficiency	0.95	[-]

Cushion information		
C.O.R.	0.85	[-]

Pile parameters		
Length	12	m
Elastic Modulus	210000	MPa
Spec. Weight	77.5	kN/m^3
Pile size	1220	mm
Perimeter	3.83	m

Soil Parameters					
Quake			**Damping**		
Shaft	2.5	mm	Shaft	0.25	s/m
Toe	2.5	mm	Toe	0.5	s/m

Hammer parameters *Stroke*, *Assembly weight* and *Helmet weight* are adjusted based on the hammer choice and cushion information. The values input for the selected Hydrohammers S-30 and S-70 are found in Appendix C.1, Table 10 and Table 11. The pile geometry parameters *Section area*, *Toe area* and *Wall thickness* are changed for every new iteration. From the obtained blowcounts, the drivability is assessed. A blowcount around 100 blows per 0.25 meter penetration indicates refusal. The preferred normal performance of a Hydrohammer is around 30 blows per 0.25 meter penetration.

4.1.2 Methodology

The following methodology is adopted to find a suitable pile geometry for the set prerequisites; to maintain a relevant comparison to mono piles (L/D-ratio = 4-10), possible comparison between Hydrohammer and Blue Piling installation (thus similar penetration depths) and availability of the material.

1. Perform drivability analysis with S-70 hammer
2. Perform drivability analysis with S-30 hammer
   > Choose hammer based balance between ease and efficiency of driving
3. Add Safety factor 1.25 to soil data to find heaviest possible driving conditions
4. Check drivability under reduced energy settings
5. Check influence of driving shoe
   > Change pile geometry if necessary
6. Propose suitable pile/hammer configuration
7. Adjust design based on available material
8. Check drivability for other site conditions
9. Propose a final pile geometry that fulfills the prerequisites

4.1.3 Results

The following work flow was adapted to find a suitable pile geometry and the most suitable hammer for driving the pile in the Maasvlakte test site. The initial pile geometry is as follows from the Table below.

	Interval [m]	**t [mm]**
Top	9	25
Bottom	3	50

Table 1: First iteration Pile Geometry

1. **S-70 hammer - Drivability**:

   The smallest Hydrohammer after S30 and S40 IQIP Hydrohammers at full energy (full stroke = 2.02 meter) for first iteration pile geometry.

   - Refusal is not reached at 10 meter depth.

2. **S-30 hammer - Drivability**:

   To check if driving to similar depth is possible at full energy (full stroke = 1.88 meter). The use of the smaller S-30 hammer has economic and time planning benefits since handling is lighter.

   - Value around 10 meter depth closer to refusal (63 blows /0.25 meter penetration).
   - Top 2 meters of soil indicate refusal, but refusal is unlikely at this depth because of smaller confinement pressures at soil horizons close to ground level.

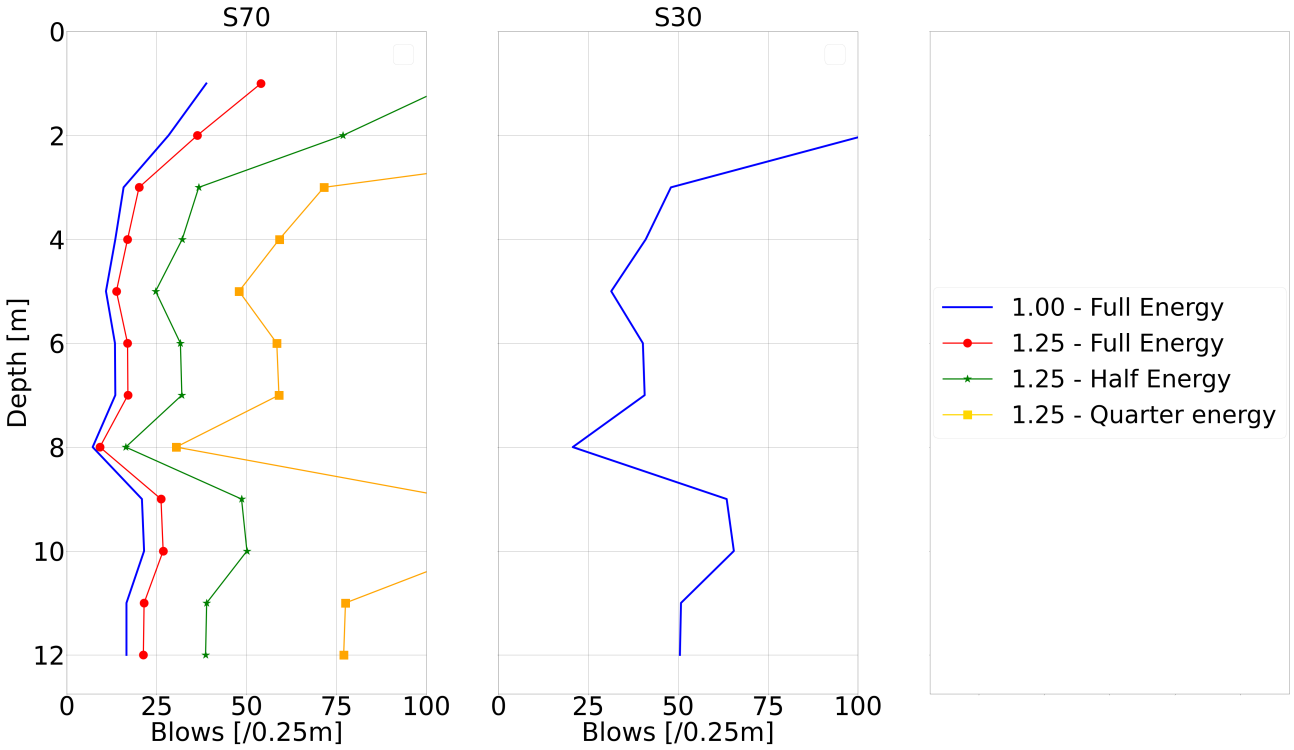

Figure 19: Blowcounts obtained for (a) S70 - Safety Factor and Energy adjustments, (b) S30

3. **S-70 hammer - Adding Safety Factor**:

   Safety Factor of 1.25 is added to the design calculations to check heaviest possible driving conditions and verify penetration possible to at least 9 meters depth.

4. **S-70 hammer - Reduced Energy settings**:

   The Hammer *Stroke* is positively linearly correlated to the acceleration of the hammer block and thus the hammer energy that can be reached during installation. By replacing the initial value by a *Virtual Stroke*, the energy exerted scales directly.

   • The pile can be driven to a depth of around 9 meters on quarter energy and including safety factor. Ensuring drivability of the pile geometry with an S-70 Hydrohammer with a large margin.

5. **S70 hammer - Changing shoe thickness and height**

   For half the driving energy levels (*Virtual Stroke* = 1.01 meter), geometry input parameters are changed to check the effects in Weap Drivability analysis as follows from the following table. Results can be found in Appendix C.1, figure 56.

	Interval [m]	**t [mm]**	**Interval [m]**	**t [mm]**
Top	9	25	11.4	25
Bottom	3	50 and 40	0.6	50 and 40

Table 2: Further iteration Pile Geometry

   • Driving shoes of 3 meters from the pile tip of 50 and 40 mm thickness are tested. The increase in base resistance is felt mostly in the first gravelly sand layer above 2 meters depth and towards final penetration.

   • The effect of the driving shoe in GRLWeap analysis is changing the amount of blows necessary for 0.25m penetration by 10 blows between length of shoe equal to 3 to 0.6 meters around final penetration values.

   • Driving shoes of 0.6 meter from pile tip of 50 and 40 mm are tested. Rise in blowcount is not significant compared to the case without driving shoe. In practise, implementation of a shorter driving shoe may relieve driving resistance as found in Literature research, but most relevant effects are seen for higher penetration ratios (Byrne, 1995) than currently introduced.

6. **Proposition of Pile/Hammer configuration**:

   The proposed pile geometry consists of diameter (D) = 1.22 meter, homogeneous thickness (t) = 25 mm along the pile. Implementation of no driving shoe is deemed reasonable due to plugging being unlikely for the large diameter implemented as found in Chapter 2.1.2. Penetration to around 9 meters depth is governed for Hydrohammer S-70 and Blue Piling hammer (Leon Martens, Blue Piling Team) with this geometry.

7. **Adjusting design to the available material**:

   Only an S-30 hammer is available in the time frame for the Maasvlakte tests. An already existing steel pipe pile of length (L) = 11.9 meters, diameter (D) = 1.22 meters and homogeneous thickness (t) = 21 mm is available. Further elaborations are done for full energy (*Stroke* = 1.88 m) settings.

8. **S-30 Hammer - Changing Site Conditions**:

   The drivability analysis is performed for S14 throughout. As preparation for differing site conditions during the test, results are shortly elaborated for soil profile S1 as found by Fugro, Chapter B. Safety factor is included in both analyses.

   • No refusal conditions are reached for the shallow high q_c values found in the gravelly sand layer above 2 meters depth.

   • For both soil profiles considered, the pile can be driven to at least 8.5 meters depth.

9. **S-30 and Blue Piling Hammer results for Final Geometry**:

Results of the Simulations performed by Leon Martens, Blue Piling Team are plotted against the blowcounts obtained for the S-30 Hydrohammer as predicted by GRLWeap. Blue Piling Simulations are performed with two different statistic models: Alm and Hamre, (2001) and ICP method by Jardine, (2005) as further elaborated in Chapter 2.2 and Appendix A.3, respectively.

- Penetration to around 8.5 to 9 meters depth is governed for Hydrohammer S-30 and Blue Piling hammer (Leon Martens, Blue Piling Team) with this geometry.
- There is a large difference in the amount of loading cycles during installation.

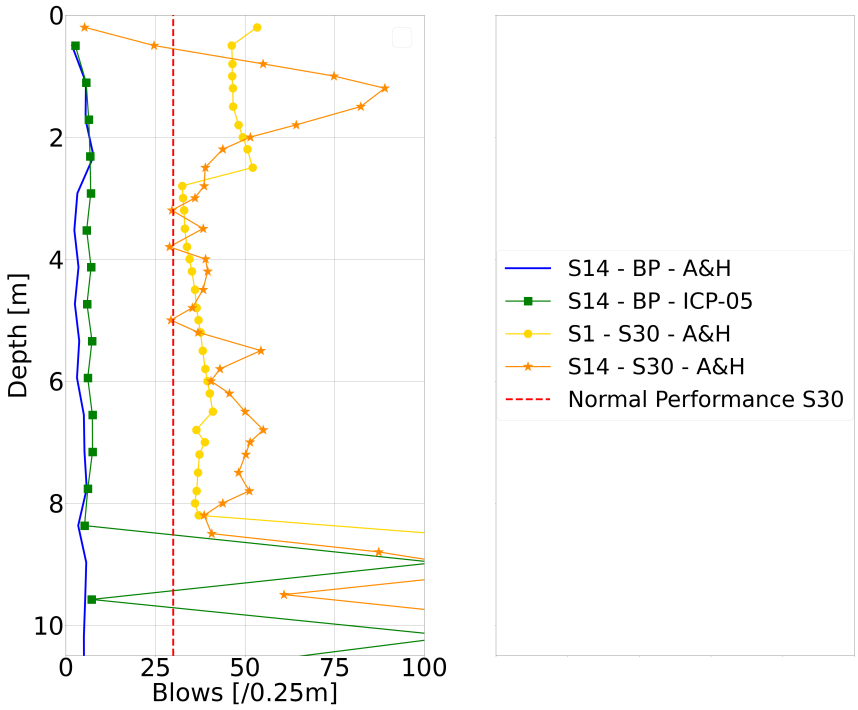

Figure 20: Blowcounts obtained for S-30 and BP Hammer

4.1.4 Revisiting GRLWeap after Maasvlakte tests

One of the results of the Experiments executed on the Maasvlakte is transferred energy. It is measured in the PDA apparatus aswell as the Hammer control unit. A cross-check between transferred energy to the pile as found by the hammer control unit and PDA data is performed. Any adjustments to the raw data are elaborated and visualized. Secondly, a comparison is made between the in-situ results, measured in the hammer control unit, and the initial GRLWeap blowcount prediction. By comparing the outcomes and performing a parametric study, the quality of prediction based on hammer and soil input can be judged.

Based on the average blow energy $[kJ]$ delivered per 0.25m of penetration as taken from the hammer control data, a 'Virtual Stroke' (VS - Avg. Blow Energy) can be formulated since energy scales linearly with fall height of the ram. This virtual stroke is implemented as hammer parameter in the initial prediction done using GRLWEAP to form comparative value to the in-situ data. A second 'Virtual Stroke' (VS - ENTHRU) of the average EMX over the total of blows every 0.25m available is formulated to compare the obtained energy transfer data, see Figure 58. For the first blow, the same value as the second value of virtual stroke is appointed. Any virtual stroke being equal to zero is adjusted to the same value as the previous stroke. In both graphs below, the efficiency has a value of 0.95 and the Coefficient of Restitution (C.O.R.) equals 0.85. Other parameters are considered as can be found in Appendix C.2.1.

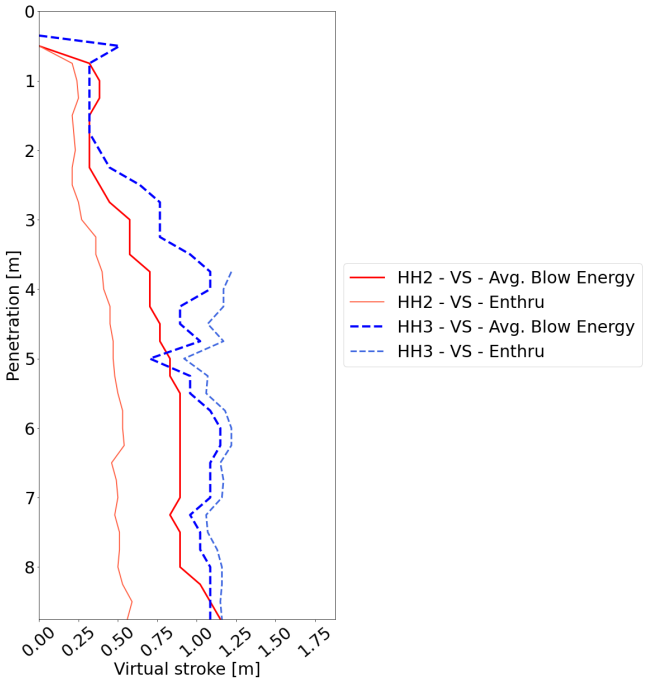

Figure 21: Virtual stroke comparison HH2 and HH3 during respective pile installation

GRLWeap Blowcount prediction
The geometry of the pile and the soil profile are not adjusted. A parametric study will be performed adjusting hammer parameters. Figure 59 and 60 in Appendix C.2.1 shows the adjustments of the Efficiency and Coefficient of Restitution (C.O.R.).

For the in-situ results of HH2 and HH3, it can be seen that the peak in resistance between 0.5 and 2.5 meter depth is overestimated by GRLWeap. This can be appointed to high values of cone resistance (q_c) found during CPT investigation, see Chapter 3. These high values are directly translated into static resistance as found using Alm and Hamre, (2001) which is direct input into GRLWeap. The top soil consists of gravelly sand to sand and is classified as loose sand based on its relative density from Site Investigation. A CPT test is monotonic whereas pile installation causes a cyclic loading. As a result of the cyclic loading of pile and lack of confinement due to shallow depth, the (gravelly) sand may have loosened, causing a much lower encountered resistance in-situ during monopile installation than initally predicted.

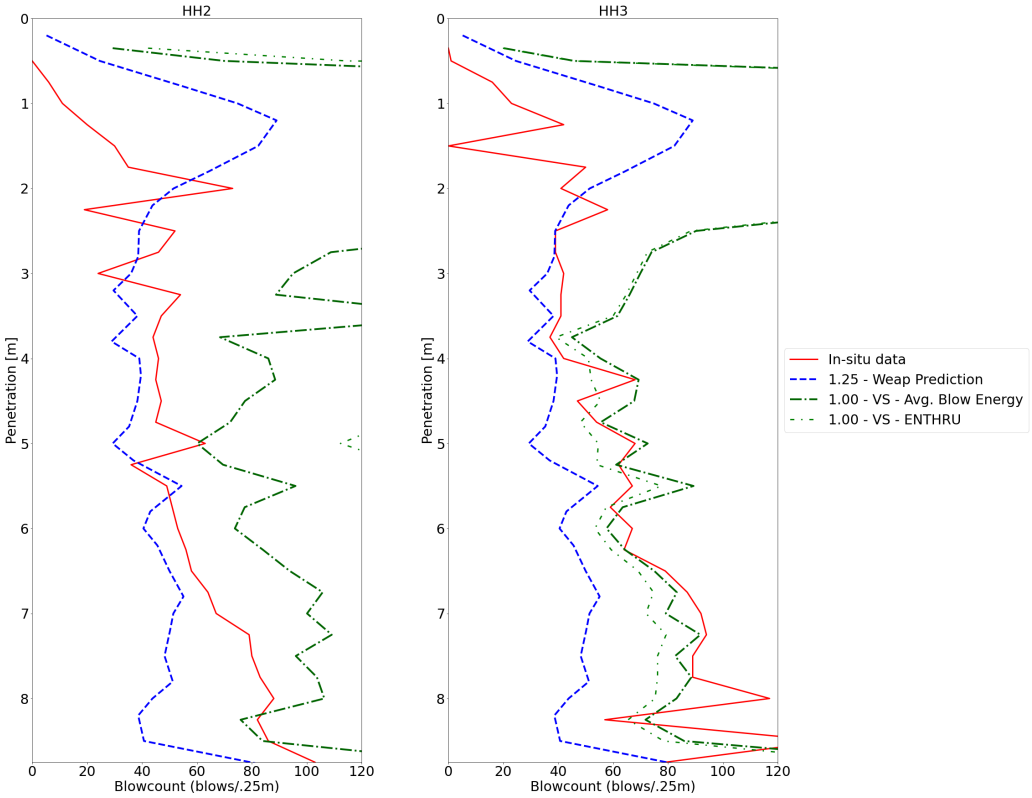

Figure 22: Blowcount measurements vs. Blowcount (GRLWeap) prediction

- **HH2:** The in-situ data does not match well the prediction based on the virtual stroke based on average blow energy. Since Enthru energies registered are a factor 2 lower than the ones obtained from average blow energy they fall outside the scale of comparison. No parametric study in Weap is performed on the hammer parameters. Adjustment of the soil parameters may yield a better result.
- **HH3:** The prediction done with adjusted stroke and safety factor 1.25 applied to the soil parameters overpredicts the blowcount significantly. Going back to the values of soil parameters obtained in CPT (safety factor = 1) and their adjusted strokes, a good match can be found from a depth of 3.5 meters onwards. This is true both for virtual stroke based on average blow energy and Ethru. Input parameters can be found in Appendix C.2.1.

Parametric study is only performed on the data adjusted based on the average blow energy virtual stroke since it yields the best match. The adjustment of the Efficiency and C.O.R. was performed for values between 0.9 and 1 and 0.8 and 0.9 respectively. The initial prediction performed without safety factor already matches the in-situ obtained data well, but the effect of the adjustments of parameters can be seen in Figure 60. From this, it can be seen that for depths between 3.5 - 5.5 meters, where the blowcount was overpredicted slightly, a higher efficiency or higher coefficient of restitution gives a better match. For depths below 6.5 meters, where the blowcount was underpredicted slightly, a lower efficiency gives a better match, or lower coefficient of restitution. This can be explained by the optimal blowcounts for a hydro hammer lying around values of 40. For higher blowcounts as can be found for higher resistances and deeper installation depths, the efficiency and blow energy that can be restituted drops.

Concluding statement
From the performed comparison of available transferred energy it is found that the data for HH3 gives a better match than HH2 between initial prediction and encountered soil resistance from a penetration depth of 3.75 meters onwards.

4.2 Measurement devices

Measurement devices are installed on the pile to assess the installation effects of every different installation method. Accelerometers and strain gauges are placed on the pile to be able to obtain information about the stress wave and mobilized resistance between pile and soil. Radial total pressure and pore pressure sensors are placed on the pile to be able to quantify friction fatigue and set-up. Displacement of the pile is measured as reference for all measurements. A measuring tape is used to quantify the pile plug after (or during) driving. Recording the blowcounts and exerted energy levels is a standard procedure in the hammer control unit. The values obtained in the field are compared with the initially determined Static and Dynamic Resistance to Driving predictions.

The following instrumentation devices are installed along the penetration depth of the pile. Figure 24 shows the placement of the measurement devices on the five levels that were prepared for placement. The sections elaborate on the purpose of measurement device application in the performed experiment. In this thesis, the data is only visualised, no further processing is performed.

Sensor	Total	Product Name	Provider	Measured Unit	Measurement Frequency [kHz]
(QB) Strain Gauge	14	3/350 CLY41-3L-10M	HBM	$[\mu\epsilon]$	10
(FB) Strain Gauge	6	TLM FLA-2-350-23	Allnamics	$[\mu\epsilon]$	20
Accelerometer	6	EGCS-S055B-5000	Allnamics	$[g]$	20
Total Pressure	3	PDB-PB Miniature Pressure Transducer	Athen Sensors	$[MPa]$	10
Pore Pressure	3	KPE-PB Small Pore Pressure Gauge	Athen Sensors	$[MPa]$	10

From here onwards the Total Pressure transducer is referenced to as Soil Pressure transducer, referring to the total stress component in Terzaghi's Principle, Equation 15 (Terzaghi, 1943). **PDA - Stress wave monitoring**

During the hammer blow, a compression wave is sent down the pile and reflections occur where the soil generates resistance. Stress wave monitoring is performed by measuring the strain and acceleration at one or more points above the mudline during the hammer blows. The distribution of the mobilised resistance can be back-analysed using numerical programs (M. F. Randolph & Gourvenec, 2011). This will be executed using a Pile Driving Analysis (PDA), which requires a pair of strain gauges combined with a pair of accelerometers. The top strain gauges should be around least 1-2 times the diameter away from the pile top (Jan van Rooij, Jasper Winkes, personal communication on the 17th of August 2022), (Santos, Instituto Superior Técnico (Lisbon, of Soil Mechanics and Foundation Engineering, & de Geotecnia, 2008). This is because due to local stress, towards the top the stresses are more distributed towards zero. Thus a sufficient distance should be accounted for to obtain representative values during testing. At the same time, a distance with regard to the installation sleeve should be accounted for which is feasible with the availabe material and chosen pile geometry.

Figure 23: PDA (a) Receiver connected to module on 0° and 180° (b) Full bridge strain module with accelerometer

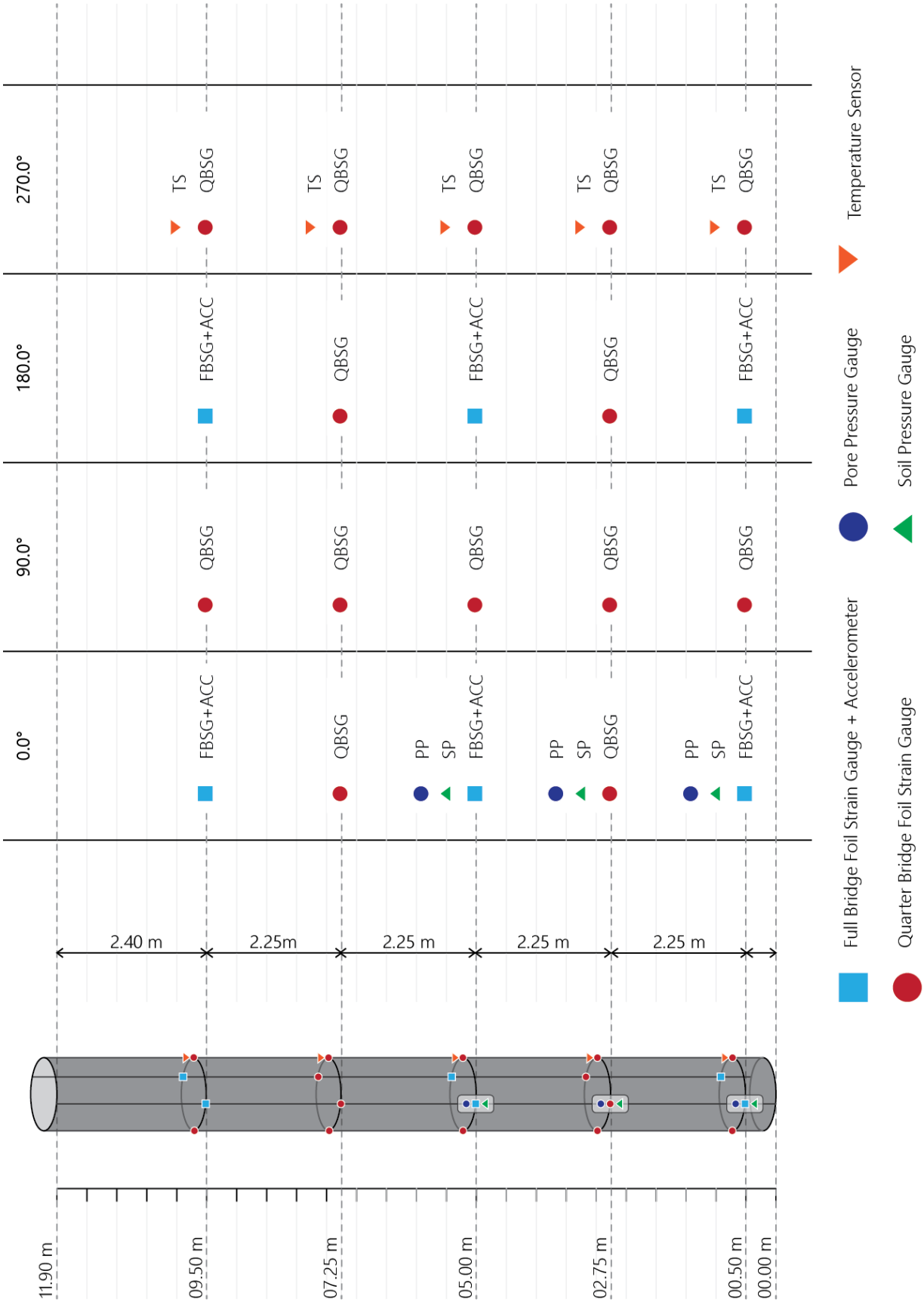

Figure 24: Schematic of pile and measurement devices

Strain gauges

Strain gauges provide point measurements which may be used to study axial as well as flexural behaviour (Klar et al., 2006). Transforming the measured strain to axial force can be performed under the assumption of plane-strain condition. An uneven distribution of strain in the cross-section may be appointed to eccentric loading or irregular soil resistance since the total strain is the sum of axial and bending strain. The forces at various depth can be differentiated to estimate force dissipation into the soil (Sinnreich, 2021) Strain measurements will serve as extra boundary conditions for the signal matching procedure as discussed in Section 4.2.

Per horizon, two pairs of strain gauges (four in total) are installed along the pile length. For this, a configuration of 0°, 90° 180° and 270° is chosen at 5 levels along the pile. The arrangement of the strain gauges should be symmetrical since then the average of the strain gauges gives strain at the centroid. Possible strain malfunction is accounted for since when one strain gauges fails, the average of the remaining pair of strain gauges yields an accurate measure of strain at the pile centroid. The third single strain gauge should then not be considered since the average is away from the centroid, which is not representative when strain is distributed unevenly in the cross-section (Sinnreich, 2021). Theoretically, it is beneficial to place strain gauges closer together in spacing towards the pile tip since load transfer rate tends to be higher (?, ?). However, practically the strain gauges installed close to the tip are at higher risk of loss during pile installation (Personal communication Jan van Rooij, on the 17th of August 2022). The compromise is equal spacing of the strain gauges as indicated in Figure 24.

The principle of a strain measurement by a foil strain gauge is a change in resistance that is strain-initiated. Foil strain gauges have metal foil photo-etched in a grid pattern on an electric insulator of thin resin. The pattern of the grid serves to maximize the amount of metallic foil that an be subjected to strain in the parallel direction. Gauge leads are attached to transfer the received signals, see Figure 25.

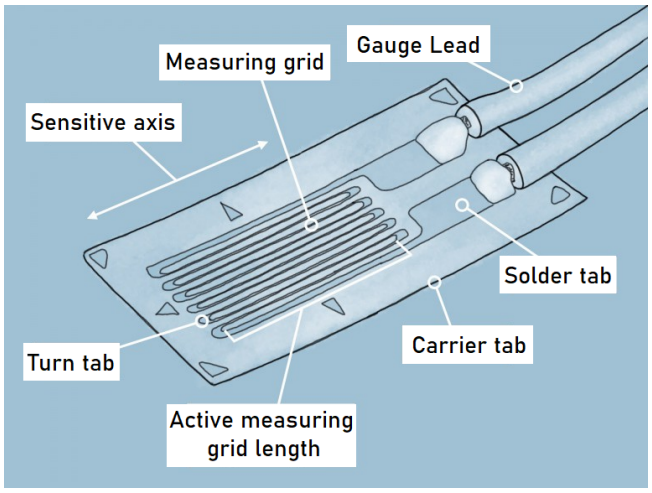

Figure 25: Foil Strain Gauge, (Meijer, 2010)

The following Figures show the configurations of strain gauges installed on the pile. More elaboration can be found in Appendix C.3.1. The foil strain gauges are indicated by the white squares.

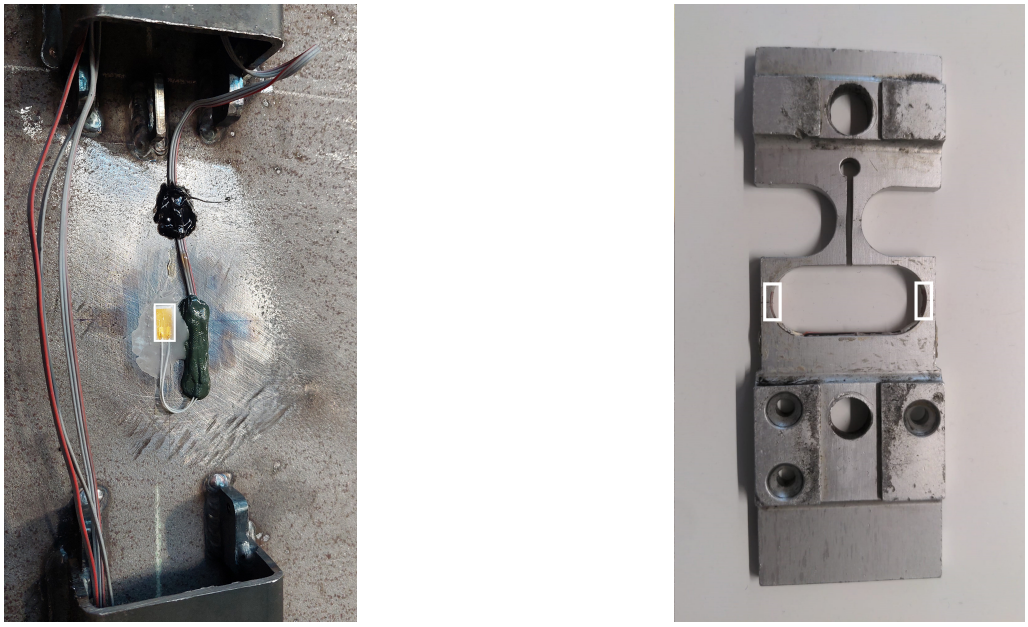

Figure 26: Strain gauges installed under U profile (a) Quarter bridge set-up (Roest, A.) (b) Full bridge module

Accelerometers

The accelerometers measure the acceleration of the piles at different levels which can be integrated to velocities and displacements. The measured displacements can be verified by differentiating the values found but noise should be filtered out beforehand since the differentiation process generally amplifies signal noise. Measuring accelerations independently increases accuracy of analysis since the numerical integration process is more stable than differentiation (Brown & Hyde, 2006). In the same way as the displacement data, the signals can be used as additional matching conditions in the PDA signal matching analysis to contribute to more accurate predictions (Hölscher et al., 2012).

From the velocities, also the energy transferred into the pile can be calculated as it is the workflow FxV through the steel sections. In addition to this, recording acceleration can be used to judge the behaviour of the pile as a rigid body during installation (expected for Blue Piling) or not (as expected for Conventional driving).

Accelerometers are installed along the pile at a total of 3 levels. The measurement devices will be installed at a distance from the pile tip around 0.5, 5 and 9.5 meters on 0 and 180 °. The following figure displays the accelerometer as implemented on the pile inside the U-profile.

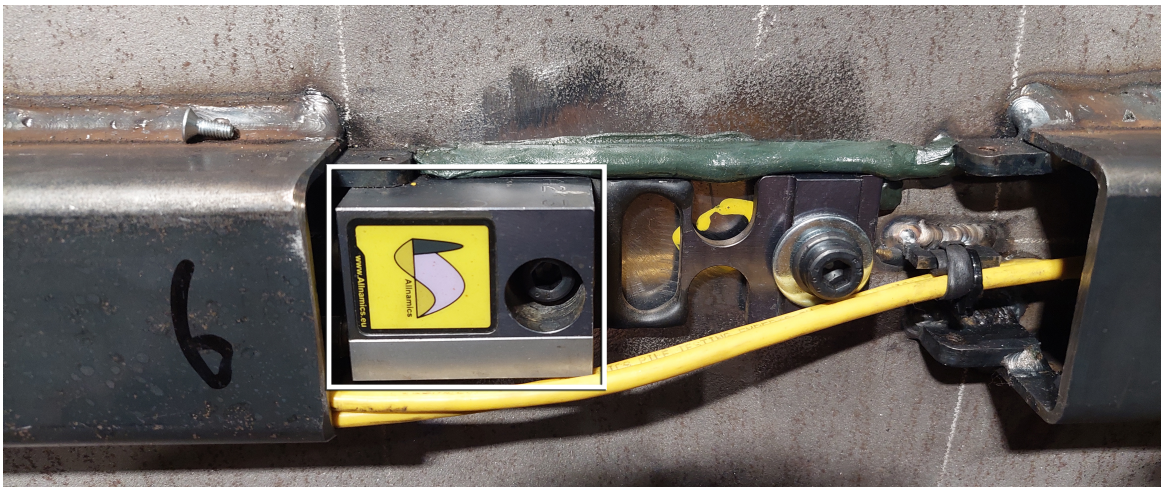

Figure 27: Accelerometer on Full bridge module

Laser Displacement measurements
Pile displacement is registered to reference the performed measurements of total pressure, pore pressure, accelerations and strains to the achieved pile penetration.

A photovoltaic sensor is installed to measure pile penetration, using a static reference to determine displacements. The laser is bound to the Hydrohammer and Blue Piling Hammer respectively. Due to the vibrations of the Vibrohammer, the displacements cannot be measured using the photovoltaic sensor.

Figure 28: Laser displacement measurement installed on (a) the Blue Piling hammer (b) the S-30 Hydrohammer

Pore pressure transducers
The measurement of pore pressure transducers in combination with Lateral stress sensors will allow for the analysis of effective stresses in-situ. Also a check for the hydrostatic water pressure can be performed during driving stops.

The pore pressure gauge is calibrated with a constant voltage excitation type and gives a rated output based on factors established by the producer, see Appendix C.3, Table 13. The model of pore pressure transducer used in set-up is the KPE-PB Small Pore Pressure Gauge, provided by Athen Sensors, see Figure 29(a). The gauges selected can measure up to 1 and 2 MPa and is marketed for model testing. The KPE-PB Small Pore Pressure Gauge is built up out of the pressure gauge main body, a filter and a cap. The filter is installed on the main body. The latter houses the sensing part and is hermetically sealed. The dual construction ensures that measurements are not affected by lateral pressure. The mesh in the filter and the space between the pressure-sensing surface and filter are saturated to make for an accurate measurement, (Athen Sensors, 2022).

The pore pressure transducers are installed on the piles on only one place along the circumference on three different levels: LVL5 - L/D = 0.4, LVL4 - L/D = 2.3 and LVL3 - L/D = 4.1.

Lateral stress sensor
The presence of friction fatigue and set-up can be studied by introducing a method to measure the change in lateral earth pressure. The sensing area gives a rated output based on a measured excitation, further described in Appendix C.3, Table 13, (Tokyo Measuring Instruments Lab, 2022).

The model of soil pressure transducer that is installed is the PDB-PB transducer, as can be seen in Figure 29(b). The gauges selected can measure 1, 2 and 3 MPa, based on their location on the pile, see Appendix D. They are only installed on the piles one place along the circumference on three different levels, the same levels as the pore pressure transducers: LVL5 - L/D = 0.4, LVL4 - L/D = 2.3 and LVL3 - L/D = 4.1 as can be found in Figure 24. They are located a bit above halfway in the U-profiles as can be seen in Figure 29(c).

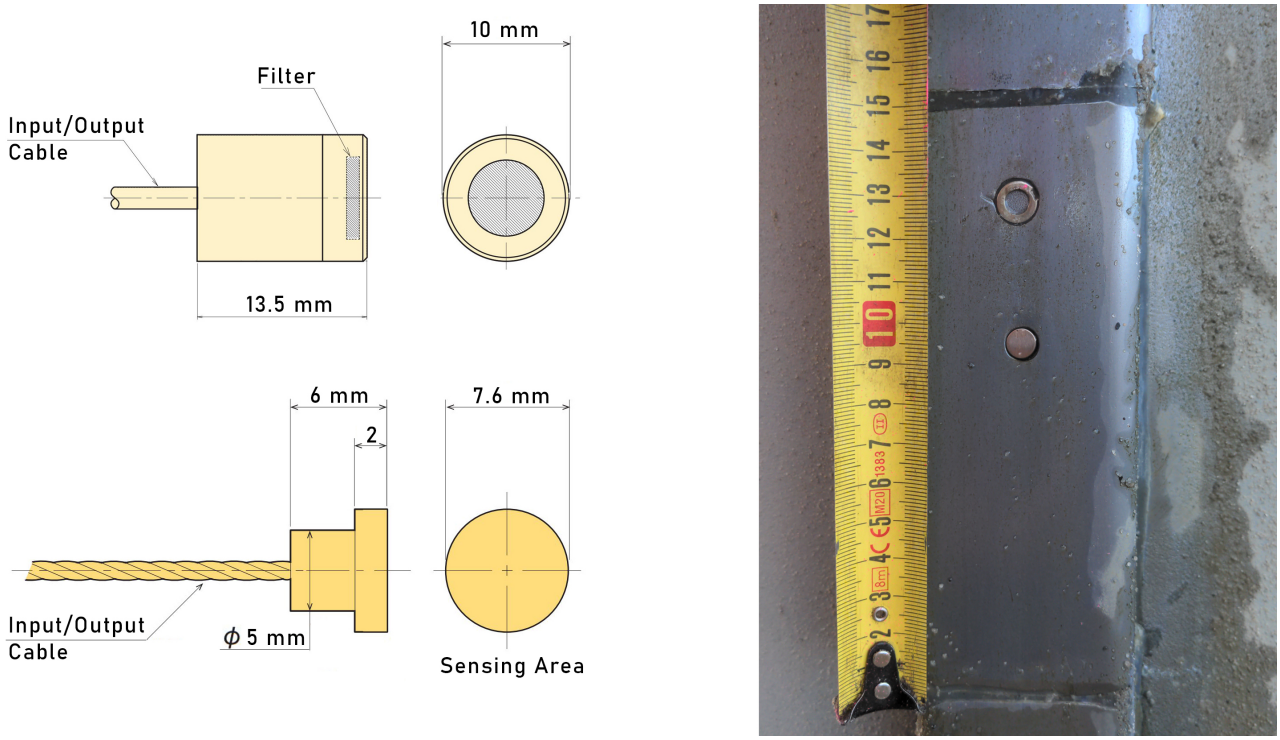

Figure 29: (a) KPE-PB Miniature Pore Pressure gauge, (Athen Sensors, 2022) (b) PDB-PB Miniature Pressure Transducer, (Tokyo Measuring Instruments Lab, 2022)(c) Lay-out in-situ

Plug height measurements

To acquire the plugging behaviour of a pile during installation, the height of the plug with respect to ground level can be measured during installation. In combination with the pile penetration, the Internal Filling Ratio can be established as described in Chapter 2. The plug heights are measured using a measuring tape, reaching through a hole in the pile.

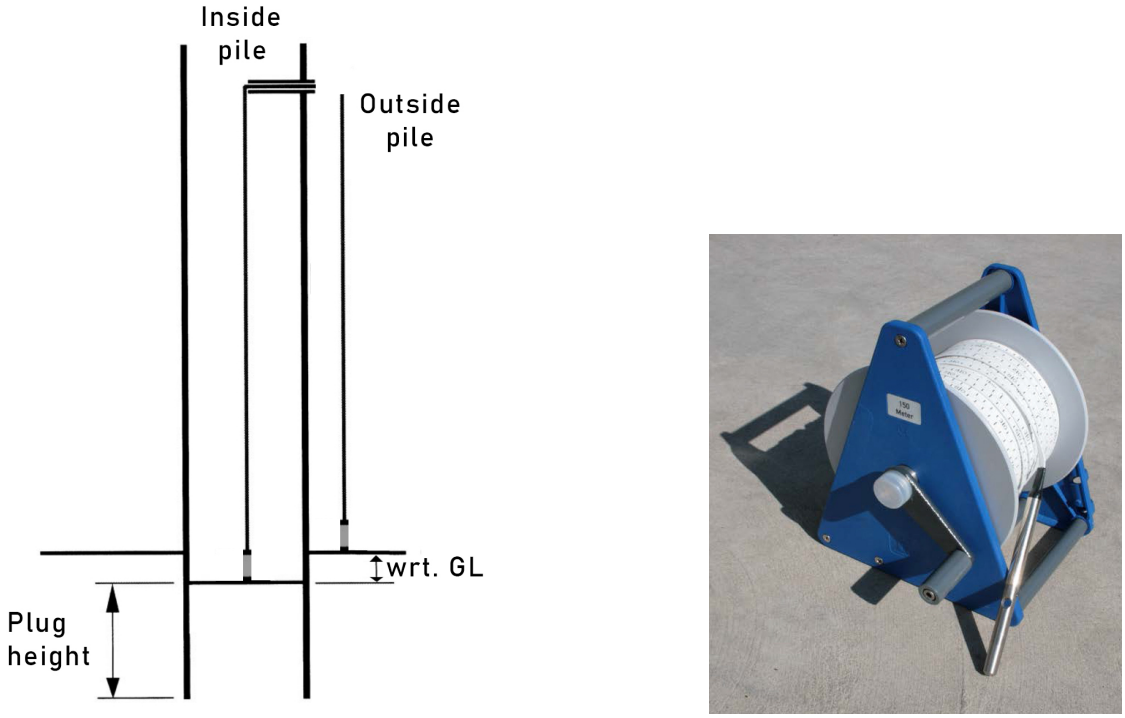

Figure 30: (a) Measuring the pile plug with respect to ground level (b) Used device (Tecso, n.d.)

Strain gauges were installed along five levels on the pile, four places around the perimeter. Accelerometers were installed at three levels on the pile, two places around the perimeter. Total radial stress and water pressure transducers were installed on one place along the perimeter on the bottom three levels of the pile. Plug measurements are performed by measuring the inside distance to plug and the outside distance to ground level.

5 Execution of the Maasvlakte field tests

In November 2022, in-situ field test are executed on Maasvlakte 2 near the Port of Rotterdam. Using a prototype Blue Piling hammer, a 1.22 diameter steel pipe pile is driven to a depth of 9 meter. As reference, two other installation techniques (conventional hammering and vibratory installation) are executed on piles of the same diameter in soil with little spatial homogeneity within two weeks time. Execution of the test was performed for 3 Hydrohammer installations (HH1, HH2 HH3), 4 Bluepiling installations (BP1, BP2, BP3, BP4), 3 Vibrohammer installations (V1, V2, V3) and one installation was done up to 6 meters with the Hydrohammer and finished with the Blue Piling hammer up to refusal (BP5). The reason for this was the formation of a plug. The following Chapter describes the experiment lay-out, the experiment procedure and lastly some procedural adjustments that were dealt with during execution of the tests.

5.1 Experiment lay-out

Installation location

The installation location on Maasvlakte is based on the location of the Stress Wave Conference as took place two weeks before the experiments. The Site Investigation performed and elaborated in Chapter 3 indicates piles installed for this event. A suitable distance is kept from these locations, indicated in Figure 65, Appendix C.3.1. An inter-pile distance of 15 meters is picked based on the following findings: (1) a prerequisite of at least the penetration depth, equal to 9 meters (2) a necessary minimum of six times the diameter equal to 7.3 meters (NEN 9997-1, 2016) and (3) a value of the 'magical radius' as a limit to the zone of deformation, as introduced by M. Randolph and Wroth, (1978) equal to 15.8 meters as found maximum. The final pile locations are as displayed in Figure 31, where the crane used for handling is located in the middle of the radial grid. Note that this map is the final result from Procedural adjustments as elaborated in Chapter 5.3.

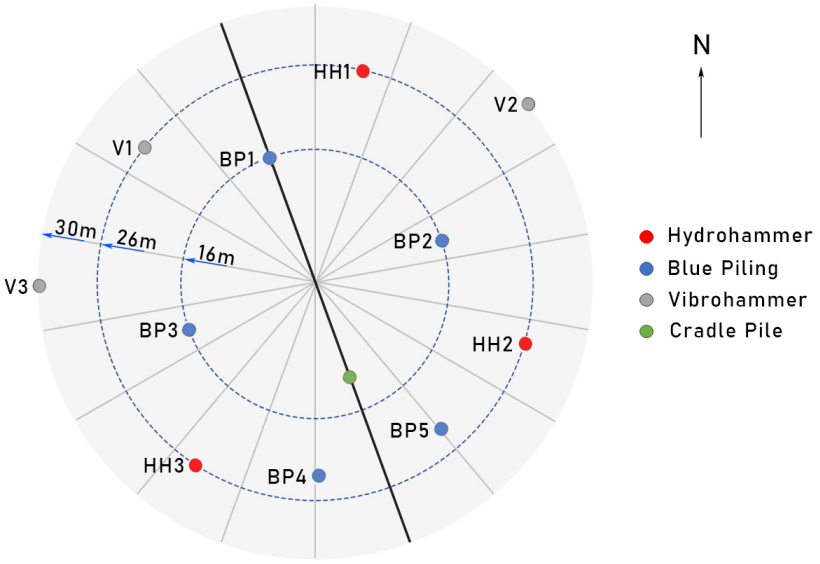

Figure 31: Installation locations

Since the Blue Piling hammer is the heaviest, installations are performed in the closest radial distance to the center of the crane set-up. The S-30 hammer including anvil can be placed in the second ring, an the vibratory hammer can be placed the furthest away due to the fast frame not having to be placed. Instead the vibratory hammer will be clamped to the pile and carried by the crane during installation.

Pile configuration

The pile used in the experiment is a total length of 11.9 meters and is installed to a maximum of 9 meters depth or until refusal is reached. The diameter of the pile equals 1.22 meter (=48 inch). A U-profile is installed along the full length of the pile to house the measurement devices, which was elaborated in Subsection 4.2. The profile is placed at 0°, 90°, 180° and 270° along the pile circumference. The same pile is installed with either of the three hammers and retrieved using the vibratory hammer. After the sixth installation of the steel pile, a hole was burned in the pile to be able to measure plug height during driving.

Pile instrumentation
The following instrumentation devices are installed along the penetration depth of the pile. For a full elaboration is referred to Chapter 4.2.

- Quarter bridge foil strain gauges: 3/350 CLY41-3L-10M, HBM
- Full-bridge foil strain gauges: TLM FLA-2-350-23, Allnamics
- Accelerometers: EGCS-S055B-5000, Allnamics)
- Pore pressure: KPE-PB Small Pore Pressure Gauge (1MPa and 2MPa), Athen Sensors
- Soil pressure: PDB-PB Miniature Pressure Transducer (50 kPa - 3MPa) , Athen Sensors
- Laser displacement measurement: D-series Dimetix Laser Distance, DPE-10-500

Driving (hammer) configuration
The following images display the pile hammer configuration as used during the Maasvlakte tests.

Figure 32: Test set-up of (a) Blue Piling Hammer (b) Hydro Hammer and (c) Vibratory driver

Prototype Blue Hammer 2022 - IQIP
The design of the hammer is an adjusted version from the large scale Blue Piling hammer. For the technical details of the hammer will be referred to '9000280100_E - GA - Hammer guide assembly', and '9000280100_J - Cons - Hammer guide construction' as found in the IQIP repository. Again, the fast-frame is deployed to ensure stability during driving. Due to the static characteristics of the Blue Piling hammer blow, the first installations to be performed were using this hammer. The main reason is to be able to use the measurement devices for more times after the first installation by avoiding damage as was also argued by (Yang, Tham, Lee, & Yu, 2006).

S-30 Hydrohammer - IQIP
For conventional pile driving, the IQIP S-30 Hydrohammer is deployed. The pile is driven by the blows delivered from a ram weight onto the anvil that is located on top of the pile. The anvil is supported by the anvil housing which, extended downwards also forms the pile guiding system. The need of a follower is avoided by the extra length of the pile above wished penetration. A fast-frame, usually applied under water, is employed during installation to ensure stability of the pile including the hammer during driving. Figure 32(a) shows the set-up of the S30 Hydrohammer aswell as the fast frame and the positioning on the pile during driving. For technical details will be referred to the IQIP repository.

PVE 2350 VM - Van 't Hek
The vibration block PVE2350VM is used for installation. No further elaboration is done for data of the Vibratory hammer. The vibro installations would be performed last because of the sensitivity of the devices to vibrations.

Installation procedure
The following table displays the driving time per installation. The hammer type used is indicated in the ID for the Hydrohammer (HH), Blue Piling Prototype hammer (BP) and Vibratory hammer (V). Also the starting (self-weight of pile and hammer) penetration, final penetration and the final plugheight with respect to ground level are recorded.

	ID	Date	Time	Start pen. [m]	End pen. [m]	Fin. plug height [m from GL]
1	BP1	15-Nov	11:30h - 13:45h	0.75	5.8	1.2
2	HH1	16-Nov	14:20h - 15:07h	0.4	5	
		17-Nov	09:06h - 09:51h	5	9	0.21
3	HH3	18-Nov	09:43h - 10:42h	0.4	9	0.14
4	BP3	21-Nov	10:15h - 11:00h	0.8	8.6	3.02
5	BP2	21-Nov	15:05h - 16:20h	0.8	8.8	2.75
6	BP4[1]	23-Nov	08:47h - 10:12h	0.75	7.9	2.2
7	HH2	23-Nov	15:57h - 16:50h	0.5	9	0.17
8	BP5[2]	24-Nov	13:38h - 14:04h	0.5	6	
			14:56h - 15:25h	6	7.85	1.6
9	V1	25-Nov	11:26h - 11:48h	0.4	9	0
10	V2	25-Nov	13:52h - 14:13h	0.5	9	0
11	V3	28-Nov	09:03h - 09:28h	0.5	9	0

Table 3: Performed installations during the Maasvlakte in-situ tests

5.2 Methodology

For the Maasvlakte procedure is adopted per installation performed.

1. **Pile markers**:
   Apply level markers on the pile.
2. **Integrity U-profile:**
   Check integrity of the U-profiles. These parts should not let in any water or soil.
3. **Fast-frame placement:**
   Move closed fast-frame to the place of installation
   > Check fast-frame is placed with the opening towards the PDA antenna. Adjust when needed.
4. **Pile placement:**
   Move the pile to the fast-frame in place of installation
   > Move the cables that reach from measurement devices on the pile to control unit accordingly.
5. **Selfweight penetration & levelling:**
   Check pile self-weight penetration and levelling after placement in fast frame.
   > Adjust when not within limits (max. +/-4° with respect to vertical).
6. **Hammer check:**
   Check measurement devices on the hammer.
7. **Start measurements:**
   Start measurement devices installed on pile/hammer
8. Check reception in control room
   > Adjust PDA antenna and/or check cable connections when unavailable.
9. **Hammer placement:**
   Place hammer on top of the pile. Move hydraulic hoses accordingly.

10. **Self-weight penetration & levelling:**
    Check self-weight penetration for hammer/pile set-up and check levelling.
    > Adjust when not within limits.
11. **Start pile installation**[3]
12. **Fast-frame opening:**
    Open fast frame between 4 - 4.5 meter penetration
13. **Driving stop:**
    Perform intended driving stop around 7.7 - 7.8 meter penetration for minimum of 10 minutes.
    > Check levelling during driving stop.
14. **Stop installation:**
    Stop pile installation at 9 maximum meter depth or when refusal conditions are reached.
15. **Stop measurements:**
    Stop measurement devices on pile/hammer 10 minutes after the last blow and save data
16. **Remove hammer**
17. **Remove pile:**
    Lie down pile for checks 1. and 2. for following pile installation.
18. **Close and remove fast-frame**

Other activities performed are registration of every driving stop by time stamp, penetration height, cause and blow-count when registered.

5.3 Procedural Adjustments in the field

The following procedural adjustments had to be made during the field tests on the Maasvlakte. The matters are noted in order of relevance. All matters were resolved in the noted matter.

- **Temporary problems Blue Piling hammer:**
  During BP1 installation, technical issues were encountered during Blue Piling installation. BP1 installation was resumed the day after but without success, causing BP1 to not be performed to target depth or refusal. The installation can however be used to study set-up since the measurement devices were turned on both days. Installations were resumed using the Hydrohammer which caused a shift in installation order.
- **Pile Plugging**
  Even though pile plugging was deemed unlikely for the diameter of the pile (=1.22 meter) and medium strength soil conditions, significant plugging took place for the installation using the Blue Piling hammer. To be able to quantify plugging during driving, a hole was burnt in the pile just above the 9 meter mark (from pile tip) around the 270° perimeter mark on the 22nd of November, see Figure 33. Every Blue Piling and Hydrohammer installation after and including BP4 was performed with extra introduced driving stop for every meter. In the two minute driving break, a plugging measurement was performed. For vibratory installation, no plugging took place so no extra driving stops were introduced.

[3]For pile installation BP4, HH2 and BP5 driving stops are introduced every meter of penetration to check pile plug height w.r.t. Ground level.

Figure 33: (a) Hole burnt in the pile around 9 meter (from pile tip) mark (b) Performing plugging measurement from aerial work platform

- **Two additional pile installations (BP4 & BP5):**

  Due to the unexpected plugging behaviour, two additional pile installations were performed, BP4 and BP5. BP4 was performed as normal with Blue Piling prototype hammer, introducing driving stops for plug measurements every 1 meter interval. Most relevant plugging takes place after 4 meters penetration depth as follows from Figure 42(d). BP5 installation was performed for the first 6 meters using Hydrohammer S-30 to see if with less plugging (less resistance), a larger final penetration can be reached. A larger final penetration was not achieved. Large IFR ratio's were found after 6 meters up to final penetration of 7.8 meters.

- **Placement of BP4 & BP5:**

  By the time of reconfiguration of pile placements, already pile BP1, HH1, HH3 and BP3 were driven. By shifting the Vibratory hammer installations further away from the center and compromising in inter-pile distance for the cradle pile, BP4 and BP5, still a reasonable distance of slightly more than minimally pile penetration depth (around 10 meters) was able to be kept.

- **Delayed driving on east side of perimeter**

  Due to neighbouring work activities on the Maasvlakte demo-site, no piles could be driven on the east side of the perimeter. As a result, installation of HH2, BP2 and V2 were delayed untill 21st of November. This caused a shift in installation order, Table 3.

The measurement devices as selected were succesfully installed on the pile for installation on the Maasvlakte. Execution of the test was performed for 3 Hydrohammer installations, 4 Bluepiling installations, 3 Vibrohammer installations and one installation was done up to 6 meters with the Hydrohammer and finished with the Blue Piling hammer up to refusal.

6 Data Obtained

The following Chapter elaborates on the data obtained from the data processing phase of the Maasvlakte test data. The data is visualized to illustrate the differences in results obtained for Hydrohammer installation (HH3) and Blue Piling installation (BP3 or BP4, depending on availability of data).

6.1 During installation - Blow investigation

The data from the total radial stress and the pore pressure transducers show a response to the blows of the hammers used for installation. The following section elaborates on a selection of the most characteristic blows for different soil horizons and different transducer levels. The differences between those measured for the Hydro- and the Blue Piling hammer are highlighted.

Blue Piling Hammer:

Total radial pressure:

- For Level 5 - L/D = 0.4 passing the horizons at 4, 5, 6.5 and 8 meter depth, the Blue Hammer blows are characterized by a strong dip, followed by a peak value and a decrease towards a plateau signified as the 'stationary' phase of the hammer blow. Where the decrease towards plateau is gradual for the first 1200 seconds of the installation as seen in Figure 34, it becomes sharp for the time it passes the 8 meter deep soil horizon, which is also towards refusal, as can be found in Appendix F.2. The blows around 4, 6.5 and 8 meter soil horizon show a minimal increase in pressure, forming a narrow plateau, before passage of a new blow. Its consistency indicates it relation to the consistent catching of the hammer weight after a blow and raising it to the required height before it is dropped to generate new blow, illustrated in Figure 34.
- For Level 4 - L/D = 2.3 passing the horizons 4 and 5 meter depth the blows immediately show sharp decrease after which the plateau value is reached, see Figure 36. The narrow plateau can be seen at the end of a blow, transferring into the next for both measurements taken.
- The total soil pressure measurements reach to and beyond zero regardless of peak value for all blows researched, except for the 6.5m depth horizon of LVL5, seen in Figures below.
- No strong drop in soil pressure measurements is observed for the blows recorded above water level, in the 1.5 meter depth soil horizon for transducer LVL3 and LVL4, as illustrated in Figure 37.

Pore pressure:

- A blow generally generates a decrease in pore pressure. During the 'stationary' phase of the blow, pore pressures increase. This behaviour is independent from hydrostatic pressure in place since it takes place when hydrostatic pressures are both higher and lower than measured in that moment, illustrated in Figure 34 and Figure 35. A strong build-up of pore pressures in sand in the stationairy phase of the blow even though hydrostatic pressure is lower may be appointed to rate effects.

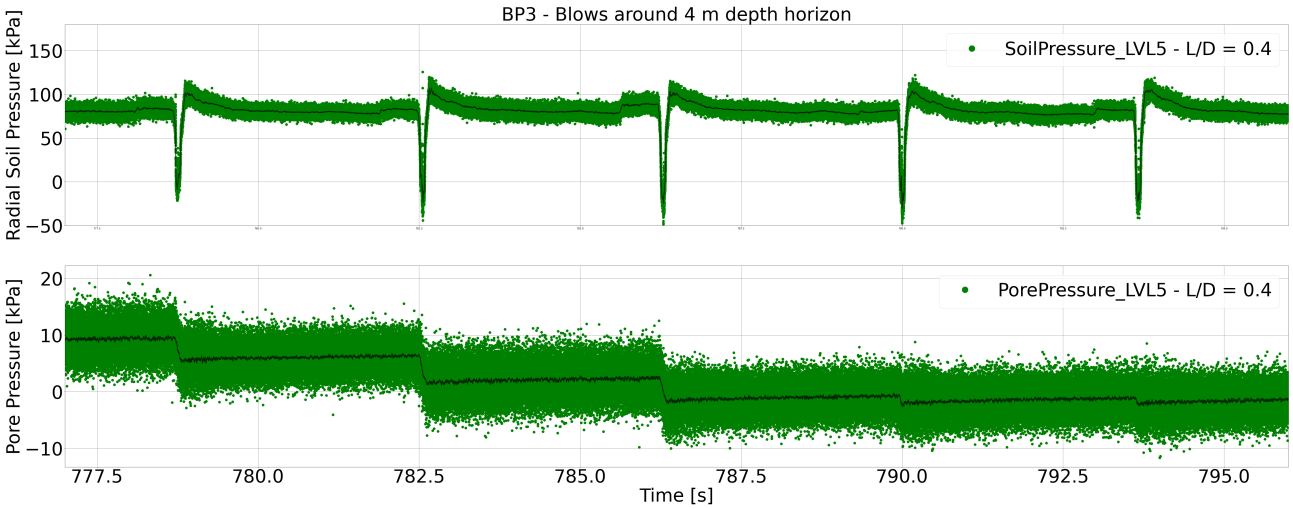

Figure 34: Illustration of (a) Characteristic BP blow with negative dip, peak value, gradual decrease towards plateau and second narrow plateau value (b) A build-up to negative pore pressures.

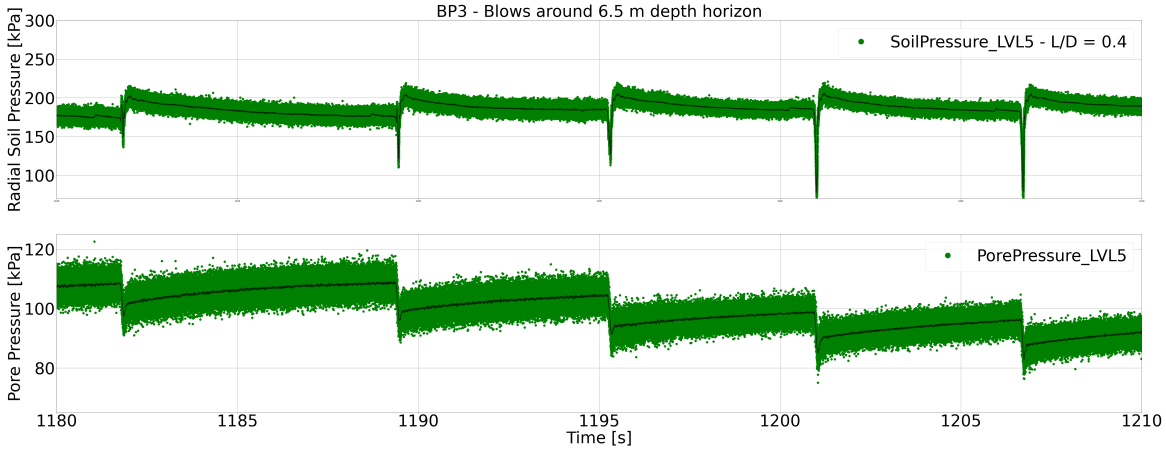

Figure 35: Illustration of (a) Characteristic BP blow without negative dip, but with peak value, gradual decrease towards plateau and second narrow plateau value (b) A strong build-up in pore pressures in 'stationairy phase' of blow in sand while hydrostratic pressure is around 45 kPa

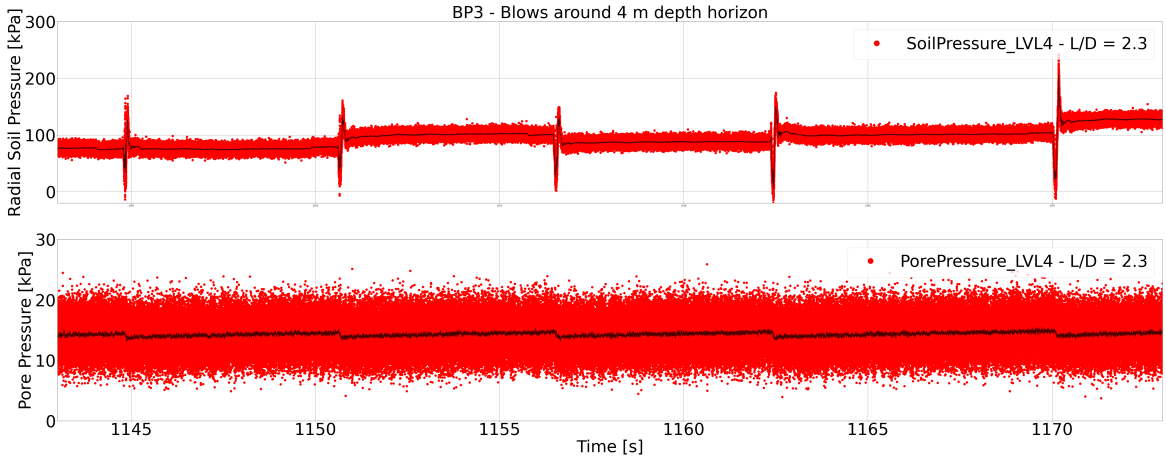

Figure 36: Illustration of (a) BP blow with sharp decrease and reach into plateau value (b) Weak response of the pore pressure with hydrostatic pressure being equal to around 20 kPa.

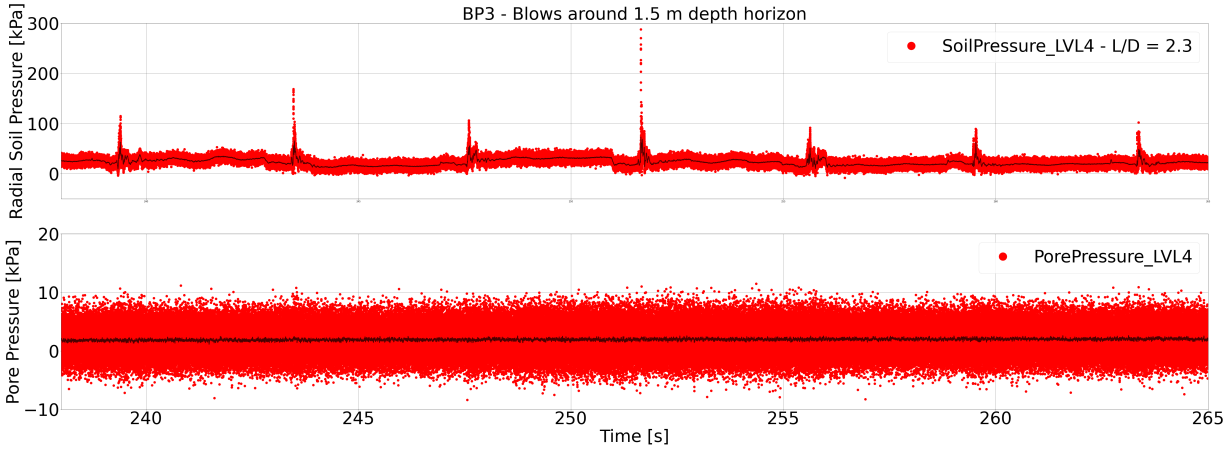

Figure 37: Illustration of (a) BP blow above groundwater table showing no strong dip (b) Pore pressure sensor showing no excitation

Hydrohammer S-30
Total radial pressure:

- The blow of the Hydrohammer is characterized by a strong peak, not completely captured in measurements (Personal communication Ken Gavin, 11th of May 2023) because the data registration frequency is not high enough to clearly catch the strong peak caused by installation. The peak is followed by a strong dip to negative values and after build-up an oscillation towards a plateau value. This oscillating plateau is held up for 0.2 seconds. The plateau ends with a drop in total radial pressure measured and leads to a second plateau which would in this case be the 'stationairy' part of the Hydrohammer blow. There may still be some oscillations dampening out in this part.
- For Level 5 - L/D = 0.4 passing the depth horizons 4, 5 meters, LVL4 depth horizon 4 meters and LVL3 depth horizon 1.5 meter, (all within installation time 1320 - 1750) the first plateau value is not very distinct, but is replaced by an oscillatory measurement of 0.2 seconds and blends in to the stationary phase value. The distance in time between the plateau values depends on the blowcount.

Pore pressure

- When pore pressures are around hydrostatic pressures at the soil horizon, no strong response in water pressures are measured as found in LVL4 for blows around 4 m depth. .
- When pore pressures are not near hydrostatic pressures at the soil horizon, the first total pressure dip is accompanied by the dip in pore pressures. They in turn quickly recover to a plateau value until the next blow is initiated.

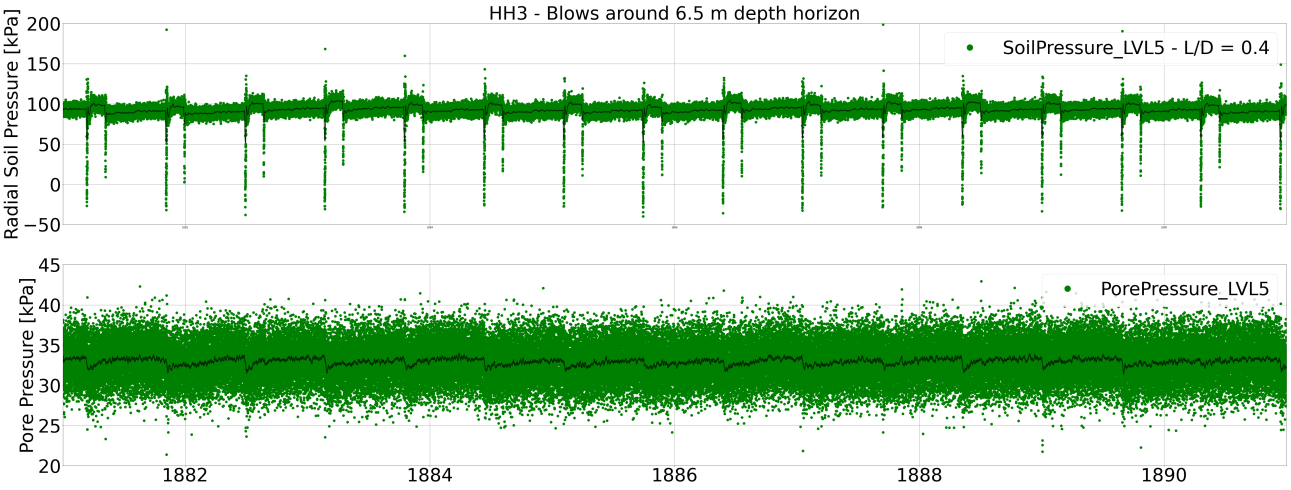

Figure 38: Illustration of (a) Characteristic HH blow with strong peak, strong dip into negative pressures, oscillating plateau of around 0.2 seconds and 'stationairy' phase plateau dependent on blow rate (b) Typical pore pressure response, dip for time of blow and quick recovery into plateau value

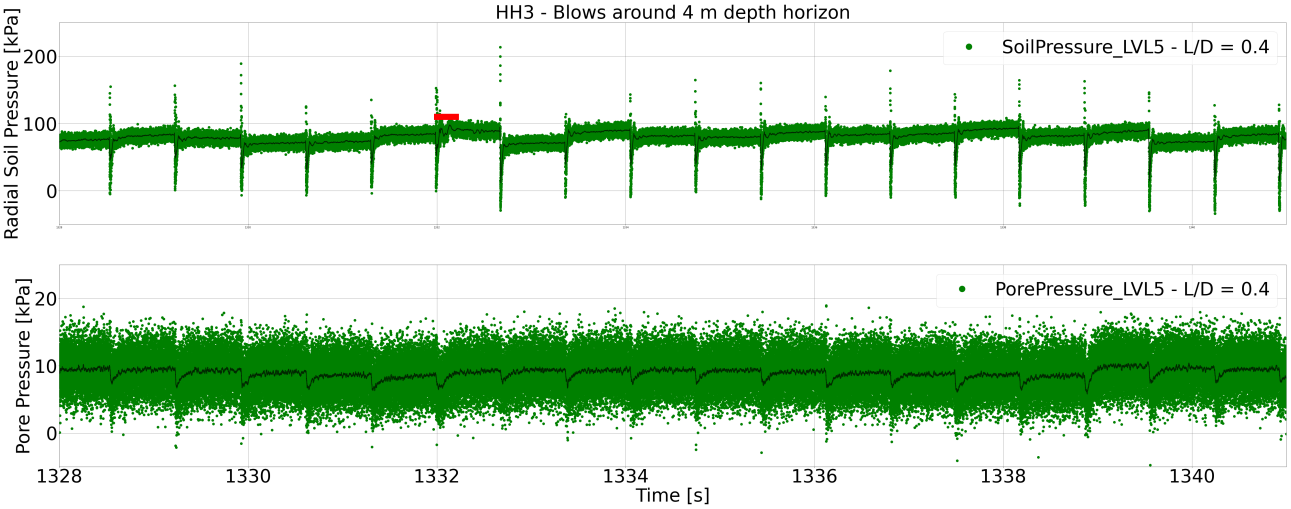

Figure 39: Illustration of (a) HH blow with strong peak, strong negative peak and non-distinct oscillatory plateau equal to 0.2 seconds (b) Typical pore pressure response, dip for time of blow and quick recovery into plateau value.

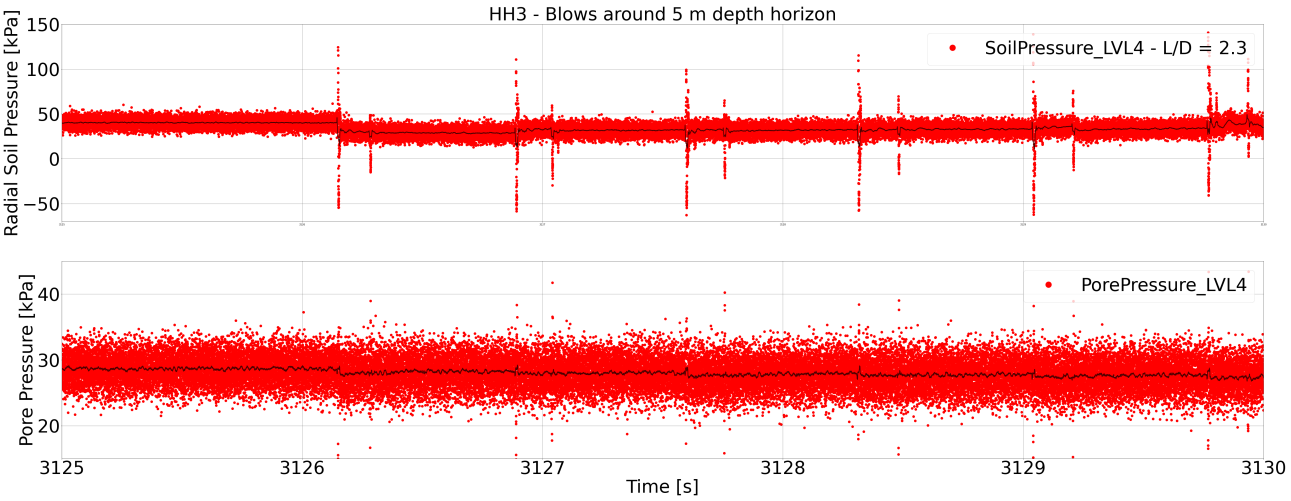

Figure 40: Illustration of (a) Characteristic HH blow (b) Feable response to to blows in pore water pressure measurements, hydrostatic pressure being around 30 kPa

6.2 During Installation - Radial Soil Pressure, Water Pressure and IFR

After removal of the pile from the place of installation, a change of the ground level with respect to the soil on the sides was perceived. Leading to the conclusion that plugging had taken place during execution of both the S-30 (although minimal) and Blue Piling hammer (significant). The figures below show the visualization of the IFR as found after consideration of the plug heights with respect to the ground level per interval of penetration. The radial total pressures and water pressures are obtained from the 'stationary' values of the blows considered in the previous subsection. Next to the radial soil pressure, the water pressures are indicated in shaded area. This shows the effective radial stresses on the left side of the shaded interval.[4]. The pore pressures are plotted next to the assumed hydrostatic water pressure and lastly measured IFR ratios for the same installation technique in a different driving location.

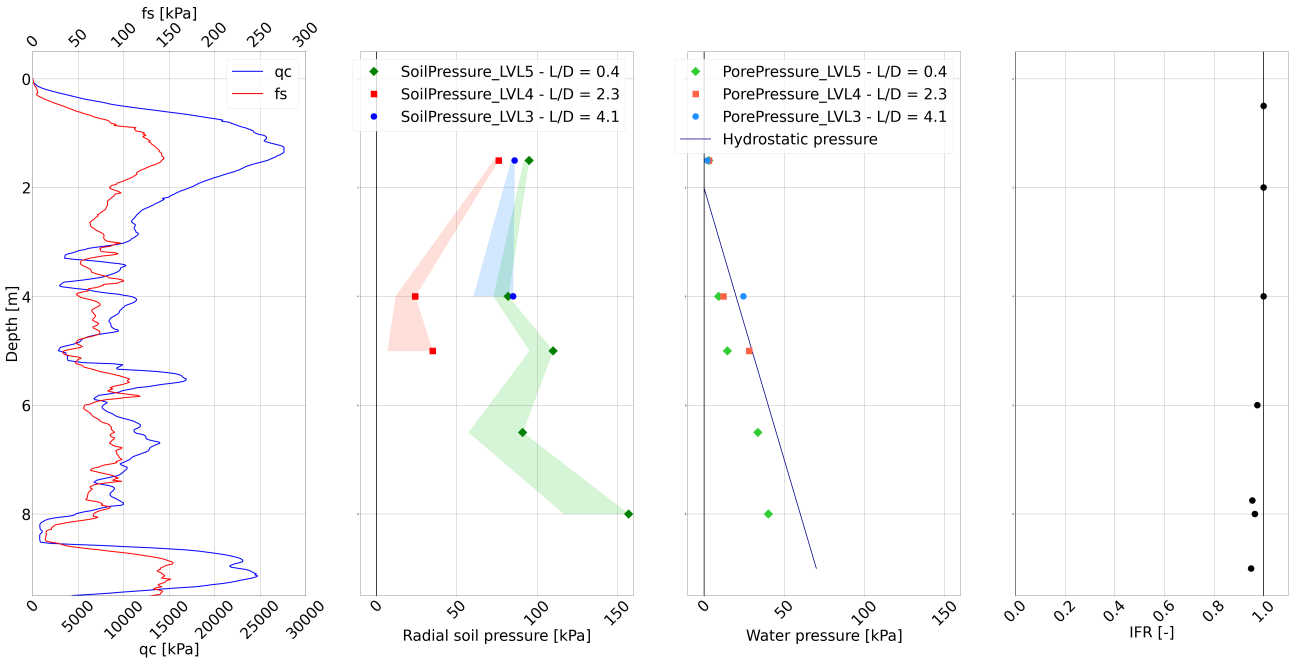

Figure 41: (a) CPT Profile S14 (b) HH3 - Radial Soil Pressures (c) HH3 - Pore Pressures (d) HH2 - IFR ratios obtained in driving stops

- The total radial pressures measured for the Hydrohammer installation show a maximum value of 150 kPa. The largest total (and effective) stresses are found for the Soil Pressure transducer at LVL5 located 0.5 meter from pile tip.
- The smallest total(and effective) pressures are measured for the transducer located at level 4.
- From the points selected for analysis, the effect of friction fatigue could be inferred between the data measured for transducer LVL5 and LVL4, seen as lower radial stresses are measured for distances h higher from the pile tip. The measurements from transducer LVL3 should according to an increased amount of loading cycles at the same soil horizon be lower than the other levels, but this is not the case.
- Pore pressures measured are always positive, and parallel in development to the hydrostatic pressure level.

[4]It is noted that the measurements are chosen manually for a specific soil horizon and thus caution is warrented in finding trends in the displayed data, see Chapter 8

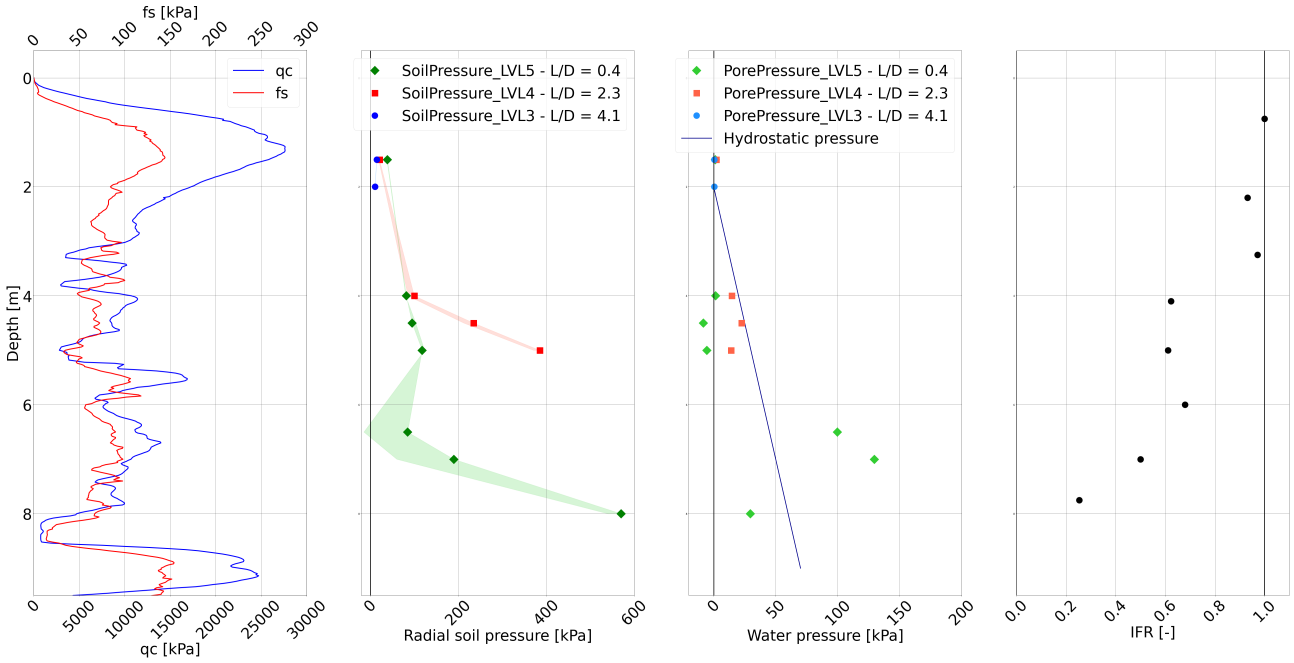

Figure 42: (a) CPT Profile S14 (b) BP3 - Radial Soil Pressures (c) BP3 - Pore Pressures (d) BP4 - IFR ratios obtained in driving stops

- The total radial pressures measured for the Blue Piling installation are a factor 2 to 3 higher than the radial soil pressures measured for LVL5 of the Hydrohammer installation after a depth of 7 meters. This is also when the most significant plugging takes place.
- The total stresses for transducer LVL4 are a factor of 2 to 4 higher for depths around 4 to 5 meters, showing the effects of reduced cycling of the Blue Piling hammer installation.
- The pore pressures generated during driving are slightly negative for soil horizon 4, 5 and 6.5, located in sand to silty sand and sandy silt. They generally do not follow the hydrostatic water pressure in place.

6.3 Plug Heights

For BP5, the first 6 meters of installation were performed using the S30, as to avoid plug formation. The goal of BP5 was to check if the pile was able to be driven to target depth if plugging was less than for a full installation using the Blue Piling hammer.

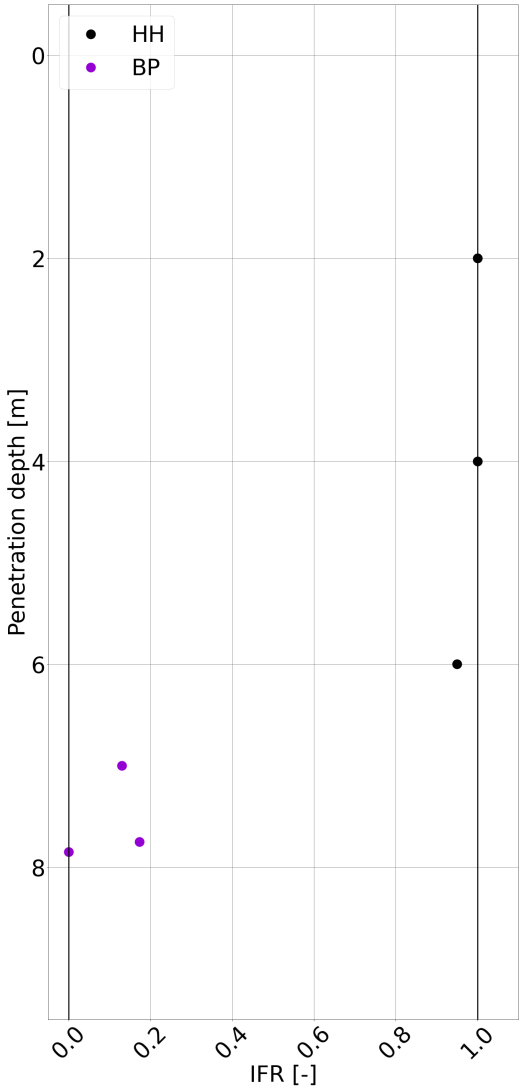

Figure 43: BP5 - IFR

Based on the plugging information of the HH2 and BP4 installation, plugging starts to take place passing from the depth of 3 to 4 meters from ground level for the Blue piling hammer. By driving to 6 meters depth using the Hydrohammer, no significant plug is formed. The pile protrudes through the soil in a coring mode, causing less pressure-build up than a plugging pile would. However from the moment the Blue Piling is used to penetrate further, immediate coring follows. Target depth is not reached for BP5.

6.4 During driving stop - Total and pore stress equalization

For HH3 and BP3, three driving stops are explored. Driving stop 1 takes place during opening of the fast-frame around 4 - 4.25 meter depth. Driving stop 2 is the intentional driving stop around penetration of 7.75m and lastly the End of Driving. The water level is assumed 2 meters below ground level, see Appendix 6.6.

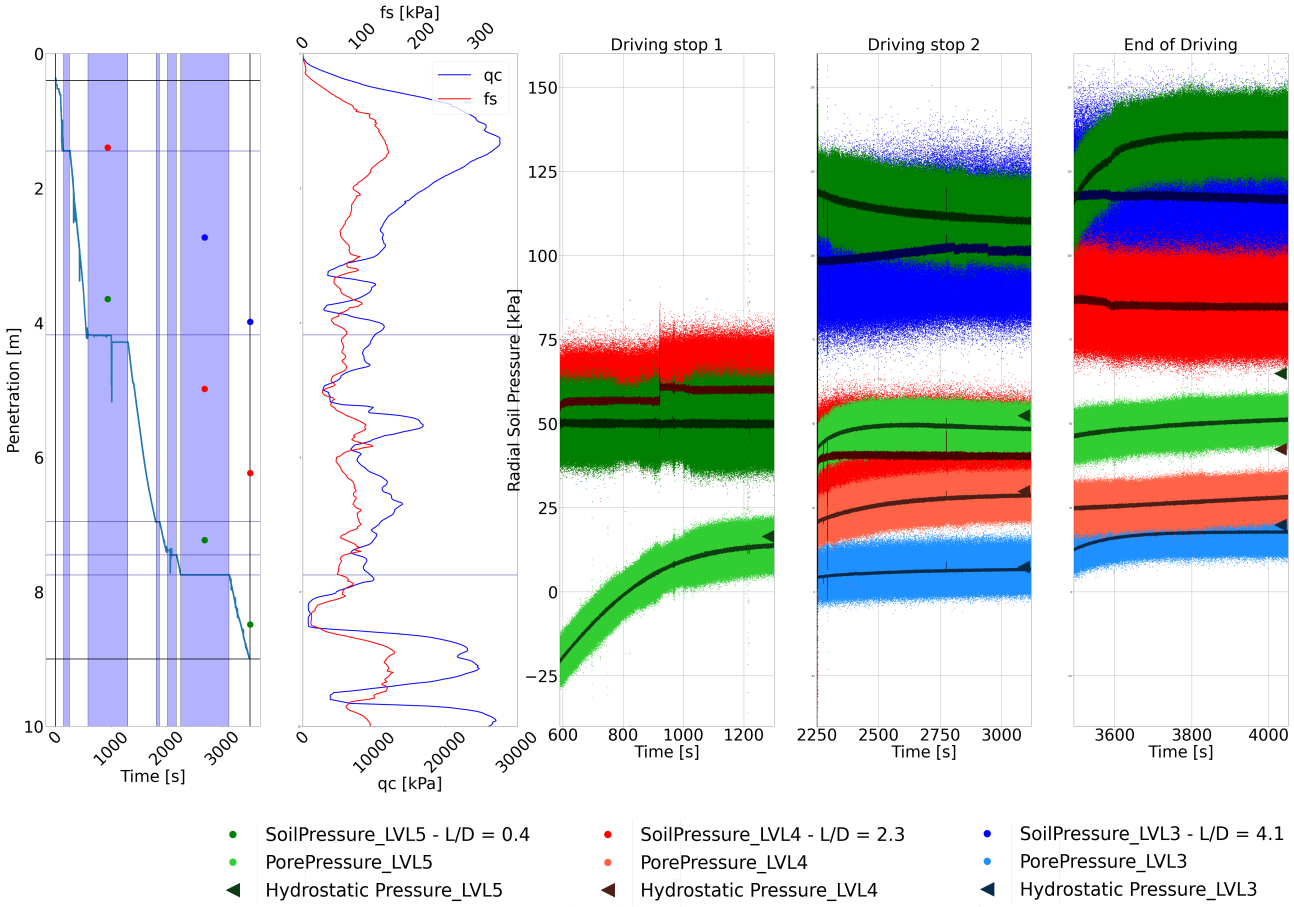

Figure 44: HH3 - Driving stops indicated over depth of pile tip and sensor levels next to CPT S14

Stop 1:

- The water pressure for LVL 5 - L/D = 0.4 was developed toward -25 kPa, but recovers to a value close to the hydrostatic pressure over the driving stop of about 700 seconds.
- The total soil pressure for LVL3 - L/D = 4.1 remains constant although water pressures recover from negative to positive pressures, indicating a decrease in effective stress.

Stop 2:

- Total stress drops for LVL5. The pore pressure transducer on level 5 - L/D = 0.5 reaches slightly below the plateau value reached, indicating an effective stress decrease over time.
- Total stress reaches a plateau quickly for level 4, pore pressures slowly converge to assumed hydrostatic pressure thus indicating an effective stress decrease.
- Total stress for level 3 sightly fluctuates around 100 kPa. Pore pressures don't increase significantly, leading to almost no effective stress change.
- For all three levels the values for total stress approach the values of sleeve friction measured at their respective heights prior to installation.

Stop 3:

- Hydrostatic conditions are not yet reached for level 4 and level 5 around 500 seconds after End of Driving, the deviation is around 15 kPa. At level 3 - L/D = 4.1 the water pressures recover more quickly to their plateau level and does end at hydrostatic pressure.
- The high value of total pressure indicates the LVL5 sensor is already reaching into the denser sand layer below.

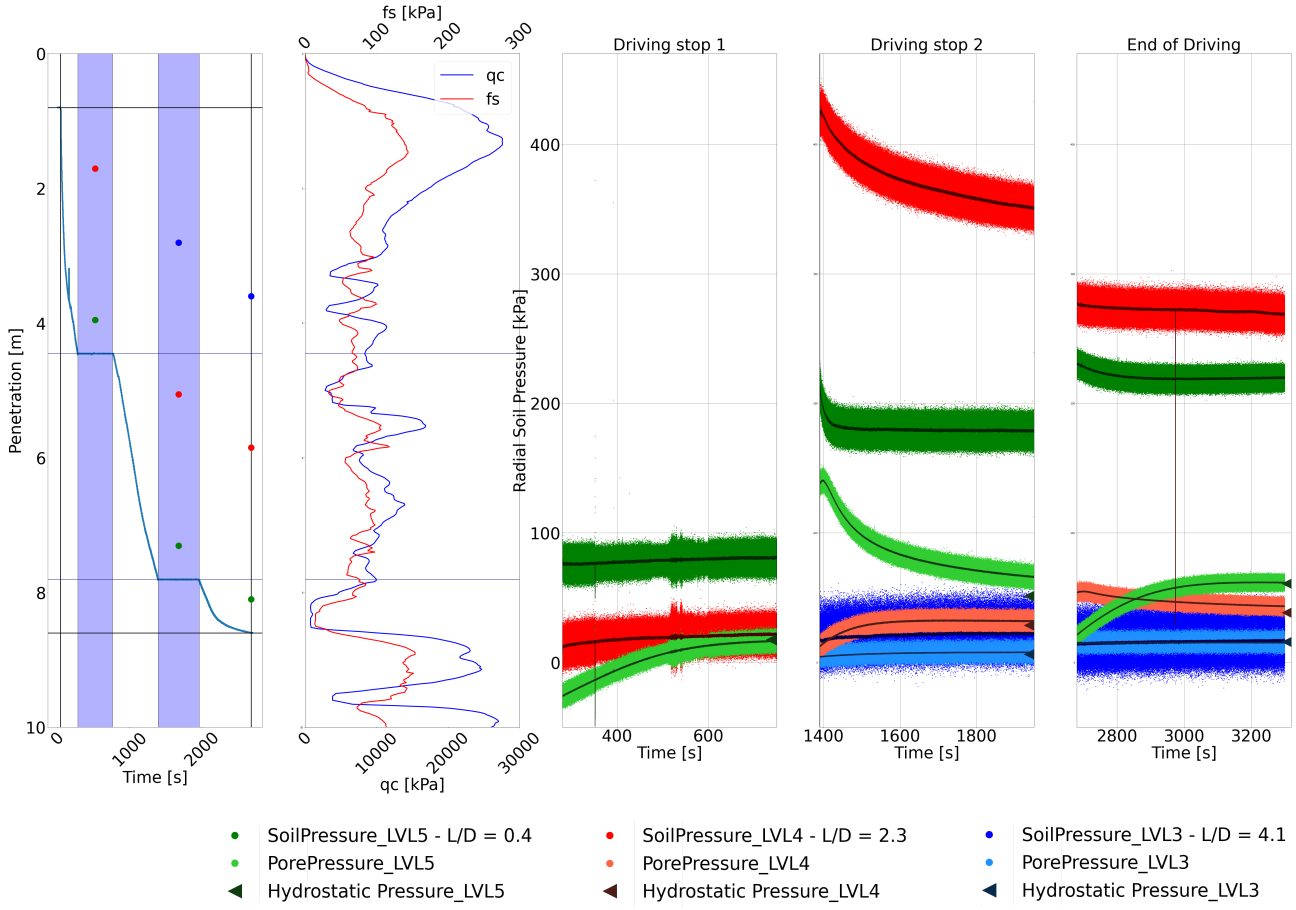

Figure 45: BP3 - Driving stops indicated over depth of pile tip and sensor levels next to CPT S14

Stop 1:

- The magnitude of total stress obtained for BP3 LVL4 with respect to the stress obtained with HH3 is much smaller, whereas the total stress reached for LVL5 is much higher than for HH3.
- Pore pressure values are around the same magnitude and also balance out at hydrostatic pressure. They are less negative at the start of the driving stop for LVL5 for BP3 than HH3.

Stop 2:

- The magnitude of the total pressures is significantly higher for LVL4 - L/D = 2.3. The value for LVL5 is slightly higher, whereas the value for LVL3 is much lower.
- A strong build-up in pore pressure up to driving break of 150 kPa can be seen for LVL 5. The water pressures then strongly come down and balance a bit above the hydrostatic level at this depth. The rest of the waterpressure levels build up to hydrostatic water level at respective depth.
- Only the effective stress for LVL5 is increasing over time with Driving stop 2.

Stop 3:

- The total stress is highest for LVL4 and lowest for LVL3.
- The pore pressures all converge to hydrostatic water level at the end of measurement registration. What can be seen is that
- Even though pore pressures of lVL3 decrease, effective stress barely changes because total stress decreases in a similar matter.

6.5 Acceleration

The acceleration data is displayed in the following Figures. To obtain the acceleration at the centroid, an average can be taken between the transducer located at 000 and 180 degrees. The only elaboration performed in this thesis is the visualization. The acceleration data is briefly assessed for LVL3 and LVL5. The figures for LVL3 can be found in Appendix F.3.

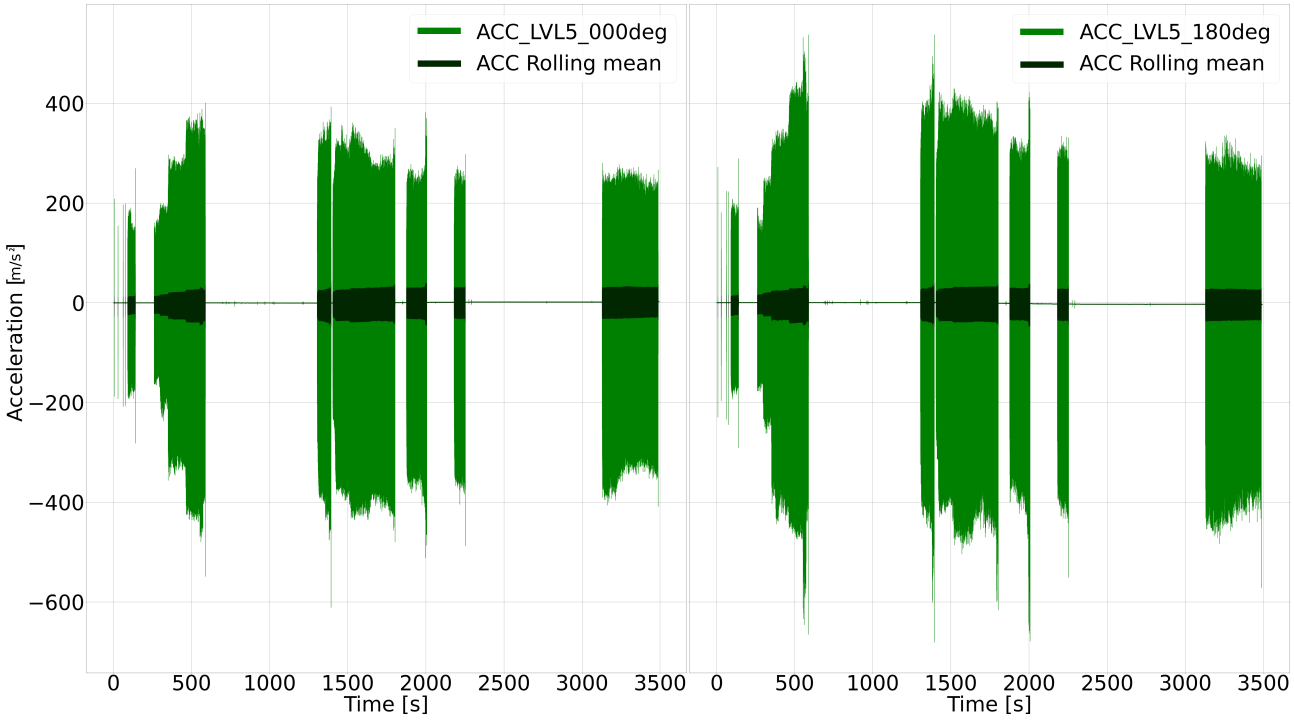

Figure 46: HH3 - LVL 5 - L/D = 0.4 - Accelerations

- During driving stops, the acceleration measurements show little excitation as measured by $ACC - LVL3 - 000deg$, $ACC - LVL5 - 000deg$ and $ACC - LVL3 - 180deg$.
- During driving, the accelerations measured by $ACC - LVL3 - 000deg$, $ACC - LVL3 - 090deg$ and $ACC - LVL3 - 270deg$ show a clear excitation in similar ranges of around -500 to +600 $[m/s^2]$.
- Accelerations measured by $ACC - LVL3 - 180deg$ do not show the same trend in measurements. The mean calculated by performing a rolling mean almost equals the registered measurements, indicating unreliable test results for this transducer.

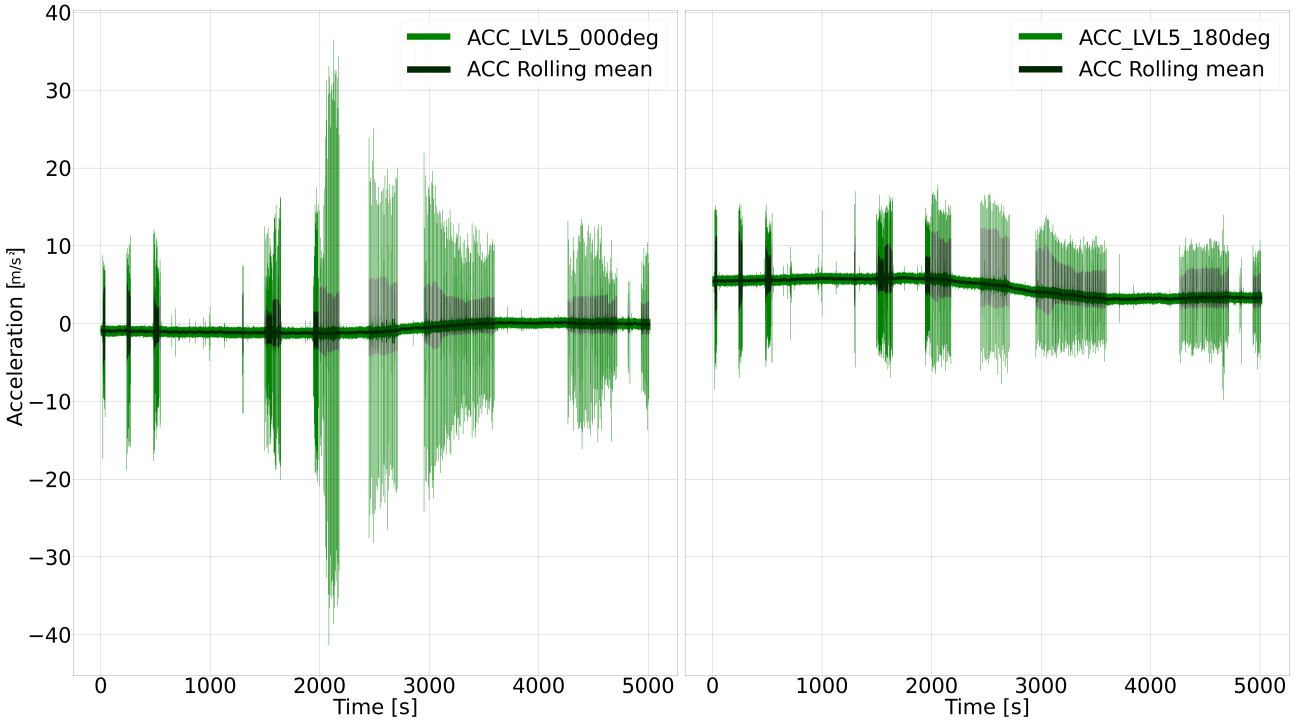

Figure 47: BP4 - LVL 5 - L/D = 0.4 - Accelerations

- BP4 shows acceleration levels that are a factor 10 lower than the acceleration levels measured for HH3. Except for the peaks registered within the first 500 seconds of installation, which fall around the same measurement range. During driving after the first 500 seconds, the accelerations measured by $ACC - LVL3 - 000deg$, $ACC - LVL3 - 090deg$ and $ACC - LVL3 - 270deg$ show a clear excitation in similar ranges of around -50 to +50 $[m/s^2]$.
- The transducer $ACC - LVL3 - 180deg$ again does not show the same shape as can be found for data of other accelerometer transducers, verifying unreliable test results for this transducer.

6.6 Field study stand pipes

During the final days of testing, close-by standpipes are investigated. This was done over 3 different days, on 3 different times during the day, to be able to investigate the tidal effects to the ground water levels around the Maasvlakte test-site. From the data found, a water level 2 meters below ground level was assumed for further elaboration. No indication of tidal effects are registered.

nr. 34	Time [hh:mm]	Depth stand pipe [m wrt GL]	Water level [m wrt GL]
25 Nov	15:25	3.68	2.06
28 Nov	07:45	3.68	2.05
28 Nov	12:13	3.68	2.06
29 Nov	08:51		2.06

Table 4: Standpipe nr. 34, Loc 100 - Observed Water levels Maasvlakte 2

nr. 1041	Time [hh:mm]	Depth stand pipe [m]	Water level wrt GL [m]
25 Nov	15:33	3.31	1.87
28 Nov	07:49	3.40	2.03
28 Nov	12:17	3.40	2.03
29 Nov	08:56		2.03

Table 5: Standpipe nr. 1041, Loc 100 NWZ - Observed Water levels Maasvlakte 2

	Time [hh:mm]	Depth stand pipe [m]	Water level wrt GL [m]
25 Nov	15:30	3.38	1.87
28 Nov	07:52	3.36	1.85
28 Nov	12:21	3.37	1.86
29 Nov	09:00		1.85

Table 6: Unnamed Standpipe (located between nr. 34 and nr. 1040) - Observed Water levels Maasvlakte 2

nr. 1040	Time [hh:mm]	Depth stand pipe [m]	Water level wrt GL [m]
25 Nov	15:27	3.35	1.73
28 Nov	07:58	3.36	1.71
28 Nov	12:23	3.36	1.72
29 Nov	09:04		1.70

Table 7: Standpipe nr. 1040, Loc 100 NWZ - Observed Water levels Maasvlakte 2

7 Conclusion

The closing chapter aims to recover the most relevant outcomes of the present study and links these findings with the proposed research questions.

"In which geotechnical aspects is Blue Piling Installation different from conventional driving using a Hydrohammer?"

The designed field test consists of installing a 1.22 diameter, 21 mm thick steel pipe pile 9 meters into the engineered medium to dense sand of Maasvlakte 2 with cone resistances reaching up to 30 MPa. Three reference techniques are used to drive the pile to depth a total of eleven times. Three installations are performed using conventional driving Hydrohammer S-30 - IQIP, four installations are performed using the prototype Blue Piling Hammer - IQIP and three installations are performed using the vibratory hammer PVE 2350 VM - van 't Hek. Due to plugging being encountered for the Blue Piling technique, one extra hybrid installation was performed up to 6 meters depth using the S-30 and driven to refusal using the Blue Piling hammer. Plugging was measured for the hybrid installation, one Hydrohammer installation and one Blue Piling installation.

The main difference between the three installation techniques are the induced stress waves (governing the static or dynamic character) and the induced amount of loading cycles. From previous research, it was found that the Blue Piling blow causes a rigid body motion and falls within rapid load conditions, characterizing it as quasi-static movement. Strain gauges, accelerometers, total radial stress and pore pressure transducers are installed on the pile to be able to quantify the relevant geotechnical aspects considered: drainage conditions, resistance mobilization, likelihood of plugging, friction fatigue and set-up.

Based on the experimental data, the difference in stress wave generated was found to affect:

- **Drainage conditions:** In total pressure data for the characteristic Blue Piling blow, an increase in pore pressures was found in the stationary phase of the blow. For the Hydrohammer (S-30) blow, the pore pressures quickly equalized before the new blow could take place. However, return to hydrostatic water pressures was only found in driving stops of at least 10 minutes long. This was complemented by literature research as for dynamic methods, free draining conditions were assumed. For static methods, loading rate effects were assumed to cause a generation in pore water pressures in (silty) sand.
- **Plug formation:** For the same pile geometry, the Blue Piling set-up was found to plug significantly with respect to the Hydrohammer installation. Based on literature review, the geometry of the pile of 1.22 meter diameter into medium to dense sand was assumed to not cause plugging. In retrospect it is evident that for dynamic methods, the inertia of the soil column creates an additional component of resistance to plugging. In the absence of dynamic effects such as for the Blue Piling hammer, high normal stresses can be locked into the soil plug, encouraging plugging.

> In turn, strong presence of plugging during driving was found at the same height as 2 - 3 times the levels of stress found at the bottom transducer level. Based on literature review, plugging may cause an open-ended pile to behave more like a partially closed pile, explaining higher developed stresses near the pile tip.

The difference in load cycles influenced the following:

- **Friction Fatigue:** For the same pile geometry, values of radial stress found at higher distance from the pile ($h/D = 2.3$) were a factor 2 to 4 higher for Blue Piling compared to Hydrohammer installation performed in similar soil conditions. This is in agreement with literature which describe friction fatigue as contraction of the narrow shear zone, which becomes more significant under cyclic shearing and loading. The contraction near pile-soil interface causes surrounding soil to relax, causing a reduction in radial stress.

8 Recommendations

The following Chapter elaborates on the recommendations based on insights gained performing the research in this thesis.

1. **Testing different pile diameters**

   Based on the literature research, it was found that pile diameters around 1.22 meter are unlikely to plug. However for the quasi-static charactersistic of the Blue Piling blow, high normal stresses are locked into the soil plug which has encouraged plugging during the experiment (De Nicola & Randolph, 1997). In combination with the reduced amount of cycling during Blue Piling installation, high radial stresses are yielded around pile base and pile shaft. Since the piles installed with the Blue Piling hammer was brought to premature refusal around 8.7 meters depth, scalability of the results is brought into question. For larger pile geometries, plugging should theoretically not take place, but this should be verified in further research since for larger monopiles, the Blue Piling hammer should still be able to reach to design penetration to be a feasible driving technique.

2. **Research into Plugging**

   Plugging causes high stresses to build up inside the pipe pile along the pile shaft due to arching effects transferring the axial stresses acting on the internal soil column to the pile walls, which increases internal shaft friction (S. G. Paikowsky et al., 1989). For a next field test, the recommendation is to install total pressure and pore pressure on the inside of the pile wall. In this way, the stresses governing plugging behaviour can be quantified if plugging takes place.

3. **Further data exploration: Friction Fatigue**

   For the analysis into the radial total pressure and water pressure, the horizons of soil picked are 1.5, 4, 5, 6.5 and 8 meters. These horizons are picked based on the Site Investigation showing that these horizons are not at the border of any soil layers and availability of PDA data at these horizons. To be able to evaluate the Friction Fatigue phenomenon of the Blue Piling and Hydrohammer installation, the analysis should be refined. For starters, a point every 0.25 meter should be added to the evaluation. From this refined analysis it can be concluded if the points currently analysed are outliers or are actually part of a consistent trend that indicates friction fatigue between the different transducer levels considered. The pressures should show a trend that is consistent with the soil conditions in-situ.

4. **Further data exploration: Set-up** Set-up is described as the gain in shaft capacity of a pile as a result of disturbance brought about during installation (Chow et al., 1998). For larger induced loading cycles, the set-up will be lower as is expected to have the most effect - in order - for the vibratory installation, then for the conventional driving and lastly the Blue Piling installation. Due to unavailability of the dataset at time of round-off of this thesis, no further elaboration is possible. The recommendation would be to check the radial total stresses at the end of driving of day 1 of BP1 and compare this to the total radial stresses before driving on day 2. Recovering the resistances along the shaft using the Pile Driving Analysis for the same points in time, may serve to verify and quantify the occurrence of this phenomenon. The set-up will govern the final capacity of the pile. The relevance for drivability is quantifying the effect of a long (unexpected) driving interruption.

References

Alm, T., Bye, A., & Kvalstad, T. (1989). New interpretation of soil resistance for piel driveability analysis. In *Proceedings of the 12th. icsmfe.*

Alm, T., & Hamre, L. (2001). Soil model for pile driveability predictions based on cpt predictions.

Athen Sensors. (2022, 12). *Kpe-pb small pore pressure gauge.* Retrieved from https://www.althensensors.com/media/30123/kpe-pb-miniature-pore-pressure-gauge-en.pdf

Barnes, G. (1995). *Soil mechanics: principles and practice.* Basingstoke: Macmillan. (OCLC: 605351676)

Beuckelaers, W. (2018, October 10). *Blue piling 25m tirals - blue pilot, offshore drivability back-analysis and methodology* (Tech. Rep. No. C769R03). Cathie Associates. (Reviewed by Cathie, D.)

Brown, M. J., & Hyde, A. F. L. (2006, October). Some observations on Statnamic pile testing. *Proceedings of the Institution of Civil Engineers - Geotechnical Engineering*, *159*(4), 269–273. Retrieved 2022-07-05, from https://www.icevirtuallibrary.com/doi/10.1680/geng.2006.159.4.269 doi: 10.1680/geng.2006.159.4.269

Byrne, B. (1995). Driven pipe piles in dense sand.

Chow, F., Jardine, R., Brucy, F., & Nauroy, J. (1998). Effects of time on capacity of pipe piles in dense marine sand. *Journal of Geotechnical and Geoenvironmental Engineering*, *124*(3). Retrieved 2022-09-05, from https://ascelibrary.org/doi/epdf/10.1061/%28ASCE%291090-0241%281998%29124%3A3%28254%29

Dean, E., & Deokiesingh, S. (2013, July). Plugging criterion for offshore pipe pile drivability. *Géotechnique*, *63*(9), 796–800. Retrieved 2022-06-08, from https://www.icevirtuallibrary.com/doi/10.1680/geot.12.T.011 doi: 10.1680/geot.12.T.011

De Nicola, A., & Randolph, M. F. (1997, September). The plugging behaviour of driven and jacked piles in sand. *Géotechnique*, *47*(4), 841–856. Retrieved 2023-05-09, from https://www.icevirtuallibrary.com/doi/10.1680/geot.1997.47.4.841 doi: 10.1680/geot.1997.47.4.841

DINOloket. (n.d.). *Ondergrondgegevens.* Retrieved 03-11-2022, from https://www.dinoloket.nl/ondergrondgegevens

Dynamics, P. (2010). *Grlweap software.*

Heerema, E. P. (1978, October). Predicting Pile Driveability: Heather As An Illustration Of The "Friction Fatigue" Theory. In *All Days* (pp. SPE–8084–MS). London, United Kingdom: SPE. Retrieved 2023-03-28, from https://onepetro.org/SPEEURO/proceedings/78EUR/All-78EUR/London,%20United%20Kingdom/134806 doi: 10.2118/8084-MS

Henke, S., & Grabe, J. (2013, June). Field measurements regarding the influence of the installation method on soil plugging in tubular piles. *Acta Geotechnica*, *8*(3), 335–352. Retrieved 2022-10-03, from http://link.springer.com/10.1007/s11440-012-0191-6 doi: 10.1007/s11440-012-0191-6

Hessels, J. (2020, March). *1-d pile-soil interaction.*

Ho, T., Jardine, R., & Anh-Minh, N. (2011, March). Large-displacement interface shear between steel and granular media. *Géotechnique*, *61*(3), 221–234. Retrieved 2023-02-21, from https://www.icevirtuallibrary.com/doi/10.1680/geot.8.P.086 doi: 10.1680/geot.8.P.086

Hölscher, P., Brassinga, H., Brown, M., Middendorp, P., Profittlich, M., & Tol, F. v. (2012). *Rapid load testing on piles: interpretation guidelines* (No. 230). Boca Raton London New York Leiden: CRC Press.

Innovators, O. W. (2019). *Ihc iqip takes the next step in development blue piling technology.* Retrieved from https://www.offshorewindinnovators.nl/news/ihc-iqip-takes-next-step-in-development-blue-piling-technology

IQIP. (2021, 11 1). *Blue piling by iqip introduction.*

IQIP. (2022). *Blue piling technology.* Retrieved from https://iqip.com/products/pile-driving-equipment/blue-piling-technology/

Jackson, A., White, D., Bolton, M., & Nagayama, T. (2008). Pore pressure effects in sand and silt during pile jacking. In *Proceedings of the bga international conference on foundations.* IHS BRE Press.

Jardine, R. (Ed.). (2005). *ICP design methods for driven piles in sands and clays* (1. publ ed.). London: Imperial College.

Klar, A., Bennett, P. J., Soga, K., Mair, R. J., Tester, P., Fernie, R., ... Torp-Peterson, G. (2006, July). Distributed strain measurement for pile foundations. *Proceedings of the Institution of Civil Engineers - Geotechnical Engineering*, *159*(3), 135–144. Retrieved 2022-09-07, from https://www.icevirtuallibrary.com/doi/10.1680/geng.2006.159.3.135 doi: 10.1680/geng.2006.159.3.135

Kodsy, A., & Iskander, M. (2022, March). Insights into Plugging of Pipe Piles Based on Pile Dimensions. *Applied Sciences*, *12*(5), 2711. Retrieved 2022-07-06, from https://www.mdpi.com/2076-3417/12/5/2711 doi: 10.3390/app12052711

Kou, H.-l., Zhang, M.-y., & Yu, F. (2015, December). Shear Zone around Jacked Piles in Clay. *Journal of Performance of Constructed Facilities*, *29*(6), 04014169. Retrieved 2022-11-11, from https://ascelibrary.org/doi/10.1061/%28ASCE%29CF.1943-5509.0000659 doi: 10.1061/(ASCE)CF.1943-5509.0000659

Ligthart, J. (2019, may). *Hydrohammersim model description - pile and soil model.*

Lim, J., & Lehane, B. (2014, May). Characterisation of the effects of time on the shaft friction of displacement piles in sand. *Géotechnique*, *64*(6), 476–485. Retrieved 2022-05-09, from https://www.icevirtuallibrary.com/doi/10.1680/geot.13.P.220 doi: 10.1680/geot.13.P.220

Liu, J.-w., Zhang, Z.-m., Yu, F., & Xie, Z.-z. (2012, July). Case History of Installing Instrumented Jacked Open-Ended Piles. *Journal of Geotechnical and Geoenvironmental Engineering*, *138*(7), 810–820. Retrieved 2023-01-18, from https://ascelibrary.org/doi/10.1061/%28ASCE%29GT.1943-5606.0000638 doi: 10.1061/(ASCE)GT.1943-5606.0000638

Martens, L. (2019, Febuary 19). *Blue piling - simulation report.*

Martens, L. (2020, February 1st). *Project blue piling, theory of operation.* personal communication.

Murthy, D. S., Robinson, R. G., & Rajagopal, K. (2021, May). Formation of soil plug in open-ended pipe piles in sandy soils. *International Journal of Geotechnical Engineering*, *15*(5), 519–529. Retrieved 2022-08-22, from https://www.tandfonline.com/doi/full/10.1080/19386362.2018.1465742 doi: 10.1080/19386362.2018.1465742

nautical charts, G. (2022). *Fishing marine charts navigation.* Retrieved from https://fishing-app.gpsnauticalcharts.com/i-boating-fishing-web-app/fishing-marine-charts-navigation.html#10.76/51.9524/4.0327

of Rotterdam, P. (n.d.-a). *Nieuw havengebied in zee.* Retrieved 03-11-2022, from https://www.portofrotterdam.com/nl/bouwen-aan-de-haven/lopende-projecten/nieuw-havengebied-zee

of Rotterdam, P. (n.d.-b). *Weather tide.* Retrieved 03-11-2022, from https://weather-tide.portofrotterdam.com/desktop/

on Rapid Pile Load Test Methosd, R. C. (1998). Research activities toward standardization of rapid pile load test methods in japan. In *Proceedings of the 2nd international statnamic seminar.*

Paikowsky, S. (1989). *A static evaluation of soil plug behavior with application to the pile plugging problem.* Massachusetts Institute of Technology. Retrieved from http://hdl.handle.net/1721.1/103189

Paikowsky, S. G., Whitman, R. V., & Baligh, M. M. (1989, January). A new look at the phenomenon of offshore pile plugging. *Marine Geotechnology*, *8*(3), 213–230. Retrieved 2022-07-06, from http://www.tandfonline.com/doi/abs/10.1080/10641198909379869 doi: 10.1080/10641198909379869

Randolph, M., & Deeks, A. (1992). Keynote lecture: Dynamic and static soil models for axial pile response. *Application of Stress-Wave Theory to Piles*, 3–14. doi: 10.1201/9781315137544

Randolph, M., & Wroth, C. (1978, December). Analysis of deformation of vertically loaded piles. *Journal of the Geotechnica Engineering Division, Proceedings of the American Society of Civil Engineers*, *104*(GT12). Retrieved 2022-07-29, from https://www.yumpu.com/en/document/view/33742715/analysis-of-deformation-of-vertically-loaded-piles-mark-f-randolph

Randolph, M. F., & Gourvenec, S. (2011). *Offshore geotechnical engineering*. London ; New York: Spon Press.

Rijkswaterstaat. (n.d.). Retrieved 03-11-2022, from https://waterinfo.rws.nl/#!/details/publiek/waterhoogte/Amaliahaven(AMHV)/Waterhoogte___20Oppervlaktewater___20t.o.v.___20Normaal___20Amsterdams___20Peil___20in___20cm

Rijsdijk, K., Passchier, S., Weerts, H., Laban, C., van Leeuwen, R., & Ebbing, J. (2005, July). Revised Upper Cenozoic stratigraphy of the Dutch sector of the North Sea Basin: towards an integrated lithostratigraphic, seismostratigraphic and allostratigraphic approach. *Netherlands Journal of Geosciences*, *84*(2), 129–146. Retrieved 2022-11-07, from https://www.cambridge.org/core/product/identifier/S0016774600023015/type/journal_article doi: 10.1017/S0016774600023015

Saathoff, J., Achmus, F., Higgins, K., Ainsworth, Y., Toll, D., & Osman, A. (2005, 5). Investigation of the behaviour of jacked and rotary-jacked piles in sandy soils. In *Piling 2020. proceedings of the piling 2020 conference.*

Santos, J. A. d., Instituto Superior Técnico (Lisbon, P., of Soil Mechanics and Foundation Engineering, I. S., & de Geotecnia, S. P. (Eds.). (2008). *The application of stress-wave theory to piles: science, technology and practice: proceedings of the 8th International Conference on the Application of Stress-Wave Theory to Piles: Lisbon, Portugal, 8-10 September 2008*. Amsterdam, Netherlands : Fairfax, VA: IOS Press ; Distributor in the USA and Canada, IOS Press. (Meeting Name: International Conference on the Application of Stress-Wave Theory on Piles OCLC: ocn262427466)

Schneider, J. A., & Harmon, I. A. (2010, August). Analyzing Drivability of Open Ended Piles in Very Dense Sands. *DFI Journal - The Journal of the Deep Foundations Institute*, *4*(1), 32–44. Retrieved 2022-06-08, from https://dfi-journal.org/papers/?abstract=2010040103 doi: 10.1179/dfi.2010.003

Semple, R. M., & Gemeinhardt, J. P. (1981). Stress History Approach To Analysis Of Soil Resistance To Pile Driving. In *Offshore Technology Conference*. Houston, Texas: Offshore Technology Conference. Retrieved 2023-03-28, from http://www.onepetro.org/doi/10.4043/3969-MS doi: 10.4043/3969-MS

Sinnreich, J. (2021, September). Optimizing the Arrangement of Strain Gauges in Pile Load Testing. *Geotechnical Testing Journal*, *44*(5), 20200033. Retrieved 2022-09-07, from http://www.astm.org/doiLink.cgi?GTJ20200033 doi: 10.1520/GTJ20200033

Smith, E. (1960). Pile driving analysis by the wave equation. *Journal of the Soil Mechanics and Foundation Division*, *84*(4), 35-61.

Smith, I., To, P., & Willson, S. (1986). *Plugging of pipe piles*. Proc. 3rd Int. Conf. on Num. Meth. in Offshore Piling, Nantes.

Stevens, R. S., Wiltsie, E. A., & Turton, T. H. (1982). Evaluating Drivability for Hard Clay, Very Dense Sand, and Rock. In *Offshore Technology Conference*. Houston, Texas: Offshore Technology Conference. Retrieved 2023-03-28, from http://www.onepetro.org/doi/10.4043/4205-MS doi: 10.4043/4205-MS

Terzaghi, K. (1943). *Theoretical soil mechanics*. New York: Wiley.

Tokyo Measuring Instruments Lab. (2022). *Pda-pb / pdb-pb miniature pressure transducer 50kpa 3mpa*. Retrieved from https://tml.jp/eng/documents/transducers/PDA-PB_PDB-PB.pdf

Toolan, F., Fox, D., & BP. (1977, May). GEOTECHNICAL PLANNINGOF PILED FOUNDATIONS FOR OFFSHORE PLATFORMS. *Proceedings of the Institution of Civil Engineers*, *62*(2), 221–244. Retrieved 2023-03-27, from https://www.icevirtuallibrary.com/doi/10.1680/iicep.1977.3224 doi: 10.1680/iicep.1977.3224

van Paassen, B. (2010, October 4th). *Interpretatie grondonderzoek kraanbanen 5.3 en 5.4.* (No. BIC-R-5.0-043). personal communication.

van Zandwijk, C., van Dijk, B., Voeten, J., & Heerema, E. (1983). An Improved Pile Driveability Theory for Gulf of Mexico Soils. In *Offshore Technology Conference*. Houston, Texas: Offshore Technology Conference. Retrieved 2023-03-28, from http://www.onepetro.org/doi/10.4043/4503-MS doi: 10.4043/4503-MS

Vesić, A. S. (1977). *Design of pile foundations* (No. 42). Washington: Transportation Research Board, National Research Council.

White, D., & Bolton, M. (2002).
In S. Springman (Ed.), *Centrifuge and constitutive modelling: Two extremes*. (chap. Observing friction fatigue on a jacked pile). Rotterdam: Balkema.

White, D. J., & Bolton, M. D. (2004, August). Displacement and strain paths during plane-strain model pile installation in sand. *Géotechnique*, *54*(6), 375–397. Retrieved 2022-07-11, from https://www.icevirtuallibrary.com/doi/10.1680/geot.2004.54.6.375 doi: 10.1680/geot.2004.54.6.375

White, D. J., & Lehane, B. M. (2004, December). Friction fatigue on displacement piles in sand. *Géotechnique*, *54*(10), 645–658. Retrieved 2022-06-08, from https://www.icevirtuallibrary.com/doi/10.1680/geot.2004.54.10.645 doi: 10.1680/geot.2004.54.10.645

Yang, J., Tham, L. G., Lee, P. K., & Yu, F. (2006, January). Observed Performance of Long Steel H-Piles Jacked into Sandy Soils. *Journal of Geotechnical and Geoenvironmental Engineering*, *132*(1), 24–35. Retrieved 2023-01-17, from https://ascelibrary.org/doi/10.1061/%28ASCE%291090-0241%282006%29132%3A1%2824%29 doi: 10.1061/(ASCE)1090-0241(2006)132:1(24)

Yang, J., Tham, L. G., Lee, P. K. K., Chan, S. T., & Yu, F. (2006, May). Behaviour of jacked and driven piles in sandy soil. *Géotechnique*, *56*(4), 245–259. Retrieved 2022-05-03, from https://www.icevirtuallibrary.com/doi/10.1680/geot.2006.56.4.245 doi: 10.1680/geot.2006.56.4.245

Appendix

A Supplement to Literature Study

A.1 Soil Mechanics

The state and stress of soil fabric in-situ is changed during driving. Since the installation of open-ended piles is considered, this will be the case both on the inside aswell as on the outside of the pile. Even though the installation methods may differ, the same mechanics are at the foundation of the installation effects that occur during driving. The following chapter describes the soil mechanics behind the process of pile driving: soil state, its classification and stress-strain behaviour. It is to be noted that the installation effects will be mainly focused on installation in (silty) sand. This is due to the found in-situ soil as will be elaborated in Chapter 3.

A.1.1 Particle packing

Granular soils (eg. coarse silts, sands and gravels) are made up by particles of different sizes, shapes, surface roughness and grading (well-graded to uniformly graded). All factors mentioned above affect distance between particles, void space, contact between particles, freedom of movement and density. This can in turn be described by the relative densily which is a measure to establish whether a soil is densely or loosely packed (Barnes, 1995).
Relative density can be described as follows:

$$R_e = D_r = \frac{e_{max} - e_{in-situ}}{e_{max} - e_{min}} \tag{12}$$

where:

e_{max} = maximum void ratio [-]
e_{min} = minimum void ratio [-]
$e_{in-situ}$ = in situ void ratio [-]

The void ratios used in the above formulations have to be obtained using intricate procedures in the lab. The parameter is often only used in laboraty research because there are some limitations to establishing the values. Tests should for example not be carried out on slightly cohesive sands (>10% silt) or on crushable particles. Additionally, ranges of density values between minimum and maximum vary minimally, and outcomes of in-situ density tests can be poor, causing relatively large errors. At depth, the Relative Density is usually assessed by the Standard Penetration test, see Table 8.

	Relative density [%]	SPT [N]
Very loose	0 - 15	0 - 4
Loose	15 - 35	4 - 10
Medium dense	35 - 65	10 - 30
Dense	65 - 85	30 - 50
Very dense	85 - 100	> 50

Table 8: Relative density, (Barnes, 1995)

The relation between relative density and cone resistance found for the top sand layer is determined according to the relation by Lunne (van Paassen, 2010).

$$R_e = ln(\frac{q_c}{61\sigma_v'^{0.71}}) * 100/2.91 \tag{13}$$

where:

$R_e = D_r$ = Relative density [%]
q_c = Measured cone resistance [kPa]
σ_v' = Effective vertical stress [kPa]

R_e is also given by equation 12. $R_n = R_e$ - 20% because firstly, based on the relation by Lunne and Christoffelsen a reduction of 10 to 15% is considered to account for (medium) dense sands and secondly the difference in-situ between the established R_n and R_e equals 5% as determined by BAM. The categories that can therefore be distinguished are as follows. Elaboration of the results from Site Investigation can be found in Chapter 3:

	R_n [%]
Loose	0 - 33
Medium dense	33 - 66
Dense	> 66

Table 9: Relative density according to Lunne

A.1.2 Stress-strain behaviour of sand

The shear strength of a granular soil depends on interlocking of the particles aswell as the friction between the contact surfaces of particles. The shear strength (τ) is described by the effective stress failure criterion as follows.

$$\tau = \sigma'_v \tan(\phi) = K\sigma'_h \tan(\phi) \tag{14}$$

where:

τ = Shear strength [kPa]
σ'_v = Effective vertical stress [kPa]
ϕ = Internal friction angle [deg]
K = Coefficient of earth pressure [-]
σ'_h = Effective horizontal stress [kPa]

Uncemented soils display strength purely based on frictional characteristics, coefficient of internal friction ($\mu = \tan(\phi)$) being the primary parameter. For the interaction between granular soil and steel pile, the ratio between interface friction angle and internal soil friction angle lies between $\frac{1}{3}$ and $\frac{2}{3}$, where interface friction angle is established in design standards. Vesi[Pleaseinsertintopreamble], (1977) amongst others, recommend assuming the ratio to be unity which implies the shear along interface mostly takes place within the soil. It is to be noted that Ho, Jardine, and Anh-Minh (2011) have performed large displacement ring tests, showing that grain crushing in the shear zone and changes in roughness of the interfaces could lead to interface friction angles significantly different from values established in small-displacement direct shear tests, which can usually be found in design standards. The large-displacement conditions created by the ring-test best represent the conditions adjacent to driven pile shaft. Further elaboration of interface friction angles is outside of the scope of this Thesis. The value of th the earth pressure coefficient K depend on initial soil density, installation method and volume displacement. In the case of soil plug and large relative displacements between soil and structure interaction the K value is closely related to the interface shear resistance (S. Paikowsky, 1989).

For soils that are saturated, meaning the sand particles are surrounded by water, the frictional strength is mobilized by the normal stresses in the particles (σ'). The effective stress equals the total stress (σ) subtracted by the pore water pressure (u) (Terzaghi, 1943).

$$\sigma' = \sigma - u \tag{15}$$

In drained conditions, a change in volume can occur due to shearing, showing as either contraction or dilation. The volume change is appointed to a change in arrangement and packing of the soil particles. The critical void ratio (e_{crit}) describes the state at which a volume of soil mass does not change any more, meaning volumetric strains are zero even though continuous shearing is applied. For initially loosely packed soil, some densification (contraction) of the particles occurs. Due to particles moving closer together, more interlocking is reached, gradually increasing shear stress (strain-hardening) before steady state shear is reached. For densely packed particles (more densely packed than critical void ratio), loosening of the particles inside the matrix has to take place (dilation) before steady state shear can occur. When the angle of dilation is greatest, the maximum frictional resistance of a soil is mobilised. The same degree of interlocking cannot be maintained after the peak has occurred which decreases strength after the peak (strain-softening). Under large confining pressure, dilatancy hardly occurs.

In undrained conditions, no volume change is possible due to low permeabilities in fine-grained soils (such as clay) where draining time may be very long. In coarse-grained soils, undrained conditions could apply when very rapid rates of loading are exerted such as loading by waves or earthquakes. The maximum shear stress that can be mobilized will depend only on the initial void ratio (e_0) and consequently its water content (w). This is called the undrained shear strength. When a dense soil is sheared, negative excess pore pressures can be generated due to the constant volume present (M. F. Randolph & Gourvenec, 2011).

$$\tau_f = s_u \tag{16}$$

When stress levels increase even more under laterally confined compression, particles can yield, causing them to crush and fracture. This allows an increase in vertical strains but also an increase in amount of particles. Because of the increase in contact surface between particles and further locking, contact stress decreases and stiffness further increases (Barnes, 1995).

Shear zone development in silty clay
The field test conducted by Kou, Zhang, and Yu (2015) in silty and sandy clay was executed to study the physical phenomenon of shear zone after installation of concrete open-ended pipe piles. The change in soil parameters due to installation were investigated in the laboratory. Compaction was found in the shear zone, with increased natural water content, unit weight and friction angles. At the same time, cohesion and void ratio decreased due to installation disturbance.

A.1.3 Soil in compression

Soil in compression goes trough three stages, (1) immediate elastic compression, (2) primary compression (also referred to as consolidation) and (3) secondary compression (referred to as creep) which is a plastic deformation. The elastic compression and primary compression for sandy soil is instant due to the high permeability. Consolidation describes the transition from undrained to drained conditions as excess pore water pressures dissipate over time. The void ratio (e) reduces as a result of this. Creep is the long-term effect of mechanical deformation of a soil, most prevalent in normally consodidated clays and organic soils. It is largely negligible in overconsolidated clays, sands and silts. In modelling soil response to driving as elaborated in Chapter 2.2, different parameters are described to catch these different stages of soil in compression.

A.1.4 Mobilization of resistance

The mobilization of capacity of a pile is based on the soil resistance obtained during installation and after installation is finished. The total static capacity (Q_{ult}) is made up of a component for the ultimate shaft resistance (Q_s) and the ultimate base resistance (Q_b). Shaft resistance for steel open pile foundations can mobilize on both the inner aswell as the outer shaft. The base resistance mobilized depends on the pile annulus area aswell as the degree of plugging, as will be further discussed in Section **??**. Mobilization of resistance will be further elaborated in Chapter 2.2.

$$Q_b = q_b A_b \tag{17}$$

where:
Q_b = ultimate base resistance [kPa]
q_b = end bearing resistance [kPa]
A_b = base cross-sectional area [kPa]

$$Q_s = \sum_{0}^{L} f_s \pi d l \tag{18}$$

where:
Q_s = ultimate shaft resistance [kPa]
f_s = skin friction in sand [kPa]

The base resistance and ultimate shaft resistance can in their turn be established using different Static Resistance to Driving (SRD) models. These are further elaborated in Chapter 2.

The state and stress of soil fabric in-situ is changed during driving, depending on its original configuration and drainage conditions. These changes in turn influence the behaviour of piles during installation and during the loading phase, so are important to consider in drivability analysis. Based on different characterization methods established both in the lab and on large scales (e.g. to establish Relative density), the configuration loose, medium dense or dense can be appointed which will aid in the understanding of encountered phenomena during installation. The importance of the in-situ testing techniques based on CPT is highlighted since disturbance is likely in sampling and testing in the lab.

A.2 Installation Phenomena

A.2.1 Plugging

Plugging during dynamic driving

This subsection serves as supplement to the subsection of Plugging during driving as discussed in Chapter 2.1.2.. Dean and Deokiesingh (2013) have proposed a new objectively calculable criterion to establish whether a pile plugs during the driving processes. A shock wavefront analysis is combined with a simplified impact analysis to establish the plugging criteria, as will be shortly summarized hereafter. The criteria is based on the consideration that the shaft friction between soil and pile will largely be mobilized before the time the wave front reaches the pile tip.

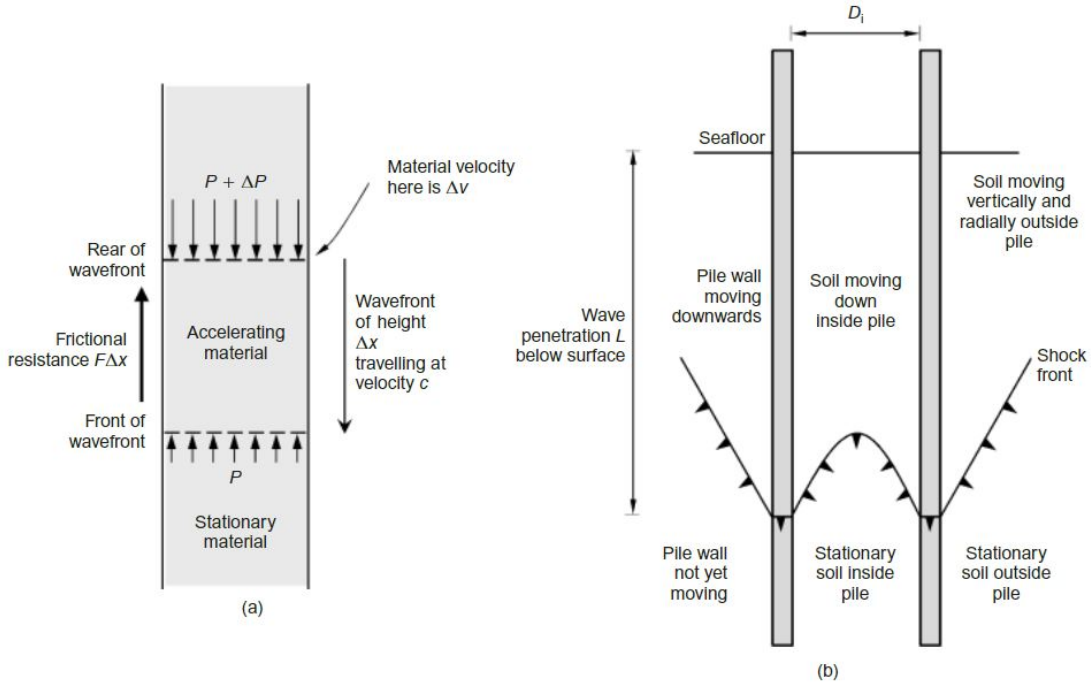

Figure 48: Shock wavefront analysis (sketches not to scale): (a) dynamics across a shock wavefront; (b) consideration of soil and pipe pile (Dean & Deokiesingh, 2013)

A shock wavefront of width Δx travels at speed c down an element with mass density ρ, Young's Modulus E and cross-sectional area A. As a result of the passing wavefront, the material mass picks up velocity Δv. The momentum of the accelerated material changes to $\rho Ac\delta t\Delta v$. The axial force P increases, accelerating the material mass inside the wavefront with an impulse of $(\Delta P - F\Delta x)\delta t$. By equating the change of momentum to the impulse and deviding by δt the result gives the following formulation. Note that the $F\Delta x$ term may be ignored if the width Δx is negligible compared to the other dimensions considered.

$$\Delta P = \rho Ac\Delta v + F\Delta x \tag{19}$$

When the soil inside the pile becomes bound to the monopile, the velocity of the shear wavefront is forced to be equal to the velocity in steel. The resulting axial force in the soil inside the pile would be similar form as Equation 19 where ρ equals ρ_{soil}, A is the area of the soil plug, c is wavespeed through steel and Δv is the velocity of the pile steel behind the shock front. ΔP can be supported by the friction mobilized between the soil and the pile between seafloor and shock wave. As a result, the average internal skin friction over the inside diameter and length of the pile would have to outweigh the resulting axial force caused by inertia of the soil plug for plugging to occur. This yields the following expression. Plugging is possible when:

$$\pi D_i L f_{av} \geq \rho_{soil} \frac{\pi D_i^2}{4} c\Delta v \tag{20}$$

An appropriate value for velocity jump at the shock front (Δv) can be taken as equal to initial velocity (v_0) as calculated in the following equation. Simplified impact analysis models the hammer blows as an infinitely rigid ram of mass (M_R) and velocity (v_R) which impacts a stationary infinitely rigid helmet of mass (M_H) (Dean & Deokiesingh, 2013).

$$v_0 = \frac{M_R v_R}{M_R + M_H} \tag{21}$$

A.3 Modelling

A.3.1 Blue Piling Hammer - Simulink

In the process of developing the Blue Piling technology, simulations in Simulink have been created of the Blue Piling technology with the goal to closely approximate results gained in the future set-up such as potential delivered energy. The model is split up in a part for the hammer, the cylinders, the sleeve, the pile and the soil in place. This subsection gives a brief outline of the mode. For the details and equations will be referred to (Martens, 2019), (Ligthart, 2019) and (Hessels, 2020). The general approach of the subdivided parts' models is applying Newton's second Law to solve for the applied forces with the input of the particular velocities and masses.

Hammer model
The model of the hammer consists of the hammer steel, the water inside the Blue piling tank and the cap, which is the volume of air entrapped between the water and the hammer top. The sum of the moving mass generates the force needed to drive the monopile. The hammer steel delivers a stiffness component, the water is compressible and the cap volume acts as an air spring.

Hammer stiffness
The hammer model consists of an infinitely stiff mass and the lower part of the hammer which does have a finite stiffness. It acts between the hammer mass and the mass of the buffer cylinders. The hammer applies a force on the shock absorber, which transfers it to the main buffer. When retracted, the force is directly exerted onto the main buffer.

Water
The water model describes the behaviour of the water masses and the force they exert because of their relative displacement on the hammer steel below. Pressures are calculated using the bulk modulus and are limited to zero bar absolute. A radial expansion term is added but to respect the one dimensional structure of the model, the additional volume is added to the initial volume of each water element.

Cap
Even when the tank of the hammer is filled to the brim with water, there is always a small amount of air present between the water and the hammer top. The pressure in the cap varies from atmospheric pressure during the process of hammering due to pressure in the tank and compressibility of the water. The pressure of the cap is exerted on the top water element and works over the water surface area.

Cylinders
Two types of cylinders are present in the system. The main pneumatic buffer cylinders are applying the hammer load on the pile. To smoothen impact between buffer rod and hammer, shock absorbers are installed. The lift cylinders are hydraulic cylinders which lift the hammer after a drop. They stay connected to the hammer so will be a source of hydraulic resistance and consequently influence the development of hammer velocity.

Main buffer cylinder
The general approach of the subdivided parts' models is applying Newton's second Law to solve for the working forces with the input of the particular velocities and masses. The main buffer cylinder is pre-pressurized which affects the stiffness of the buffer during impact. A counter-acting force is applied by pressurizing the rod side of the main buffer. The system of buffers is combined into one for simplified analysis. Gas models are used to calculate resultant forces of the gas pressures.

Lift cylinder
Again, the set of lift cylinders will be modelled as an individual cylinder and the mass is the sum of the 9 cylinders. Springs in parallel describe the sum of the stiffnesses of the rods, a spring in series is added to the hammer stiffness to describe the total, which is a factor three lower than the hammer stiffness itself (Martens, 2019).

Sleeve
A single mass without stiffness is implemented in the system for the sleeve.
Pile and soil model
The following figure displays a schematic of the pile-soil model.

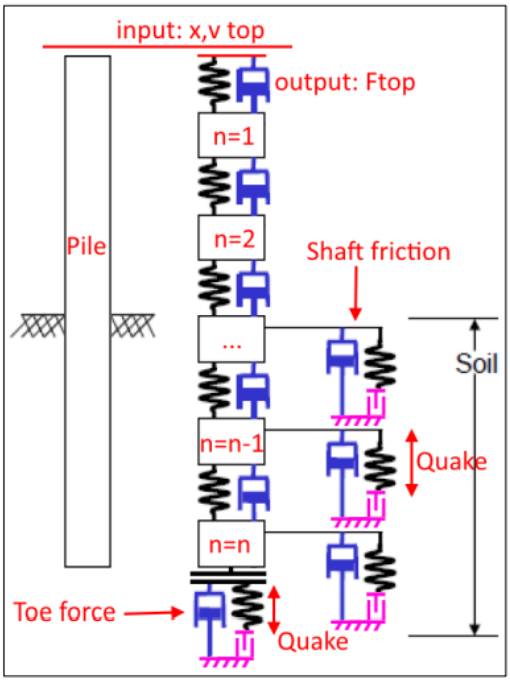

Figure 49: Schematization of the pile-soil model, (Martens, 2019)

,

Pile model

The deformation of the pile is modelled as a damped linear-elastic force. A multiple lumped-mass pile model is deployed. Internal material damping is modelled as linear damping with a damping ratio and also the gravitational force is taken into account, acting on each pile section.

Toe force model

An elasto-plastic model is deployed for approximating the toe force. Quake is the elastic contribution which in practise implies the rebound of the pile after the progression of the toe into the soil. It is the distance over which the soil contracts and expands between maximum penetration and decompression over a short distance above it. A larger value of quake means a lower stiffness (Ligthart, 2019). For a small penetration, the force at the peak is small and with increasing penetration, a plateau is reached at the ultimate toe stress (Hessels, 2020).

Damping of the soil is modelled by using Smith viscous damping. Smith damping leads to additional soil resistance, thus reduction of the displacement per blow, affecting also the speed. Linear damping could also be deployed, but shows a faster decrease of residual motions (Hessels, 2020).

Shaft friction model

The shaft friction is calculated as elastic-plastic force for all pile elements. The values obtained can be either positive or negative, unlike in the toe force model. A factor of 2 is deployed for the sum of the shaft friction since equal friction in- and outside the pile are assumed for open ended piles. Damping is present on every pile element on the shaft, which is again modelled using Smith viscous damping (Ligthart, 2019).

Extended model

The model as described above is only suitable for modelling a single sand layer. To be able to execute a more reliable approximation, the model is extended to take CPT data. The soil type (clay or sand) is determined using the Robertson graph, the actual soil resistance (toe and sleeve) is calculated using the Alm & Hamre method.

It is found in simulation that minimum force required to drive a pile with Blue piling corresponds well with the SRD of the respective pile including self-weight. Also it is noted that the effect of pile soil damping and soil layer discretization on the results in case of a pile near refusal should be further investigated (Hessels, 2020).

A.3.2 ICP - Static Soil Resistance Model

The ICP method is also elaborated since it is used as static resistance model in the calculations of the Simulink as a comparison to the Alm and Hamre method. The formulations used in the ICP method to determine shaft capacity for open ended piles are described as follows. Note that only open ended pile installation in compression is considered since this is relevant for the test set-up.

The local shear stress (τ_f) is described by the Coulomb failure criterion.

$$\tau_f = \sigma'_{rf} \tan \delta_{cv} \tag{22}$$

The interface friction angle (δ_{cv}) should be measured during the test since it depends on pile roughness amongst other factors. If not feasible, the value should be taken from Jardine et al. (1992). σ'_{rf} describes the radial effective stress which increases during pile loading according to the following relation: $\sigma'_{rf} = (\sigma'_{rc} + \Delta\sigma'_{rd})$. σ'_{rc} is the local radial effective stress which is a function of the CPT resistance (uncorrected for over consolidation ratio (OCR)), free field vertical effective stress and h/R^*. R^* is given as $R^* = (R^2_{outer} - R^2_{inner})^{0.5}$.

$$\sigma'_{rc} = 0.029\ q_c \left(\frac{\sigma'_0}{P_a}\right)^{0.13} \left(\frac{h}{R^*}\right)^{-0.38} \tag{23}$$

Here, $\Delta\sigma'_{rd}$ describes the main change in local radial effective stress associated with dilation of sand at the interface.

$$\Delta\sigma'_{rd} = 2G\frac{\Delta r}{R} \tag{24}$$

Where

$$G = q_c[A + B\eta - C\eta^2]^{-1} \tag{25}$$

$$\eta = q_c(P_a\sigma'_{v0})^{-0.5} \tag{26}$$

and A = 0.0203, B = 0.00125 and C = $1.216e^{-}6$ (Jardine, 2005).

B Site Investigation

B.1 Water table

B.1.1 Desk study water tables

Figure 50: B37A0113 Grondwaterstand

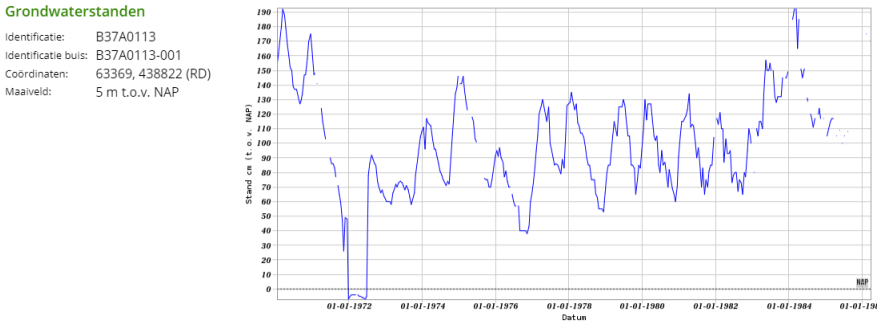

Figure 51: B37A0113 Peilbuis 001 (Dinoloket, n.d.)

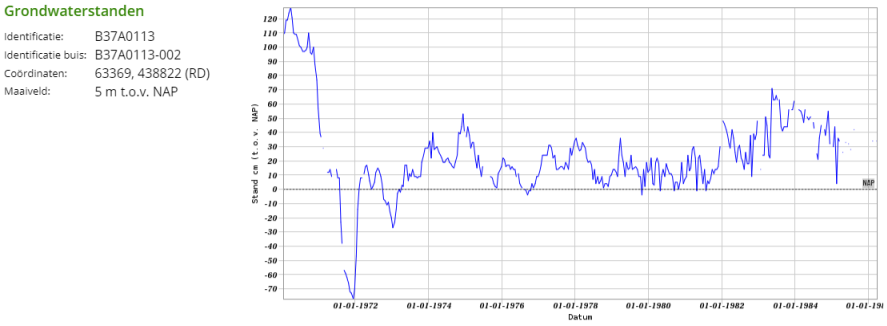

Figure 52: B37A0113 Peilbuis 002 (Dinoloket, n.d.)

Taken from (DINOloket, n.d.)

B.2 CPT comparison

Source	ID	X (m RD)	Y (m RD)	Z (m RD)	diepte (m-NAP)	Lengte (m)	max qc [5; 0]m MPa	max qc [0; -5]m MPa	max qc [-5; -10]m Mpa	max qc [-10; -15]m Mpa	max qc [-15; -20]m Mpa	max qc [-20; -25]m Mpa
Fugro	S1	58652.6	438281.8	5.42			21	33	27	59	26	21
	S2	58656.1	438271.6	5.44			23	35	27	44	32	18
	S3	58659.9	438261.2	5.24			18	38	27	53	34	27
	S4	58663.7	438250.7	5.29			21	33	29	40	29	23
	S5	58643	438278.6	5.23			18	33	30	46	26	21
	S6	58646.7	438268.3	5.27			21	32	26	49	31	26
	S7	58650.4	438257.8	5.33			14	42	35	30	28	19
	S8	58654.1	438247.6	5.43			21	33	30	46	27	17
	S9	58633.6	438275.0	5.17			18	33	26	47	29	21
	S10	58637.4	438264.8	5.15			24	31	24	52	28	26
	S11	58640.9	438254.5	5.18			25	36	22	46	24	24
	S12	58644.7	438244.1	5.39			27	30	23	45	27	20
	MAX											
Gemeente Rotterdam	S13	58595.15	438259	5.06	-21.04	26.1	25	22	29	30	29	0
	S14	58596.74	438254.2	5.08	-21	26.08	28	28	22	52	28	0
	S15	58590.34	438257.3	5.07	-21.03	26.1	24	30	29	43	28	0
	S16	58592.02	438252.6	5.04	-21.06	26.1	28	29	28	32	28	18
	S17	58585.68	438255.7	5.03	-21.07	26.1	22	20	30	42	30	28
	S18	58587.36	438250.9	5	-21.1	26.1	20	31	25	34	28	28
	S19	58580.94	438254	5.05	-21.05	26.1	24	20	32	32	31	18
	S20	58582.6	438249.3	5.03	-21.07	26.1	22	30	22	51	28	18
	S21	58576.22	438252.3	5.03	-21.07	26.1	26	30	22	41	30	16
	S22	58577.86	438247.6	5.03	-21.07	26.1	24	16	30	38	30	30
	MAX											
Van der Straaten	S23	58622.18	438268.1	5.15	-20.024	25.174	25	26	24	44	29	0
	S24	58623.51	438264.3	5.11	-19.899	25.009	25	31	26	44	28	0
	S25	58618.32	438266.8	5.11	-20.054	25.164	24	27	27	45	32	0
	S26	58619.68	438263.0	5.11	-20.035	25.145	24	28	21	47	26	0
	S27	58614.67	438265.3	5.11	-20.046	25.156	22	28	25	42	28	0
	S28	58615.89	438261.7	5.12	-20.047	25.167	20	26	26	38	30	0
	S29	58610.83	438264.0	5.12	-20.047	25.167	16	28	32	33	30	0
	S30	58612.12	438260.3	5.13	-19.797	24.927	20	31	27	33	28	0
	S31	58607.11	438262.6	5.06	-19.941	25.001	15	29	26	33	28	0
	S32	58608.35	438259.0	5.07	-19.888	24.958	17	30	29	34	29	0
	MAX											

B.3 Soil profile S14

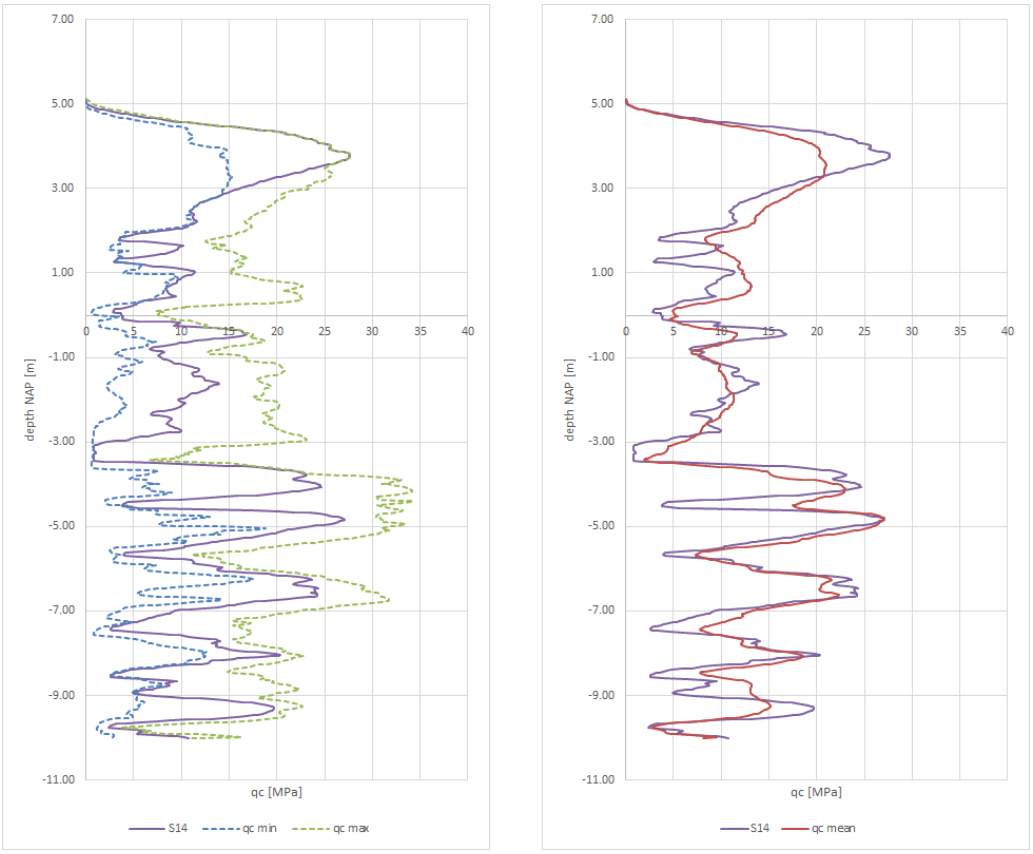

Figure 53: Soil Profile S14 - Cone resistance found in-situ compared to (a) minimum and maximum (b) mean

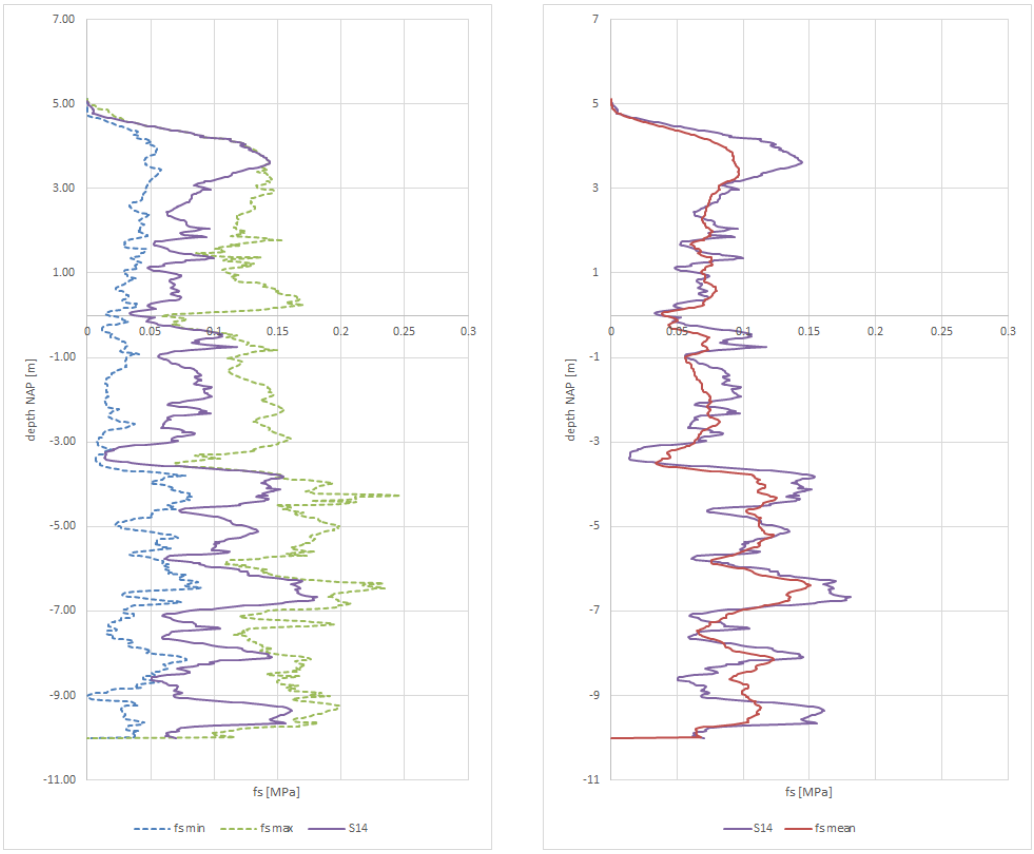

Figure 54: Soil Profile S14 - Sleeve friction found in-situ compared to (a) minimum and maximum (b) mean

B.4 Relative densities

Lunne		
Re	Rn	Kind:
#DIV/0!	#DIV/0!	
93.92	73.92	Dense
122.19	102.19	Dense
135.41	115.41	Dense
135.60	115.60	Dense
133.41	113.41	Dense
127.05	107.05	Dense
117.01	97.01	Dense
106.49	86.49	Dense
96.37	76.37	Dense
86.95	66.95	Dense
83.66	63.66	Medium dense
76.26	56.26	Medium dense
49.28	29.28	Loose
71.24	51.24	Medium dense
45.78	25.78	Loose
69.17	49.17	Medium dense
67.94	47.94	Medium dense
62.48	42.48	Medium dense
51.39	31.39	Loose
28.77	8.77	Loose
53.72	33.72	Medium dense
78.80	58.80	Medium dense
61.49	41.49	Medium dense
53.03	33.03	Medium dense
62.05	42.05	Medium dense
66.65	46.65	Medium dense
69.94	49.94	Medium dense
62.24	42.24	Medium dense
57.73	37.73	Medium dense
51.86	31.86	Loose
55.81	35.81	Medium dense
32.11	12.11	Loose
-25.26	-45.26	Loose
19.18	-0.82	Loose
81.39	61.39	Medium dense
85.28	65.28	Medium dense
82.19	62.19	Medium dense
43.43	23.43	Loose
78.41	58.41	Medium dense
66.76	46.76	Medium dense
56.98	36.98	Medium dense
40.42	20.42	Loose

Figure 55: Relative Density as found by Lunne

C Experiment Design

C.1 Supplement: Pile Design - GRLWeap

For Drivability analysis in GRLWeap, the input parameters should be established. These consist of those for the Hammer, the Cushion, the pile itself and the soil characteristics The following paragraph elaborates on the assumptions made and the values adopted for as input for GRL Weap.

The pile material consists of steel, which means the specific weight equals 77.5 kN/m^3 and the elastic modulus can be changed accordingly. The section area for a tubular open ended pile consists of the annular area as determined using the wall thickness (t) and the pile diameter. The programme calculates the perimeter accordingly. The number of sections can be established according to the provided pile geometry and cross-section. Other input parameters included are the length and the penetration depth.

Hammer parameters are type, efficiency and stroke. The weight of the hammer is accounted for when hammer type is put in. Additionally, hammer housing and sleeve/anvil housing weight should be accounted for. They are considered in the assembly weight as Hammer Override data. This assembly weight is a dead weight since it is not lifted up to generate the blow. It thus contributes to the self-penetration achieved before pile driving. The anvil is picked based on the available pile diameter (=48 inch): Hydrohammer® S-/SC-types anvil housing, pile guiding. The weight of the anvil equals 4.4 tons. Anvil housing and connection ring weights are added to the hammer assembly weight and depend on the hammer that is chosen. In this case, the anvil is compatible with hydrohammer S-30/40, S70-90, S-120/150 and S-200/280/350. Efficiency could theoretically be established as equal to 1 but is more likely established at 0.95. This can be appointed to energy loss in the force transfer. Stroke depends on the selected hammer, on which will be elaborated in the following subsection.

For the cushion information, coefficient of restitution (C.O.R.) is an input parameter describing the decay of the energy used for pile installation per blow. For conventional pile installation this value is taken equal to 0.85. Helmet (anvil) weight is established based on the hammer that is picked which is calibrated to the pile diameter. The stiffness of the cushion is equal to the pile stiffness for conventional pile installation.

The input soil parameters are Quake = 2.54 mm and Damping = 0.5 s/m for the toe, 0.25 s/m for the shaft (likely for sand). Additionally, the available CPT information is put in.

Input parameter				**Remarks:**
Assembly weight	Anvil connection ring weight	875	kg	
	Anvil housing	1100	kg	
	Hammer housing	2400	kg	
Ram weight		1600	kg	Accounted for in WEAP directly
Anvil weight		4400	kg	Helmet weight

Table 10: Composition hammer weight S-30

Input parameter				**Remarks:**
Assembly weight	Anvil connection ring weight	825	kg	
	Anvil housing	1100	kg	
	Hammer housing	5000	kg	
Ram weight		3500	kg	Accounted for in WEAP directly
Anvil weight		4400	kg	Helmet weight

Table 11: Composition hammer weight S-70

	Interval [m]	t [mm]	Interval [m]	t [mm]
Top	9	25	11.4	25
Bottom	3	50 and 40	0.6	50 and 40

Table 12: Further iteration Pile Geometry

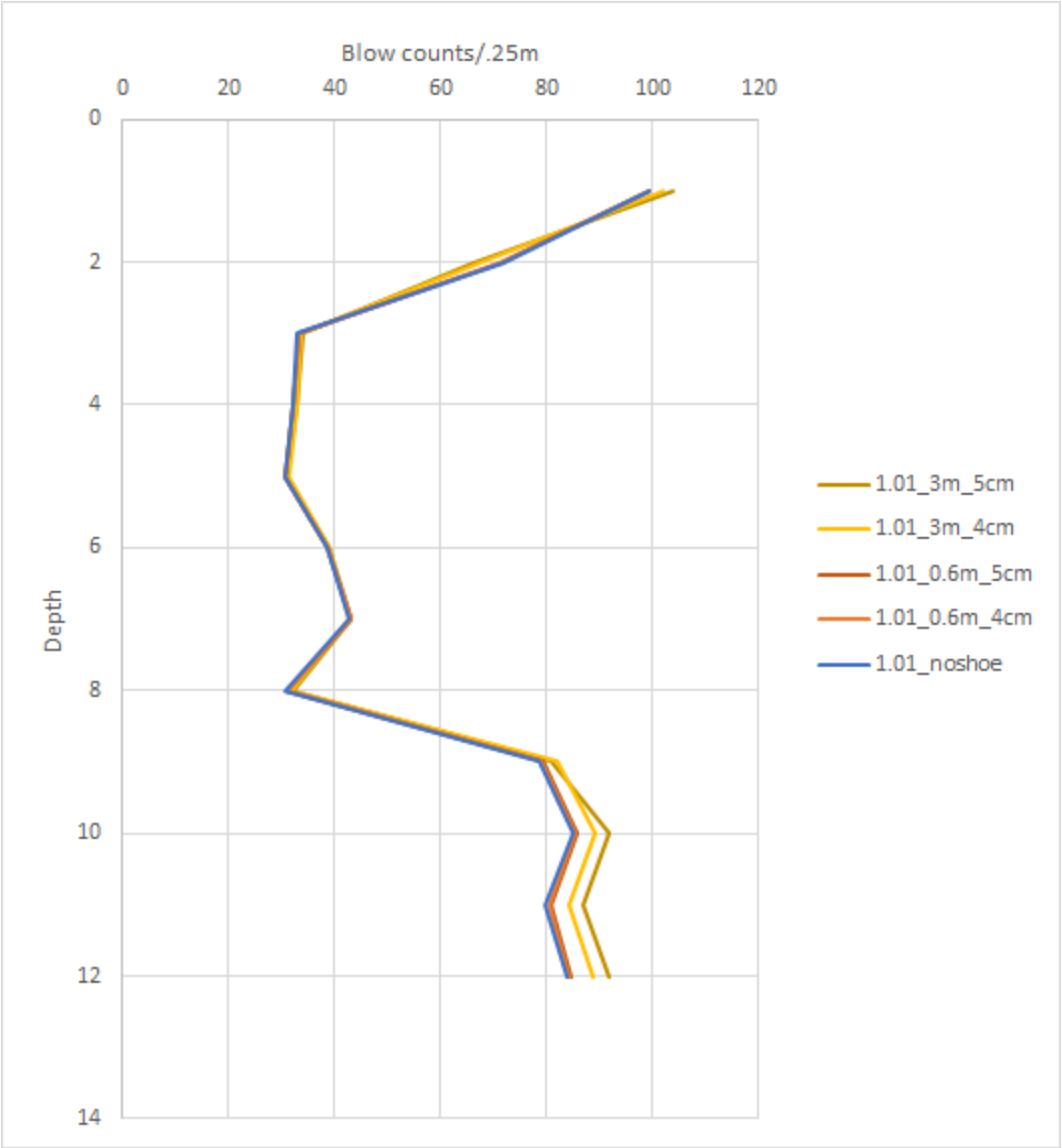

Figure 56: S-70 hammer half energy - Blowcounts obtained for different Pile Geometries

C.2 GRLWeap SRD Input

Soil (S/C)	Depth (m)	q_c or q_t (Kpa)	f_s (Kpa)	γ (KN/m^3)	σ'_{v0} (Kpa)	σ'_v/patm	q_{tip} (Kpa)	K	δ (DEG)	f_{si} (Kpa)	k	f_{res} (Kpa)	Setup Fact
S	0.00	0.00	0.00	0.00	0.00	0.00	0.00	0.00	29.00	0.00	0.31	0.00	5.00
S	0.25	2729.34	5.39	18.00	4.50	0.05	1474.75	5.35	29.00	13.34	0.31	2.67	5.00
S	0.50	10163.34	32.62	18.00	9.00	0.09	6218.51	10.90	29.00	54.38	0.42	10.88	5.00
S	0.75	19913.50	75.96	18.00	13.50	0.14	12852.91	15.01	29.00	112.31	0.48	22.46	5.00
S	1.00	24562.77	117.91	18.00	18.00	0.18	15608.80	14.41	29.00	143.81	0.46	28.76	5.00
S	1.25	27006.31	134.80	18.00	22.50	0.23	16726.81	13.05	29.00	162.77	0.43	32.55	5.00
S	1.50	25544.46	139.00	18.00	27.00	0.27	15086.02	10.53	29.00	157.65	0.38	31.53	5.00
S	1.75	21276.33	113.62	18.00	31.50	0.32	11746.41	7.67	29.00	133.97	0.32	26.79	5.00
S	2.00	17222.77	91.24	18.00	36.00	0.36	8874.71	5.53	29.00	110.34	0.27	22.07	5.00
S	2.25	14019.42	84.03	19.12	40.78	0.41	6762.04	4.04	29.00	91.29	0.23	18.26	5.00
S	2.50	11519.54	72.46	18.87	45.50	0.45	5226.53	3.02	29.00	76.09	0.20	15.22	5.00
S	2.75	11221.36	67.37	18.78	50.19	0.50	4966.10	2.70	29.00	75.07	0.19	15.01	5.00
S	3.00	9646.02	82.20	18.95	54.93	0.55	4067.66	2.14	29.00	65.29	0.17	13.06	5.00
C	3.25	4659.30	72.37	18.53	59.56	0.60	2795.58	-	29.00	144.74	0.11	29.98	4.83
S	3.50	9312.75	62.11	18.62	64.22	0.64	3779.68	1.81	29.00	64.33	0.15	12.87	5.00
S	3.75	4665.94	83.72	18.69	68.89	0.69	1626.25	0.85	29.00	32.53	0.10	6.51	5.00
S	4.00	9654.83	58.09	18.55	73.53	0.74	3841.43	1.67	29.00	67.88	0.14	13.58	5.00
S	4.25	9731.16	68.70	18.75	78.22	0.78	3830.27	1.59	29.00	68.96	0.14	13.79	5.00
S	4.50	8650.95	68.60	18.70	82.89	0.83	3287.50	1.34	29.00	61.77	0.13	12.35	5.00
S	4.75	6511.75	60.94	18.46	87.51	0.88	2312.71	0.97	29.00	46.83	0.11	9.37	5.00
S	5.00	3491.81	43.06	17.82	91.96	0.92	1084.01	0.50	29.00	25.27	0.08	5.05	5.00
S	5.25	7472.45	54.39	18.38	96.55	0.97	2674.80	1.02	29.00	54.43	0.11	10.89	5.00
S	5.50	15766.62	95.81	19.32	98.88	0.99	6521.57	2.10	29.00	115.19	0.16	23.04	5.00
S	5.75	9682.43	95.12	19.12	101.16	1.01	3616.32	1.27	29.00	70.95	0.12	14.19	5.00
S	6.00	7683.02	65.21	18.60	103.31	1.03	2728.34	0.99	29.00	56.45	0.11	11.29	5.00
S	6.25	10141.69	71.38	18.81	105.52	1.06	3791.06	1.28	29.00	74.73	0.12	14.95	5.00
S	6.50	11769.54	87.07	19.09	107.79	1.08	4513.23	1.46	29.00	86.96	0.13	17.39	5.00
S	6.75	13149.58	90.12	19.18	110.08	1.10	5133.83	1.60	29.00	97.42	0.14	19.48	5.00
S	7.00	10663.12	90.76	19.10	112.36	1.12	3975.86	1.27	29.00	79.21	0.12	15.84	5.00
S	7.25	9482.91	77.95	18.88	114.58	1.15	3440.32	1.11	29.00	70.62	0.11	14.12	5.00
S	7.50	8101.00	70.81	18.71	116.76	1.17	2837.13	0.93	29.00	60.48	0.10	12.10	5.00
S	7.75	9207.98	66.96	18.70	118.93	1.19	3296.31	1.05	29.00	68.91	0.11	13.78	5.00
C	8.00	4677.46	70.47	18.50	121.06	1.21	2806.48	-	29.00	140.94	0.08	33.81	4.17
C	8.25	889.50	23.74	16.61	122.71	1.23	533.70	-	29.00	47.48	0.03	6.99	6.79
C	8.50	3280.89	70.77	18.37	124.80	1.25	1968.54	-	29.00	141.53	0.06	24.52	5.77
S	8.75	20329.75	112.09	19.59	127.20	1.27	8413.03	2.18	29.00	153.48	0.16	30.70	5.00
S	9.00	23080.08	144.39	19.93	129.68	1.30	9758.86	2.43	29.00	174.68	0.17	34.94	5.00
S	9.25	21378.83	142.82	19.89	132.16	1.32	8868.59	2.21	29.00	162.20	0.16	32.44	5.00
S	9.50	7006.86	127.26	19.33	134.49	1.34	2317.30	0.71	29.00	53.28	0.09	10.66	5.00
S	9.75	19628.27	83.72	19.25	136.80	1.37	7949.36	1.97	29.00	149.59	0.15	29.92	5.00
S	10.00	25341.85	116.41	19.72	139.23	1.39	10763.41	2.51	29.00	193.58	0.17	38.72	5.00
S	10.25	19303.00	128.00	19.73	141.66	1.42	7737.31	1.88	29.00	147.78	0.15	29.56	5.00
S	10.50	12057.98	102.78	19.29	143.99	1.44	4384.87	1.16	29.00	92.51	0.11	18.50	5.00

Figure 57: Input Parameters Weap calculated according to Alm Hamre, 2001

C.2.1 Revisiting Pile design after Maasvlakte tests

Input Parameters GRLWeap

Hammer parameters		
Efficiency	0.95	[-]
Stroke	1.88	m
Assembly Weight	42.9	kN

Cushion information		
C.O.R.	0.85	[-]
Helmet Weight	43.2	kN
Assembly Weight	42.9	kN

Pile parameters		
Length	12	m
Penetration	9	m
Section area	790.49	cm^2
Elastic Modulus	210000	MPa
Spec. Weight	77.5	kN/m^3
Toe Area	790.49	cm^2
Perimeter	3.83	m
Pile size	1220	mm

Soil Parameters					
Quake			**Damping**		
Shaft	2.5	mm	Shaft	0.25	s/m
Toe	2.5	mm	Toe	2.5	s/m

GRLWeap Blowcount Prediction

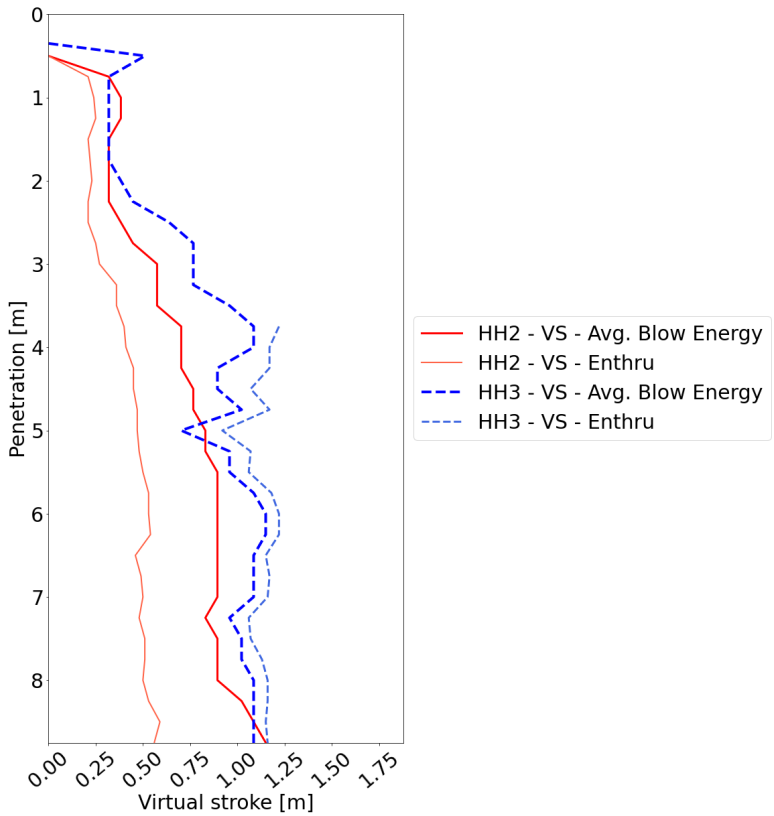

Figure 58: Virtual stroke comparison HH2 and HH3 during respective pile installation

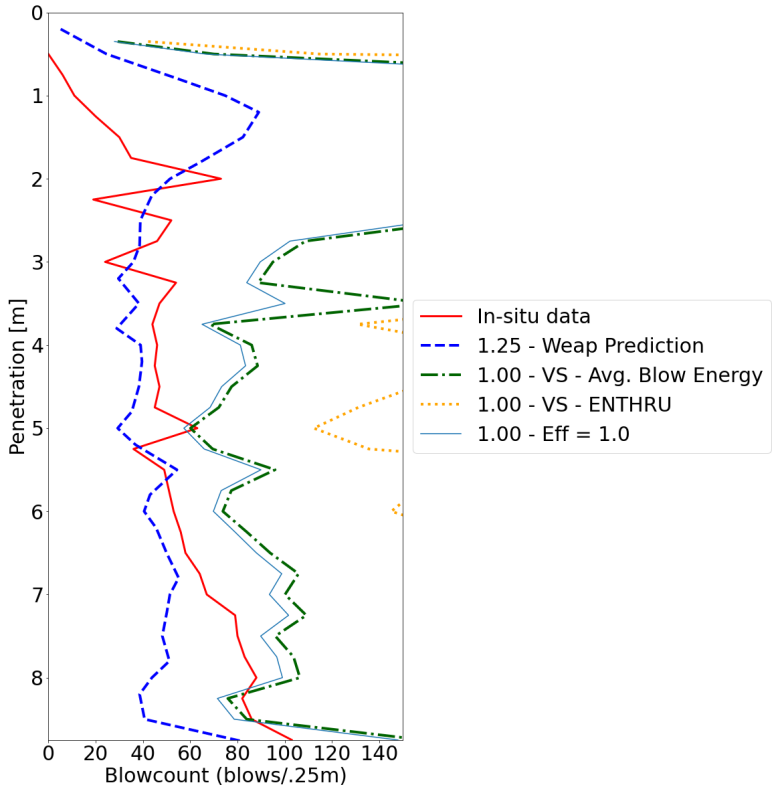

Figure 59: HH2 - Comparison of In-situ data with GRLWeap prediction (original vs. adjusted 'virtual' stroke (VS))

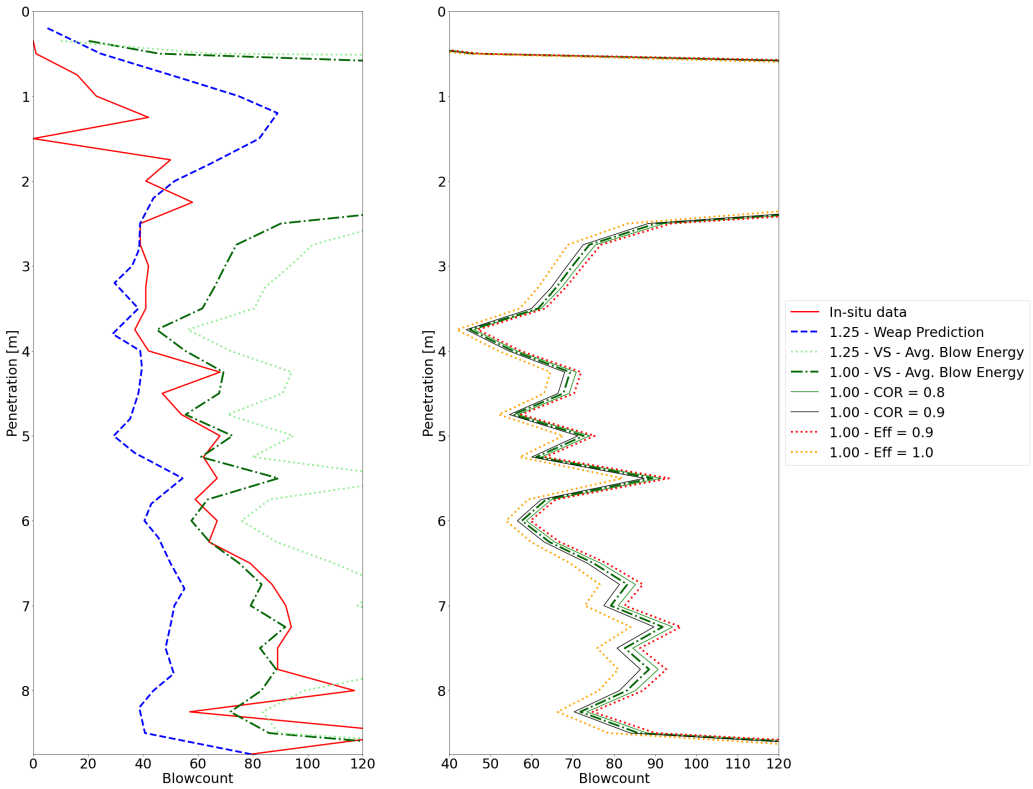

Figure 60: HH3 - (a) Comparison of In-situ data with GRLWeap prediction (original vs. adjusted 'virtual' stroke (VS)) (b) Parametric study, effect of adjusting C.O.R. and Efficiency (Eff)

HH3		Per 0.25m	Cumulatief	Dit is voor het totaal aantal slagen de Cumulatief		Per minuut	Dit is voor de totale energie/het aantal slagen dus het gemiddelde per blow			Virtual stroke willen we bepalen per blow over de energie die er per stuk in gestopt is.				
Time [Date[Y/M/D] Time]	Penetratio	Blow count	Blow count total	Blow energy [kJ]	Blow energy total [kJ]	Blow rate average [min-1]	Blow energy average [kJ]	Pump Pressure [bar]	Pump Flow [%]	Virtual stroke	EMX (avg)	EMX (MAX)	Virtual stro	Weap Enth
18-11-2022 09:42	0.35	0	0	0	0	0	0	0	0	0.51				5.2
18-11-2022 09:44	0.5	1	1	8	8	13	8	191	19	0.51	6.866346783	6.87		5.1
18-11-2022 09:45	0.75	16	17	81	89	72	5	200	20	0.32	12.14285714	19.00		3.3
18-11-2022 09:45	1	23	40	114	203	96	5	210	20	0.32				3.3
18-11-2022 09:46	1.25	42	82	200	403	98	5	208	20	0.32				3.3
18-11-2022 09:47	1.5	0	82	0	403	0	0	0	0	0.32	Oftwel een foutje in het doortellen van de stopjes en startjes			3.3
18-11-2022 09:48	1.75	50	132	232	635	97	5	205	20	0.32				3.3
18-11-2022 09:49	2	41	173	253	888	106	6	222	24	0.38				3.9
18-11-2022 09:49	2.25	58	231	402	1290	110	7	231	26	0.45				4.5
18-11-2022 09:50	2.5	39	270	391	1681	95	10	229	29	0.64				6.4
18-11-2022 09:50	2.75	39	309	456	2137	85	12	225	30	0.77				7.7
18-11-2022 09:51	3	42	351	494	2631	85	12	225	30	0.77				7.7
18-11-2022 09:51	3.25	41	392	489	3120	84	12	226	30	0.77				7.7
18-11-2022 09:52	3.5	41	433	634	3754	80	15	254	34	0.96				9.5
18-11-2022 09:52	3.75	37	470	621	4375	79	17	267	35	1.09	12.19728938	12.71	1.22	12.3
18-11-2022 09:53	4	42	512	711	5086	79	17	268	35	1.09	11.72799994	17.73	1.17	11.5
18-11-2022 09:53	4.25	68	580	922	6008	117	14	290	35	0.89			0.00	11.5
18-11-2022 10:06	4.5	47	627	657	6664	87	14	279	33	0.89	10.70130265	11.27	1.07	10.6
18-11-2022 10:06	4.75	54	681	885	7549	87	16	313	36	1.02	11.74738733	12.57	1.17	11.5
18-11-2022 10:07	5	68	749	766	8315	123	11	276	33	0.70	9.177209359	22.44	0.92	9.1
18-11-2022 10:08	5.25	62	811	924	9239	93	15	320	35	0.96	10.74470826	10.97	1.07	10.5
18-11-2022 10:09	5.5	67	878	996	10235	94	15	326	39	0.96	10.6294113	11.09	1.06	10.5
18-11-2022 10:09	5.75	59	937	1001	11235	90	17	322	40	1.09	11.84798499	12.86	1.18	11.6
18-11-2022 10:10	6	67	1004	1180	12416	89	18	324	44	1.15	12.20378163	12.65	1.22	12
18-11-2022 10:11	6.25	64	1068	1126	13541	89	18	326	45	1.15	12.16451265	12.52	1.22	12
18-11-2022 10:12	6.5	79	1147	1310	14852	89	17	305	36	1.09	11.51941135	12.24	1.15	11.3
18-11-2022 10:13	6.75	87	1234	1454	16306	85	17	284	35	1.09	11.73024478	12.92	1.17	11.5
18-11-2022 10:15	7	92	1326	1530	17836	87	17	269	36	1.09	11.61823106	20.22	1.16	11.4
18-11-2022 10:16	7.25	94	1420	1423	19259	90	15	257	35	0.96	10.55650494	11.30	1.06	10.4
18-11-2022 10:20	7.5	89	1509	1417	20676	81	16	234	36	1.02	10.73918071	21.70	1.07	10.5
18-11-2022 10:21	7.75	89	1598	1432	22109	87	16	258	36	1.02	11.32425411	17.83	1.13	11.1
18-11-2022 10:37	8	117	1715	1993	24102	82	17	250	37	1.09	11.60818855	12.17	1.16	11.4
18-11-2022 10:38	8.25	57	1772	981	25083	83	17	252	37	1.09	11.57816271	12.03	1.16	11.3
18-11-2022 10:39	8.5	138	1910	2362	27445	83	17	252	37	1.09	11.52945828	12.31	1.15	11.2
18-11-2022 10:40	8.75	79	1989	1364	28810	83	17	253	37	1.09	11.5612586	12.16	1.16	11.3
18-11-2022 10:42	9	104	2093	1809	30619	82	17	253	37	1.09	12.03669511	16.98	1.20	11.7

Figure 61: HH3 - Enthru research, comparing EMX and result virtual stroke from Weap

C.3 Supplement: Transducer design

C.3.1 Information Strain Gauge configuration

The full, half or quarter bridge configurations are dependent on the number and orientation of active elements in the Wheatstone bridge. The Wheatstone bridge is a circuit construction of known electrical resistances, used to measure an unknown resistance, which in this case is caused by the change in strain experienced by the foil strain gauges. The unknown resistance (e.g. strain gauge R3) is connected in parallel with the fixed resistors (R1-R2) and in series with another fixed resistor (R4). The current over both branches (R1-R2 and R3-R4) is the same. By measuring the change in voltage caused by applied strain (and consequential resistance) in R3, following Ohm's Law and applying a calculation factor specified by the manufacturer, the wanted measurement can be obtained. By using the Wheatstone bridge configuration, errors in measurements are minimized.

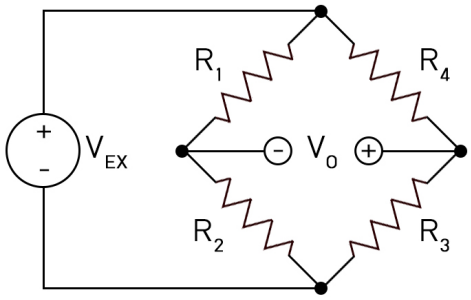

Figure 62: Wheatstone Bridge configuration

Quarter bridge
Quarter bridge strain gauges measure axial or bending strain. Additionally, a half-bridge configuration would be needed to complete the Wheatstone bridge configuration. These parts are fixed resistors located in the external control device, thus is applicable in situations where the distance to where the measurement needs to be obtained is within practical limit distance.

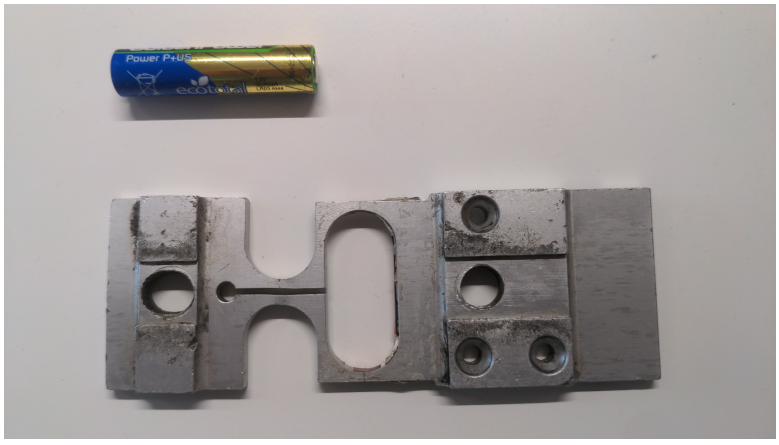

Figure 63: Full bridge strain module - AAA battery for scale

Full bridge module
A full bridge strain gauge has four foil strain gauges actively measuring on the deforming module. Two bolts keep the structure in place on the pile. The suspension between the two bolts make for a longer distance over which strain is measured, which cause more damping of the measurement, subsequently causing a higher signal to noise ratio (SNR). The shape ensures that the signal is amplified in the places of the foil gauges of which four are present. The presence of four allows for minimization of temperature effects, all within one module. Some cons may be that high-frequency effects are registered less well and that the material has an eigenfrequency, which may be disturbing measurements. Sensitivity and accuracy increase in full bridge configuration, but so do costs.

Soil and Pore Pressure

ID	159301	159302	159303	159304	159305	159306	
Brand	TML	TML	TML	TML	TML	TML	
Type	KPE-1MPB	PDB-2MPB	KPE-2MPB	PDB-3MPB	KPE-2MPB	PDB-3MPB	
Serial No.	EFJ221006	CYL221004	EFK221001	CYM221002	EFK221003	CYM221003	
Input	1	2	2	3	2	3	MPa
Output	1017	820	1002.5	918	1017	950	μV/V
Excitation	10	10	10	10	10	10	V
Rated outp.	0.01017	0.0082	0.010025	0.00918	0.01017	0.0095	V
Scale	98.3284	243.9024	199.5012	326.7974	196.6568	315.7895	MPa/V
Zero Balance	-230	640	610	-450	280	1430	-
	-0.11	0.78	0.61	-0.74	0.28	2.26	MPa

Table 13: Taken from 'Soil Sensor Calibration Data.xls' by Arjan Roest, IQIP

PileName:	BP1	BP2	BP3	BP4	BP5	HH1	HH2	HH3	V1	V2	V3
PorePressure_LVL3			0.8626	0.9054		0.7549	0.895	0.7744			
PorePressure_LVL4			-0.7411	-0.8439		-0.689	-0.8471	-0.7173			
PorePressure_LVL5			1.2673	1.3174		1.3267	1.3444	1.2942			
SoilPressure_LVL3			-0.1123	-0.1127		-0.1138	-0.1137	-0.1127			
SoilPressure_LVL4			0.6975	0.6968		0.6958	0.6947	0.6968			
SoilPressure_LVL5			0.415	0.4158		0.4136	0.4165	0.4158			

Table 14: Taken from 'Logbook.xls', tab Sensor Offset Correction by Arjan Roest, IQIP

D Experiment Execution

Figure 64: Maasvlakte 2 - Locatie In-situ test

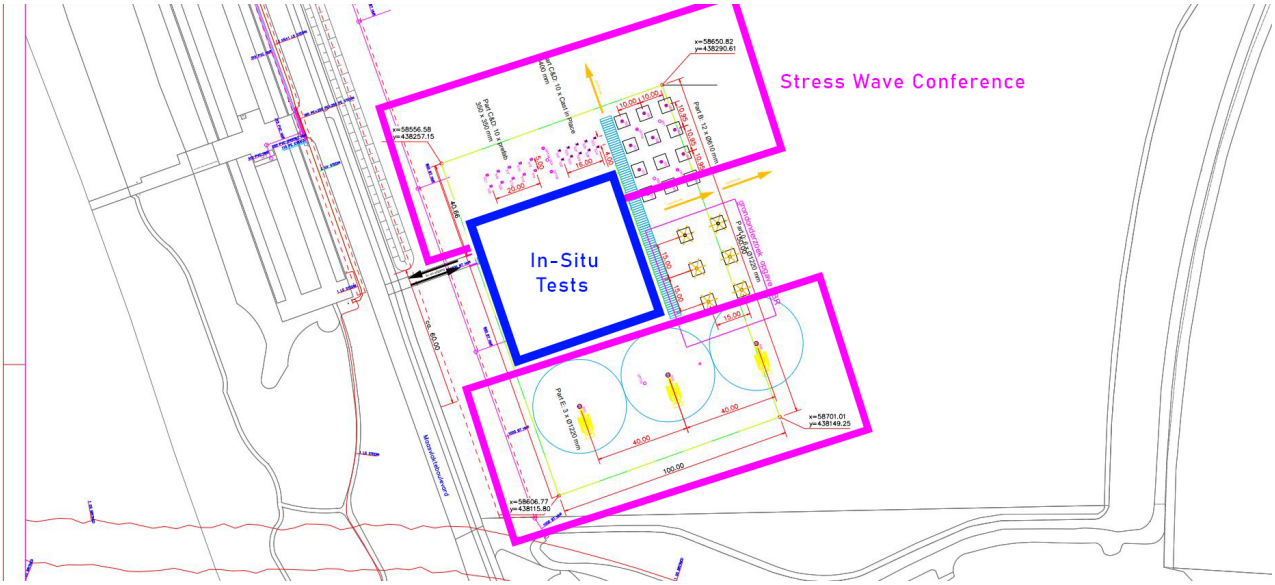

Figure 65: Location with respect to the Site Investigation done for the Stress Wave Conference 2022

E Data Processing

The following Chapter elaborates on the steps taken in the data processing phase. The raw data is processed in Matlab by Arjan Roest, IQIP. Further elaboration and visualisation is performed by Charlotte Stokman in Python. Any assumptions done will be elaborated below.

E.1 Time and pile penetration

The pile penetration [m] and UNIXTime [s] are the base of all the datasets, having the measurements ordered for all transducers.

Loading in the data
The data is loaded into the program and the names of the different pile installations are established. To control the size of datasets, the datasets are cut off a few seconds before the first blow registered by the hammer system. The datasets are not truncated at the end.

Read displacement measurements
The displacements measured with the Dimetix DPE-10-500 are asynchronized since the measurement of the laser displacement is digital and only registers when a significant change in displacement is measured. Since other measurements are done in a frequency of 10 kHz, values are supplemented in between the measurements done. The laser displacement measurements performed are then corrected from UTC (Coordinated Universal Time) to GMT+1 as is relevant for the Netherlands (+3600 seconds) and UNIXTime (also known as Epoch Time), which is the time in seconds after 1st of January 1970.

Corrections to the Laser displacements measured are necessary since the laser displacement device is very sensitive to movement of either anchor point or pivoting of the laser, which may have changed the anchor point to for example the fast frame, which was located around the pile to be installed at all time during the process. The following corrections are implemented: (1) Firstly, for different time intervals along the displacement measurement for one pile installation, interval specific offsets are implemented. This entails that measured trends in displacements are lifted to the peaks that are registered in that domain. This maintains the trend but displays the correct total displacement, satisfying the continuous increase as should be found in-situ. (2) Secondly, by considering a 'moving median', outliers are filtered.

The parameter pile penetration length is established based of the value measured by the laser. The reference from the laser until ground level is registered as refMeas. RefReal defined as the distance from pile tip to ground level. The sensor offset is calculated based on the total pile length and is described by the following formula, where sensor offset will become negative.

$$Sensoroffset = refReal - (Pilelength + RefMeas) \tag{27}$$

E.2 Retrieving Soil and Pore Pressures

Before retrieving the soil and pore pressures, the specifications of the transducers need to be considered. A rated output is defined by the manufacturer, as can be found in Appendix D, Table 13, in the range of 1000 $\frac{\mu V}{V}$. The output registered by the transducer is based on the voltage supply, which amounted to 10 Volts throughout the test. Based on the total capacity of the transducer, which is either 1, 2 or 3 MPa, the voltage registered by the transducer is scaled to display the registered pressure. The manufacturers establish a zero balance value per transducer. In addition to this, the factors affecting accuracy such as non-linearity, hysteresis and temperature are given in %RO when established.

Based on the average of the first values of soil or pore pressure measured before the laser device registers movement, the offset is defined. The offset throughout installations must be checked since a changing value may indicate drift. This could be indication of damage to the pressure transducers. The manufacturers state that also an exceeding excitation voltage compared to the recommended and allowable bridge excitation may cause drift. The found values are displayed in Appendix D, Table 14. For the resistance induced by temperature change or the length of the cable is not corrected.

During installation, a drift is registered

E.3 Noise filtering

During installation of piles in the Maasvlakte, different types of noise are present which are registered by the measuring devices. Different sources are for example the natural frequency of the pile, mechanical noise but also surrounding noises such as soil deformations, fluid pressures, heterogeneities found in the soil and machine installations. To filter the noise, a rolling mean function is implemented. No real data processing is performed in this thesis but the rolling mean is displayed in data visualizations to give a clearer indication of development of measurements.

pandas.DataFrame.rolling($window$**=100,** $center$**=True**.mean()
First, a rolling mean is introduced, meant to roughly filter out noise throughout the data. The $window$ input as integer is constant throughout the measurement devices (= 100). This is the fixed number of observations. By setting $center$ = True, the window labels are the center of the window index, meaning 50 values before and after are taken to establish the mean. All points are equally weighted so win_type is left at None as default.

A Fourier transform is performed on a domain of the original data where measured values are constant. The moment that this is true is in a driving stop. The analysis is performed on transducers only installed at level 5, which at the first driving stop can already be found below the ground level. The amplitudes which make up the signal (and noise) are visualized for the total radial pressure measurement device for both installation with Hydro- and Blue Piling hammer, see Appendix E.4. Noise can be found in both high and low frequencies (e.g. 50 Hz and multiples is caused by the 230 V of the power grid).

All the available data is partially imported and processed into datasets using first Matlab for the coarse selection and then Python for the more sensitive selection of data. For the latter, rolling mean and resampling was used to decrease the dataset size further.

E.4 Fourier Transform - Frequency Amplitude space

Soil Pressure

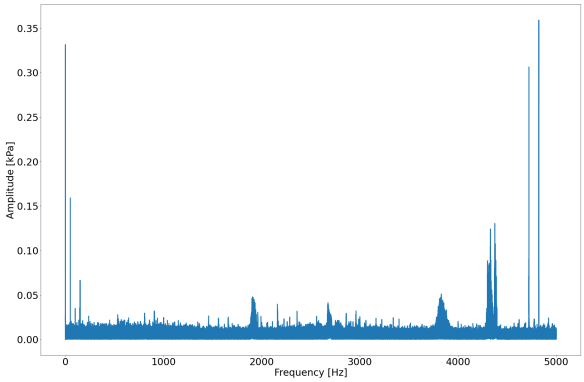

Figure 66: HH3 - Soil Pressure

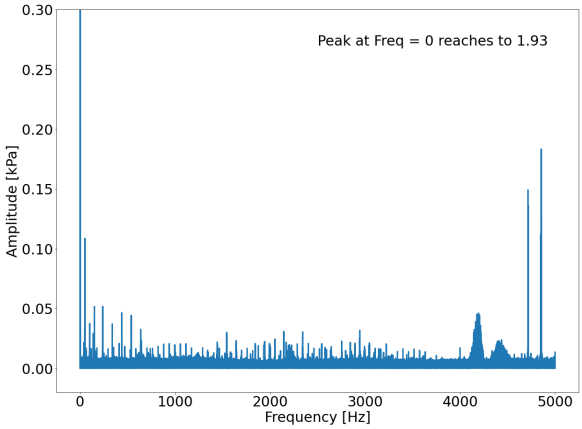

Figure 67: BP3 - Soil Pressure

Water pressure

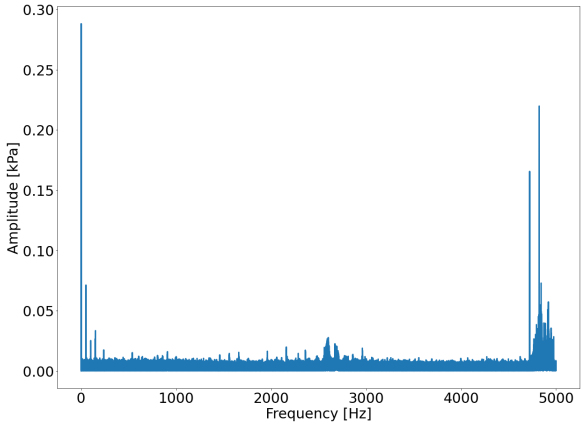

Figure 68: HH3 - Pore Pressure

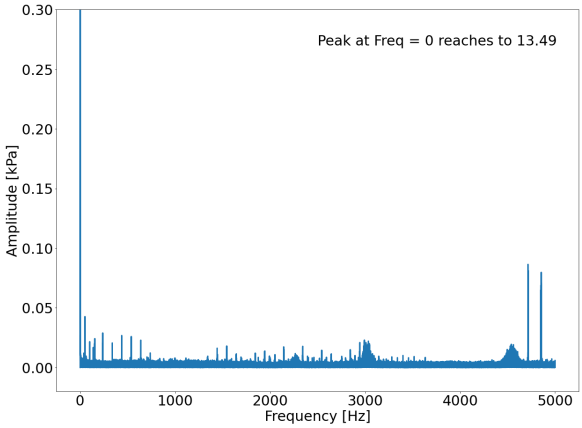

Figure 69: BP2 - Pore Pressure

Accelerations

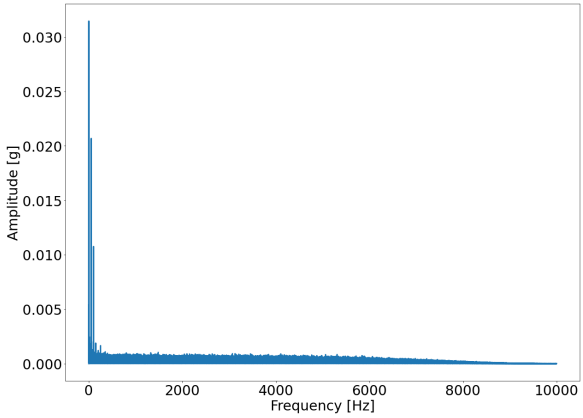

Figure 70: HH3

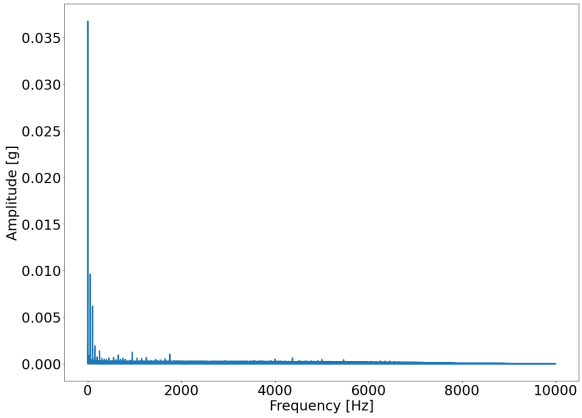

Figure 71: BP2

Strains

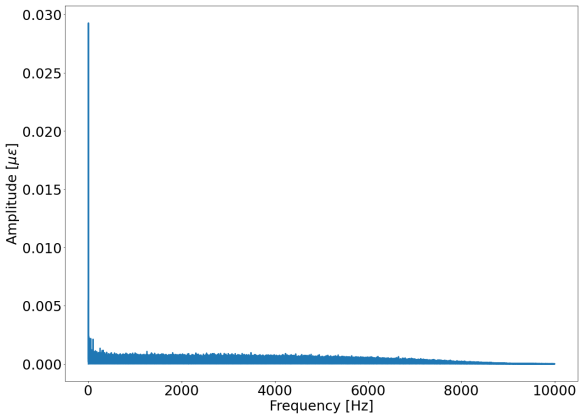

Figure 72: HH3

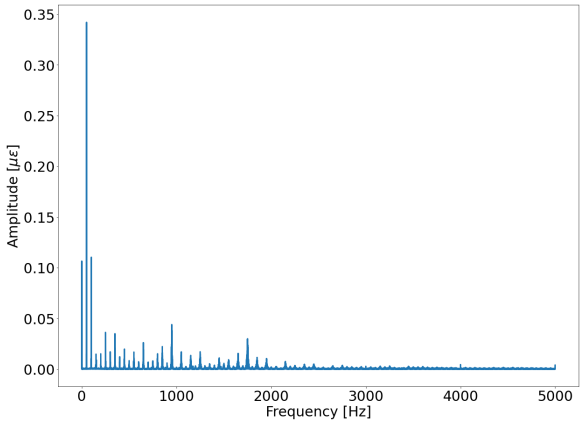

Figure 73: BP4

F Data Obtained

F.1 Driving stops

F.1.1 Table Overview

Hydro hammer installations

	Time [hh:mm:ss]	Epoch Time	From start [s]	Depth w.r.t. GL [m]
Start of driving 16/11	14:20:50	1668608450		0.4 m
			570	4.8 m
End of driving				5 m
Start of driving 17/11	09:06:00	1668675960		5 m
			240 - 400	
				7.8 m
End of driving				9 m

Table 15: Driving stops for HH1

	Time [hh:mm:ss]	Epoch Time	From start [s]	Depth w.r.t. GL [m]
Start of driving 23/11	15:57:00	1669219020		0.5 m
			330 - 550	2 m
			930 - 1620	4 m
			1710 - 1800	6 m
			To be determined	7.75 m
			To be determined	8 m
End of driving				9 m

Table 16: Driving stops for HH2

	Time [hh:mm:ss]	Epoch Time	From start [s]	Depth w.r.t. GL [m]
Start of driving 18/11	09:43:55	1668764635		0.4 m
			140 - 250	1.4 m
			580 - 1300	4.25 m
			1810 - 1870	7 m
			2010 - 2170	7.5 m
			2250 - 3120	7.75
End of driving			3500	9 m

Table 17: Driving stops for HH3

	Time [hh:mm:ss]	Epoch Time	From start [s]	Depth w.r.t. GL [m]
Start of driving 24/11	0	0		0.5 m
			unknown	2 m
			unknown	4 m
End of driving				6 m

Table 18: Driving stops for HH5 - *Dataset not available for processing*

Blue Piling installations

	Time [hh:mm:ss]	Epoch Time	From start [s]	Depth w.r.t. GL [m]
Start of driving 15/11	0	0		0.75 m
			unknown	4.5 m
			unknown	5.6 m
End of driving				5.8 m

Table 19: Driving stops for BP1 - *Dataset not available for processing*

	Time [hh:mm:ss]	Epoch Time	From start [s]	Depth w.r.t. GL [m]
Start of driving 21/11	15:05:55	1669043155		0.8 m
			220 - 1380	4.5 m
			2170 - 2800	7.75 m
			3000 - 3720	8.5 m
End of driving			4320	8.8 m

Table 20: Driving stops for BP2

	Time [hh:mm:ss]	Epoch Time	From start [s]	Depth w.r.t. GL [m]
Start of driving 21/11	10:15:30	1669025730		0.8 m
			280 - 760	4.45 m
			1390 - 1960	7.8 m
End of driving			2680	8.6 m

Table 21: Driving stops for BP3

	Time [hh:mm:ss]	Epoch Time	From start [s]	Depth w.r.t. GL [m]
Start of driving 23/11	08:47:40	1669193260		0.75 m
			40 - 220	2.2 m
			280 - 470	3.25 m
			540 - 1280	4.1 m
			1330 - 1480	4.25 m
			1640 - 1920	5 m
			2200 - 2440	6 m
			2740 - 2920	7 m
			3600 - 4240	7.75 m
			4720 - 4800	7.85 m
			4840 - 4920	7.85 m
End of driving			5020	7.9 m

Table 22: Driving stops for BP4

	Time [hh:mm:ss]	Epoch Time	From start [s]	Depth w.r.t. GL [m]
Start of driving 24/11	0	0		6.1 m
			unknown	7 m
			unknown	7.75
End of driving				7.85 m

Table 23: Driving stops for BP5 - *Dataset not available for processing*

F.1.2 Visualization

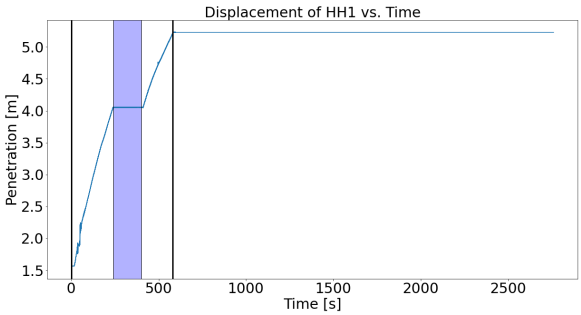

Figure 74: HH1 Start driving 16/1 14:20:50

Figure 75: BP1 position file not available

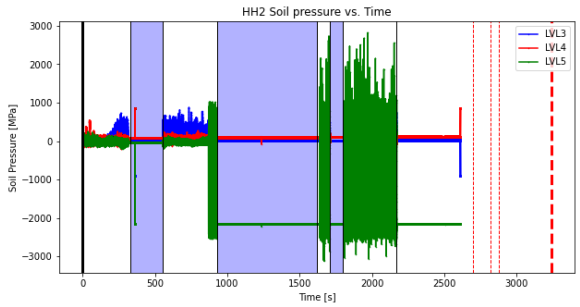

Figure 76: HH2 position file not available, based on soil pressures

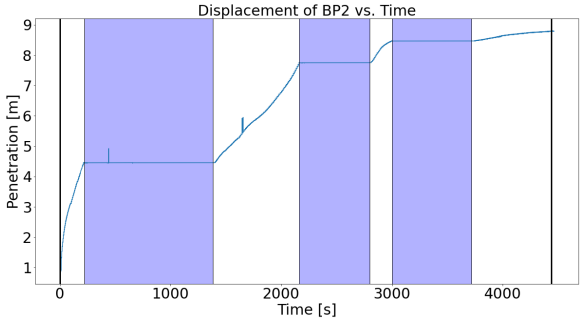

Figure 77: BP2

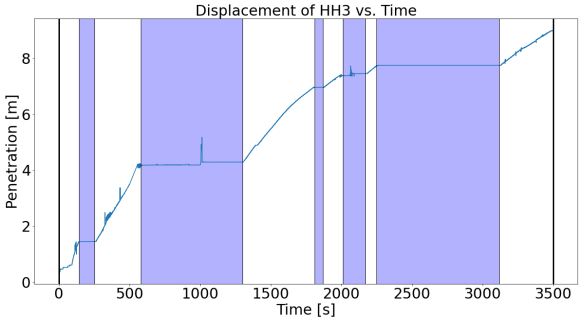

Figure 78: HH3

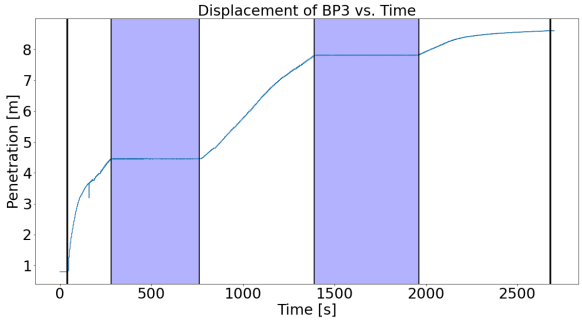

Figure 79: BP3

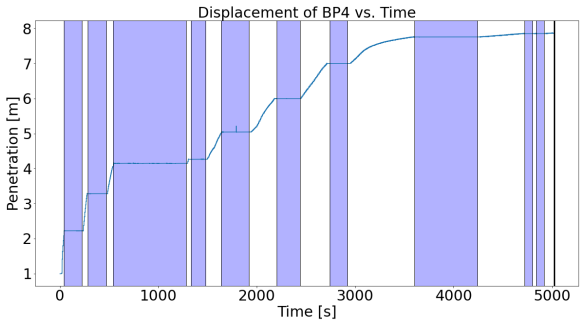

Figure 80: BP4

F.2 During installation - Blow investigation

F.2.1 Depth horizon 1.5 meters

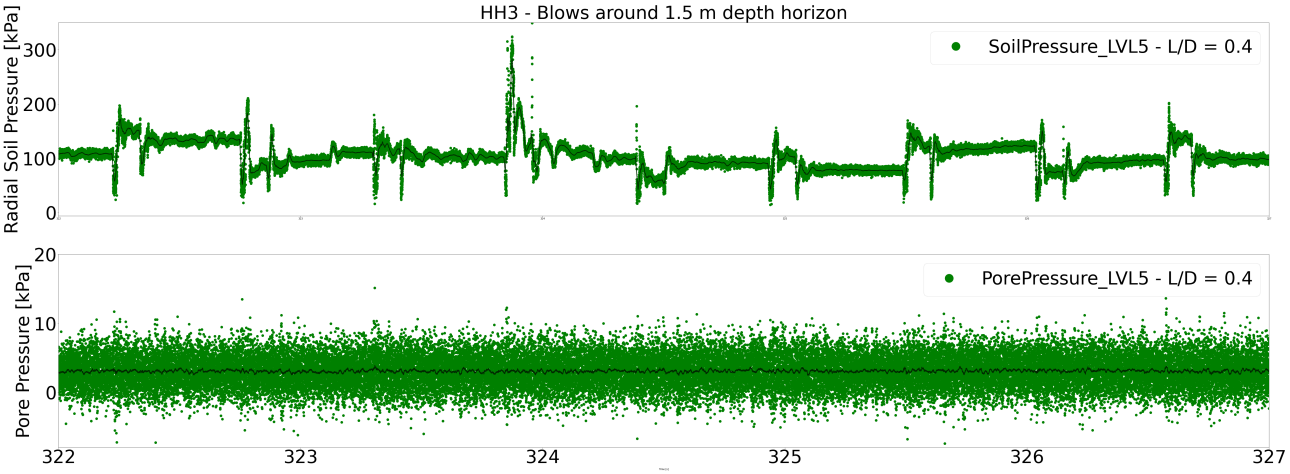

Figure 81

- Pore pressures are not changing since the sensor does not yet reach into ground water.
- The amount of blows needed to reach to this depth amounts to around 200.
- Other blows are more characteristic for the Hydrohammer.

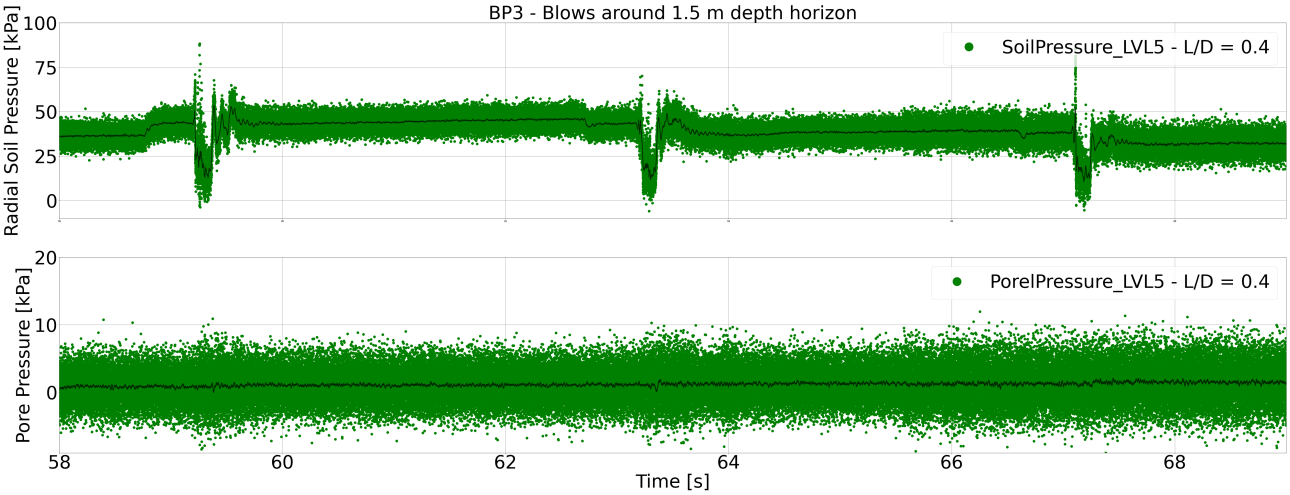

Figure 82

- Pore pressures are not changing since the sensor does not yet reach into ground water.
- The amount of blows needed to reach this depth for the Blue Piling hammer amounts to around 10.
- Other blows are more characteristic for the Blue Piling hammer.

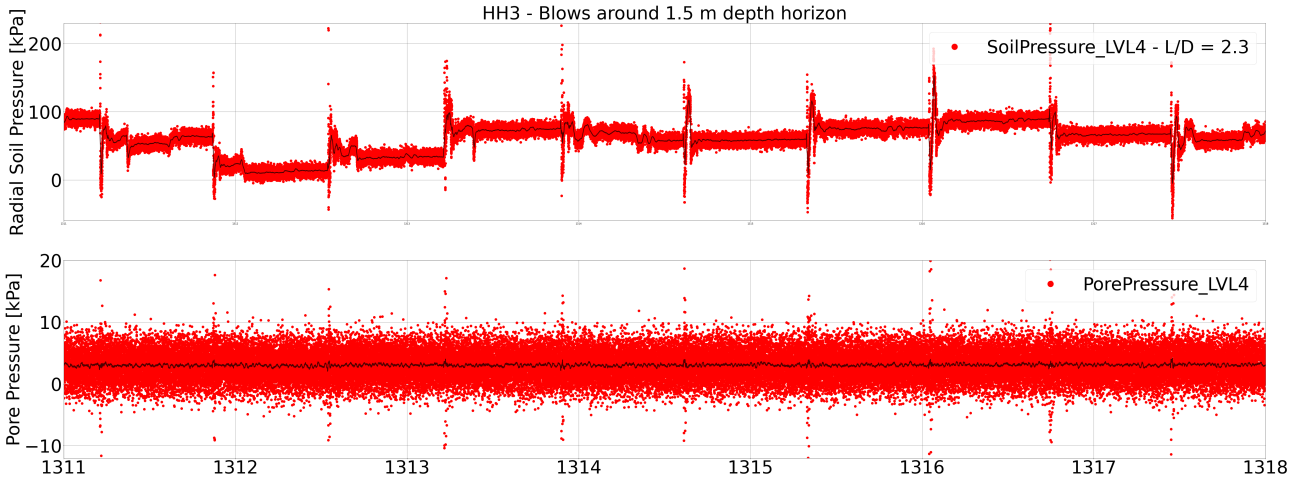

Figure 83

- The amount of blows needed to reach this depth is around 950 blows.
- No pore pressures generated since the sensor is the water for LVL4.

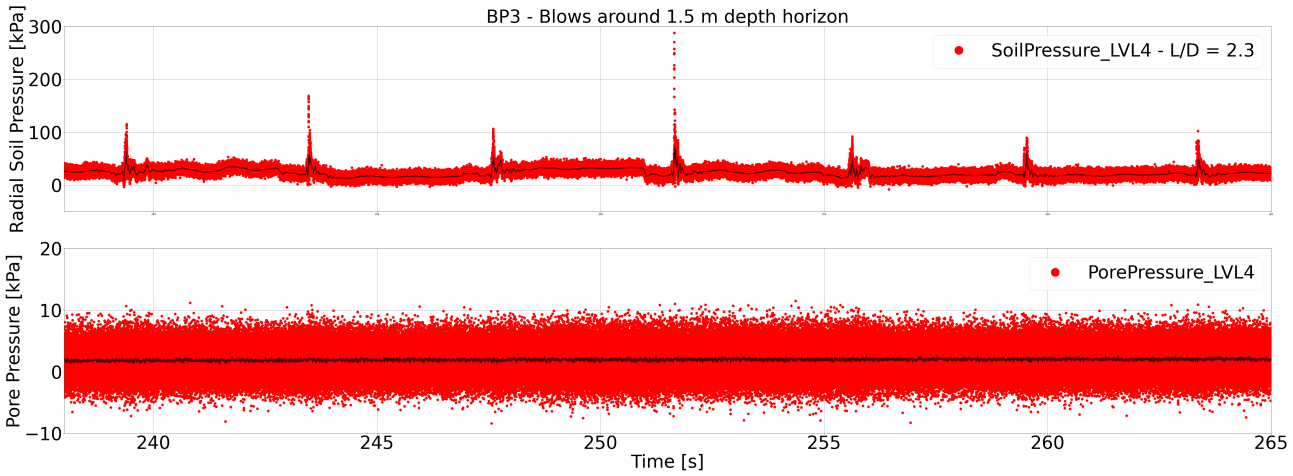

Figure 84

- No pore pressures generated since the sensor is the water for LVL4.

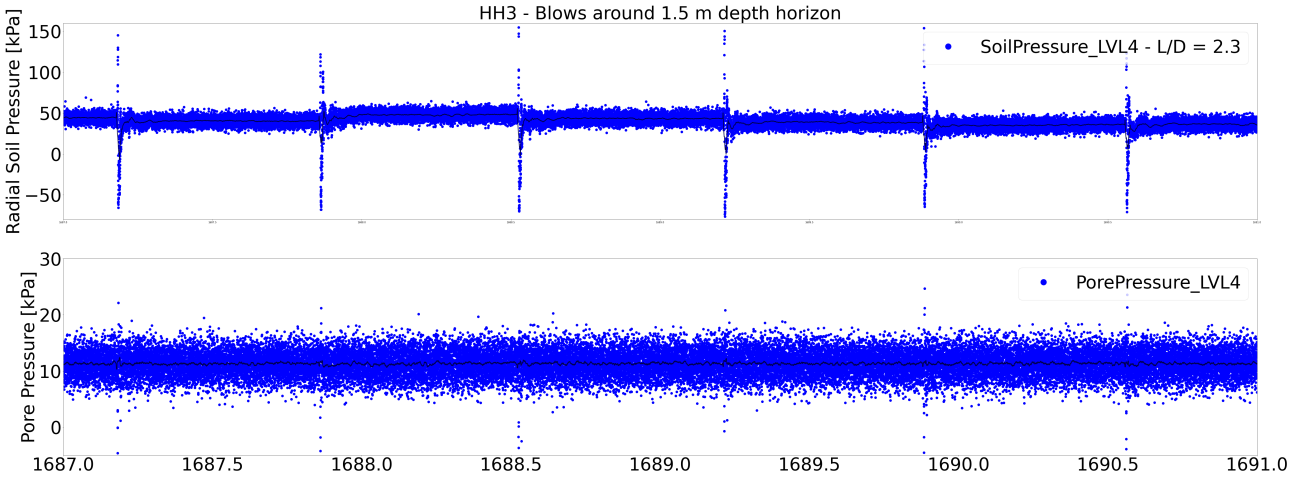

Figure 85

- Dip is strongly negative.

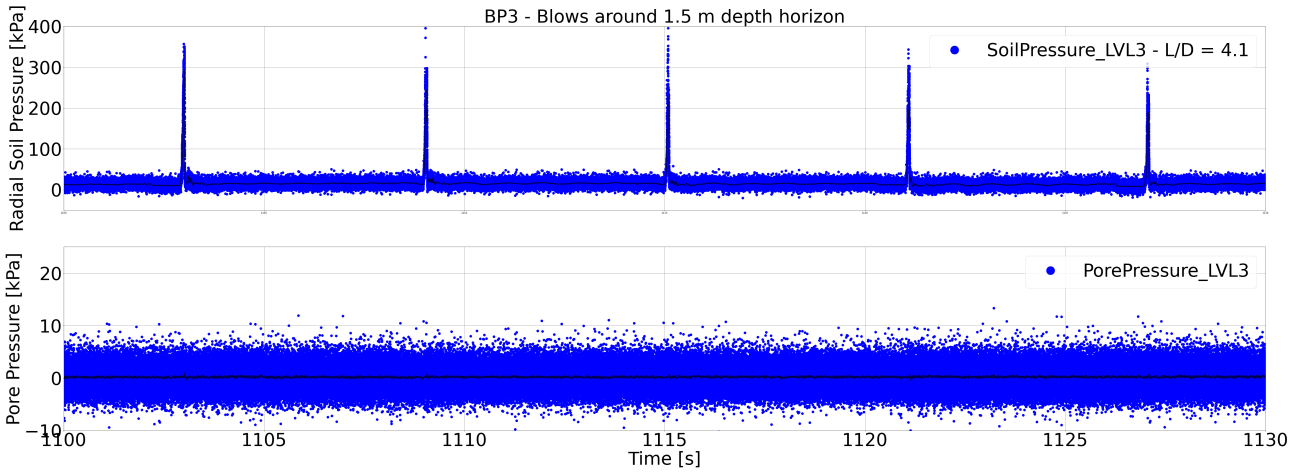

Figure 86

- No negative values in total radial pore pressures are measured for the value above water level.

F.2.2 Depth horizon 4 meters

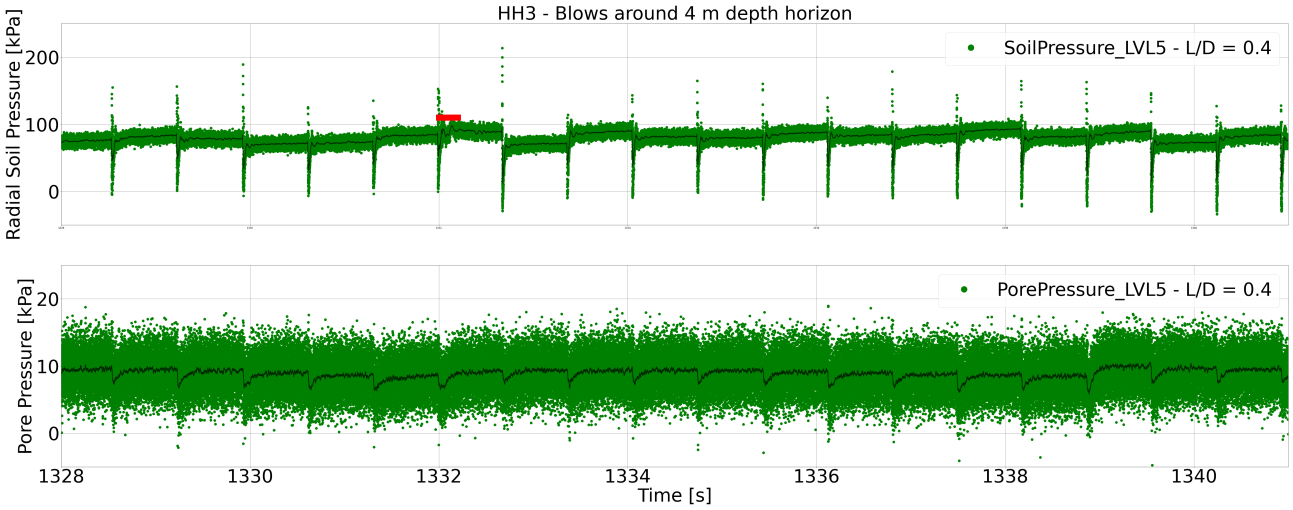

Figure 87

- At the moment of impact of HH3 installation, a small peak can be seen in the radial soil pressure measured. In combination with the other data from HH3 blows, Ken Gavin stated (Personal communication, 11th of May 2023) the data frequency is not high enough to clearly catch the strong peak caused by installation using the impact hammer. The peak is thus not found in the mean of the data indicated in solid line, but can be distinguished in the measurement readings indicated. After this peak, a strong dip in pressures is measured, followed by an increase in pressure again. The value of total radial pressure develops into a plateau value which strongly osscillates for 0.2 seconds (as indicated by the red marker, indicating loading time of the Hydrohammer). After this 0.2 seconds, the stationary' phase of the bow is reached where oscillations dampen out.

- In the pore pressures measured, a blow is characterized by a drop in pressure. After the dip, the pore pressure quickly increases and reaches a plateau which on average stays constant or increases slightly. The hydrostatic water pressure is around 20 kPa.

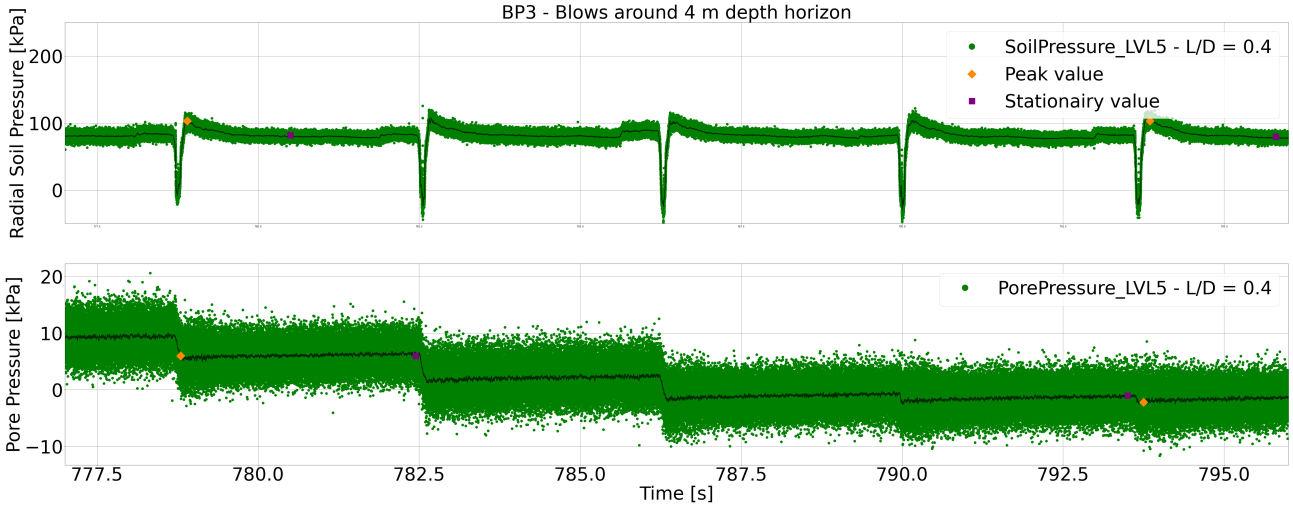

Figure 88

- At the moment of impact of BP3 installation, no peak is found in the soil pressures like in Hydrohammer installation, instead the soil pressures go straight into a strong dip, that reaches into negative pressures. After the strong dip, a peak is reached in the soil pressures, still showing slight oscillations in reaching the peak values. After the peak, the soil pressure value decreases and reaches a plateau that stays a constant value.

Right before the next blow is approached, there is a slight increase, forming a new plateau slightly higher than the previously reached value. This plateau is also visible for BP3 - LVL5 and LVL4 around 1.5 meter depth.

- The difference betweek peak and stationary value symbolizes dilation and amounts to around 20 kPa for this specific interval of blows.
- The hydrostatic pressure at this level equal 20 kPa. The water pressures recover minimally in the stationairy phase of the hammer blow. A blow causes a decrease in water pressure.

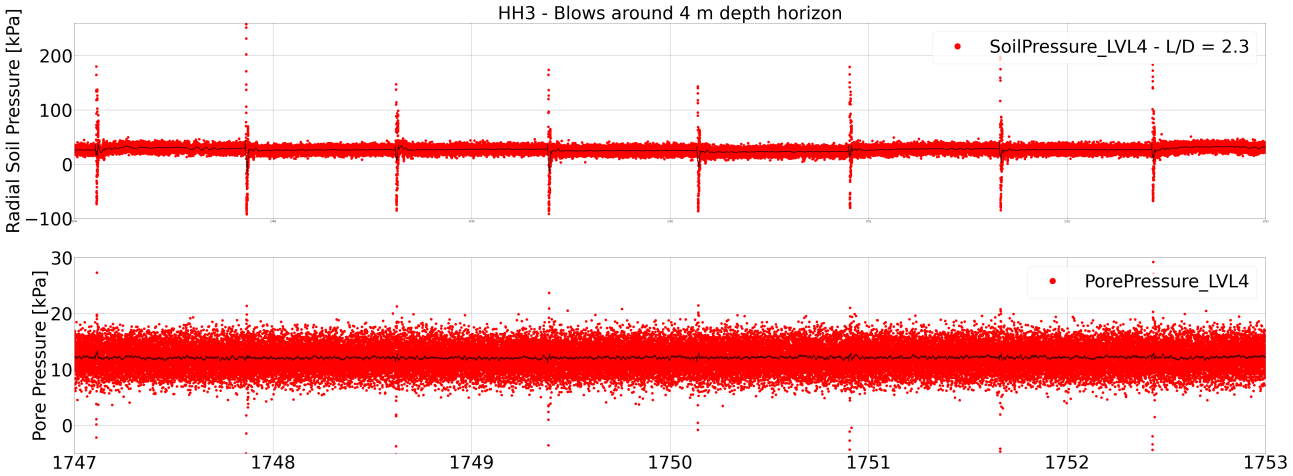

Figure 89

- Again, a small peak is measured in radial total pressure after which a strong dip takes place to negative pressures. Measurements spike up consistently.
- The pore pressures do not have a strong response to impact at the 4 meter horizon for conventional driving. This is where sand to silty sand can be found, see Chapter 3. Hydrostatic water pressure amounts to 20 kPa for this depth.

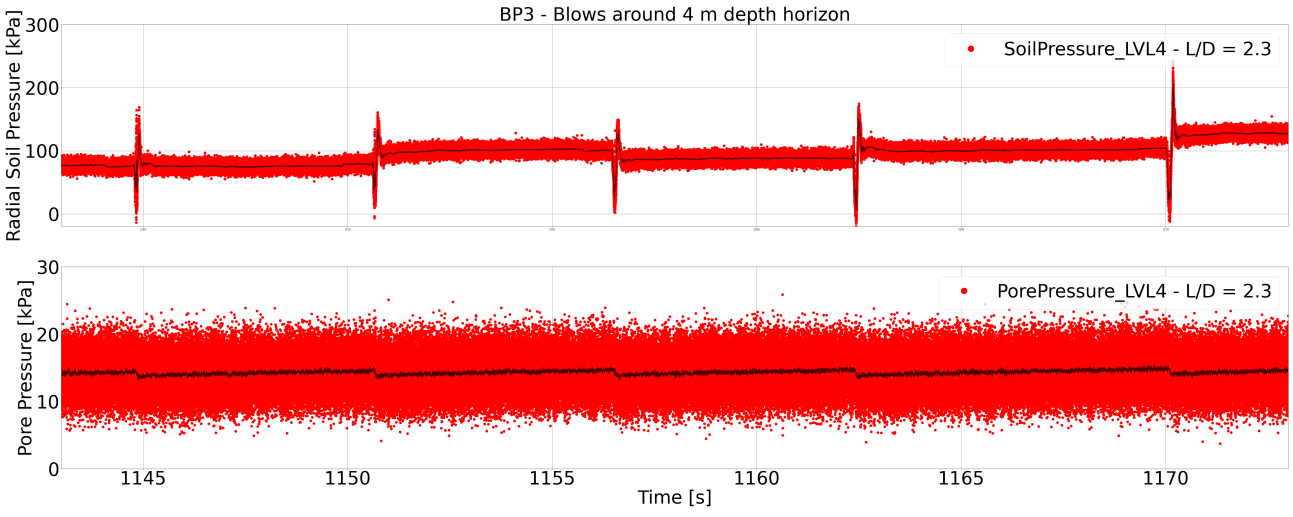

Figure 90

- For the Blue Piling installation, again the blow causes a dip in total radial stresses, reaching into negative pressures again. The peak is reached and moves much faster into the plateau value that is reached. The second small plateau is not clearly visible around this time in installation process.
- The effect of a blow on pore water pressures makes them decrease slightly. They slowly recover towards hydrostatic water pressure.

F.2.3 Depth horizon 5 meters

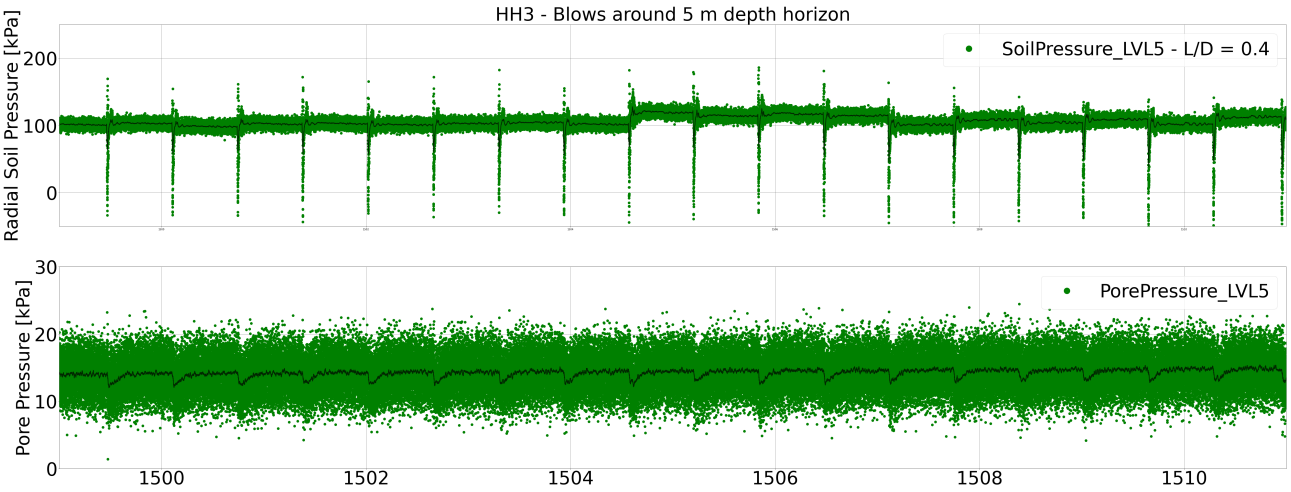

Figure 91

- A clear blow pattern can be distinguished around 5 meter depth horizon for HH3. Small peak, stronger dip, higher peak and plateau. Blow rate is around 90 a minute which means blows take around 0.6 seconds.
- The water pressures generated are slightly negative but recover very quickly, reaching a plateau that stays constant. The material at this horizon is silty sand to sandy silt.

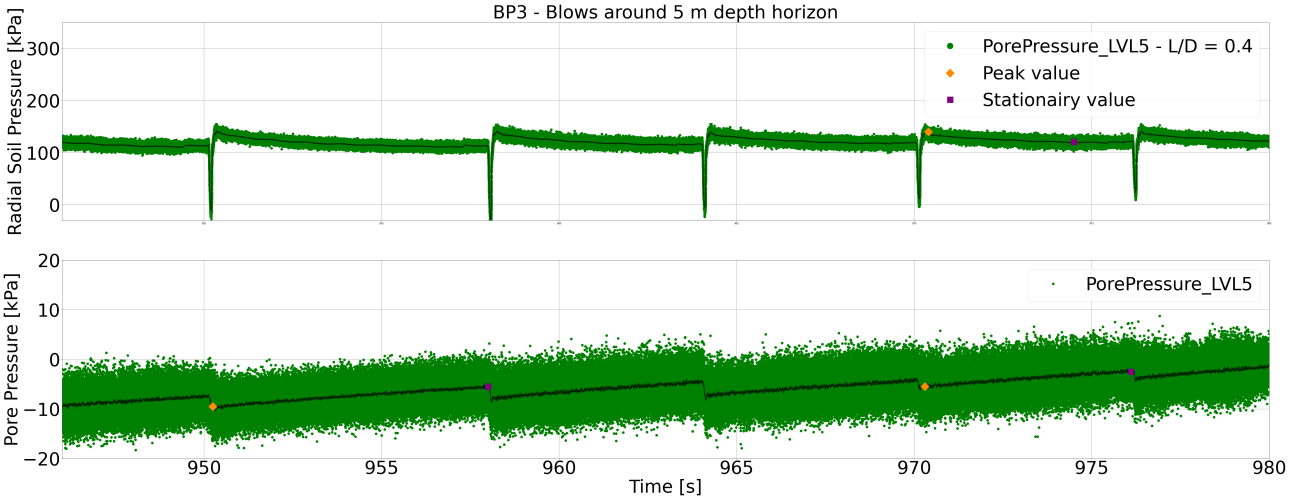

Figure 92

- A clear blow pattern can be distinguished around 5 meter depth horizon for BP3: strong dip, higher peak, balance to stationary value. The second plateau right before impact is more clearly visible for blows around 4 m depth horizon.
- Water pressures build to slightly negative in the silty sand to sandy silt. The hydrostatic pressures around this depth are 30 kPa so the pressures grow strongly positive within the stationairy part of the blow.

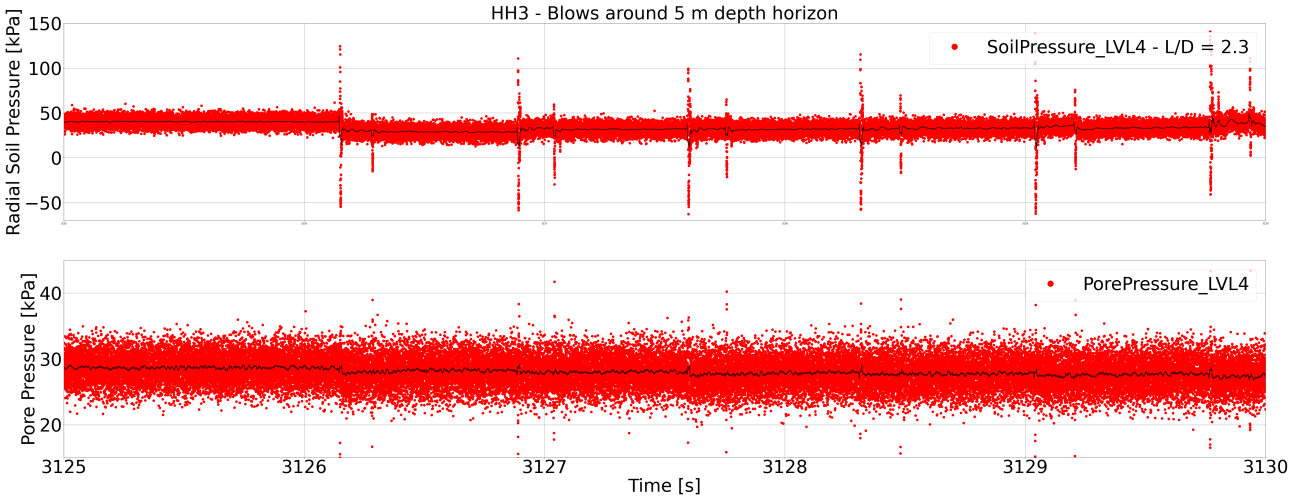

Figure 93

- The blow rate per minute around this depth is around 87, making a blow last around 0.7 seconds.
- The hydrostratic waterpressure around this depth is around 30 kPa.

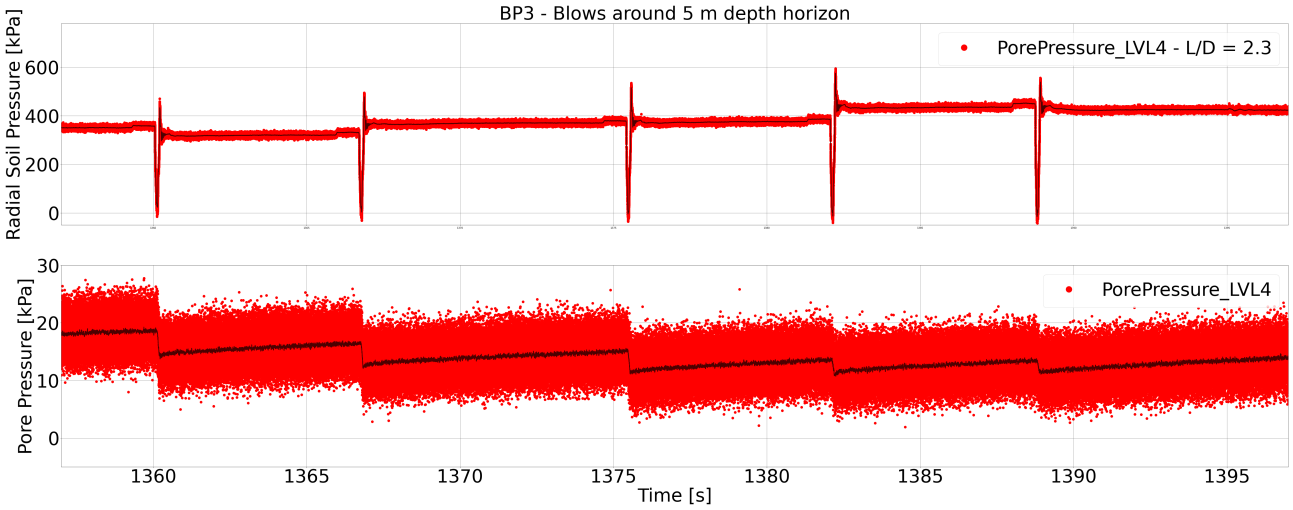

Figure 94

- The same characteristic blow can be spotted: strong dip, strong peak, however the progression into the stationairy phase of the blow is much quicker, making for a sharp decrease compared to previous blows researched.
- The hydrostatic pressure at this depth lies around 30 kPa. The pore pressures during the blow decrease again and increase during the stationairy phase.

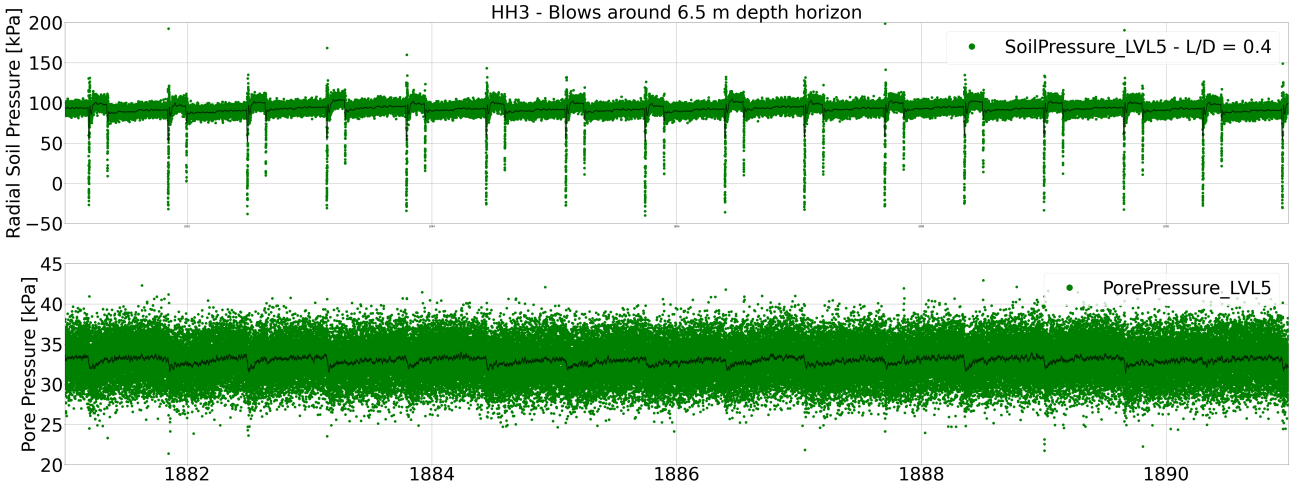

Figure 95

- The same characteristic blow can be distinguished.

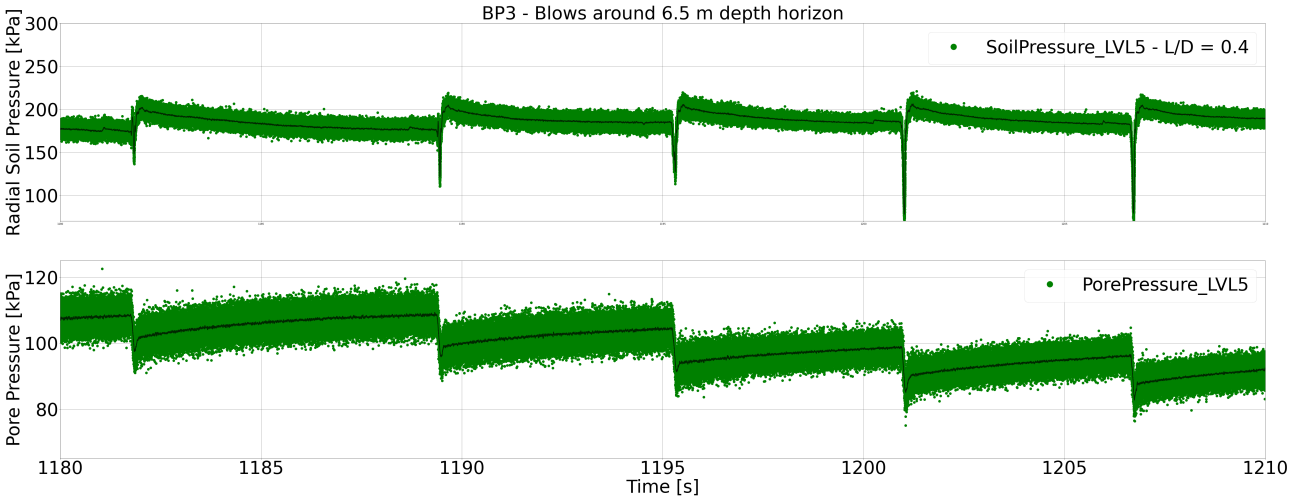

Figure 96

- The same characteristic blow can be distinguished.
- The hydrostatic water pressure equals around 45 kPa at this horizon. Again a decrease in pore pressures is generated in a blow, however in the stationairy phase, there is still a slight build-up of pore pressure. The material at this horizon is sand. This may indicate the presence of rate effects.

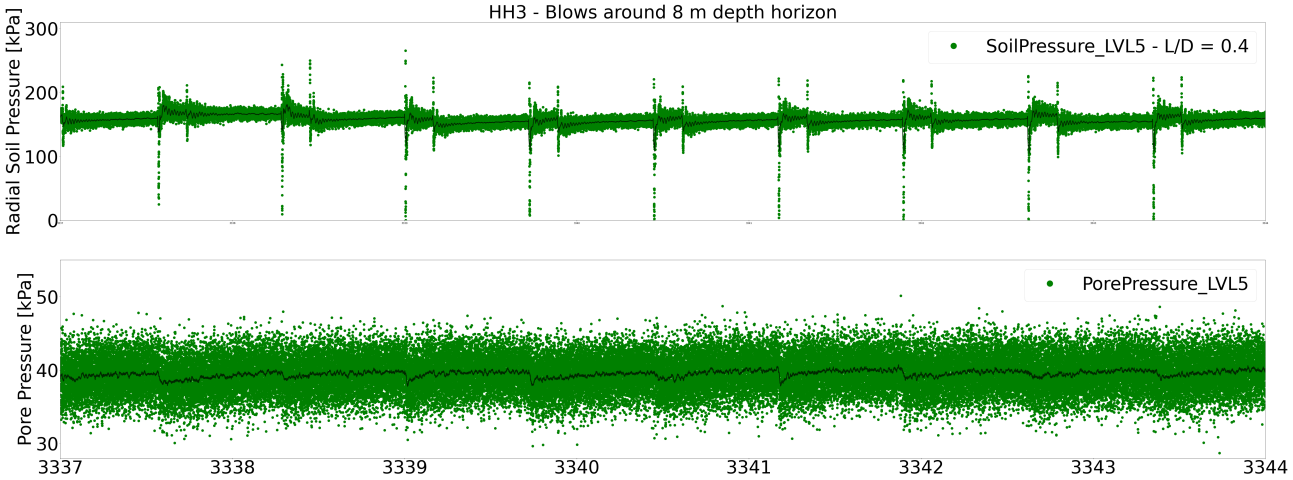

Figure 97

- The characteristic blow can be distinguished.

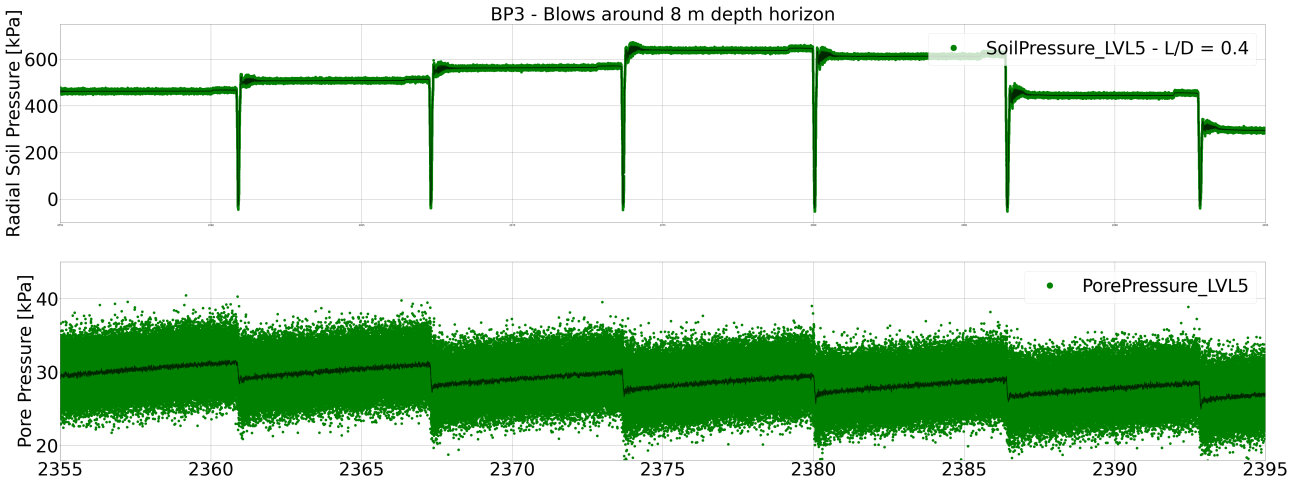

Figure 98

- A variation of the characteristic blow can be recognized for the 8 meter depth horizon. The peak is reached in an oscillatory way, quickly leading into the 'stationary' phase of the blow. The dip in the blow now reaches to and beyond 0 kPa into negative total pressures.

F.3 Accelerations

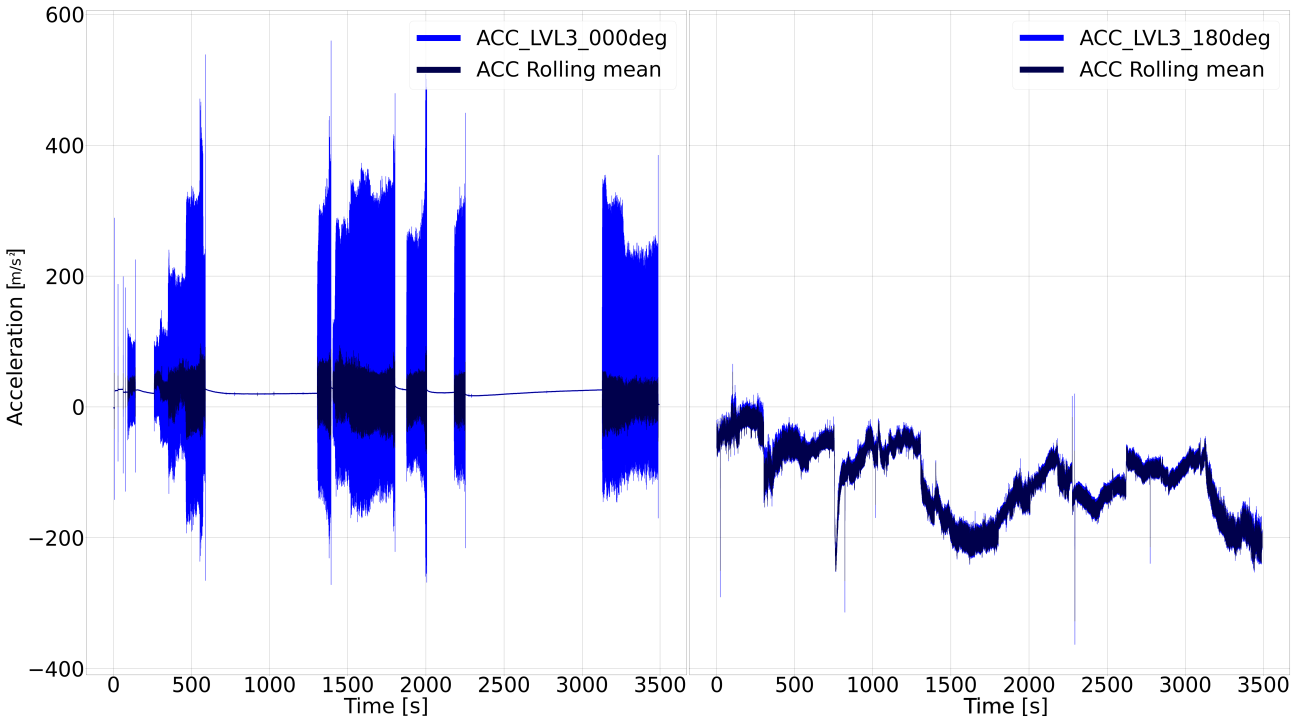

Figure 99: HH3 - LVL 3 - L/D = 4.1 - Accelerations

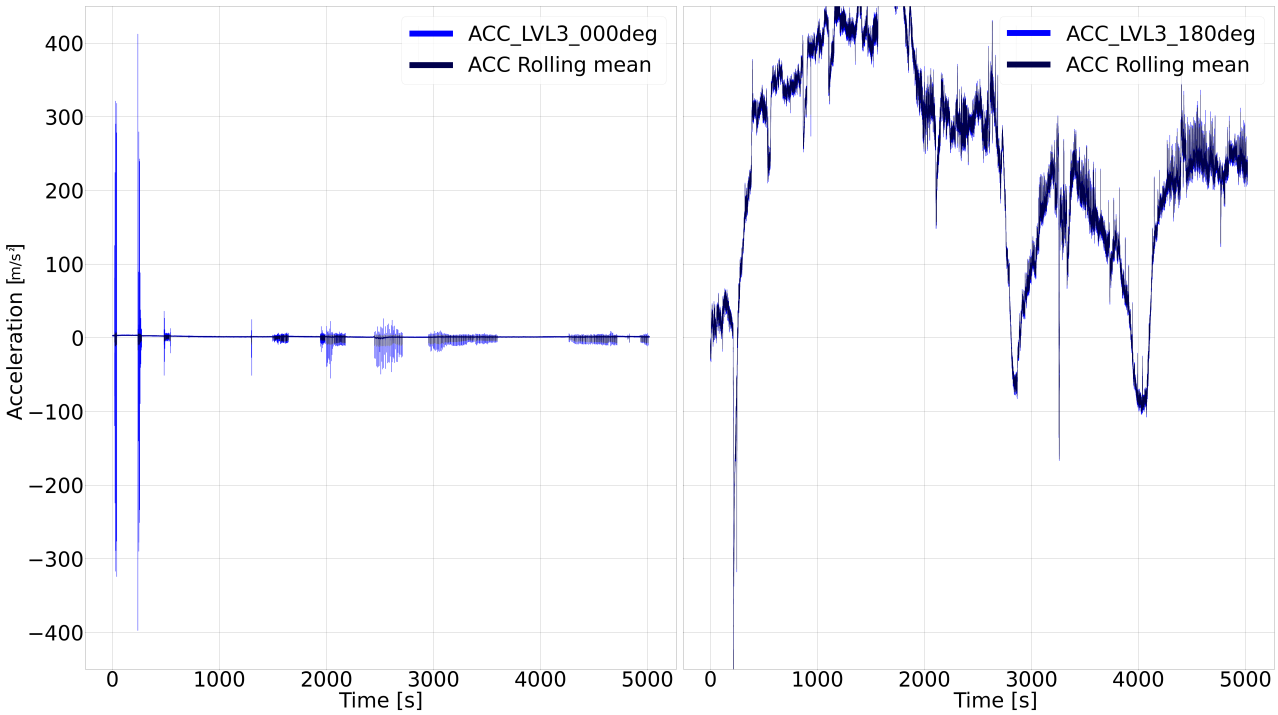

Figure 100: BP4 - LVL 3 - L/D = 4.1 - Accelerations

F.4 Strains

F.4.1 Hydrohammer Installation

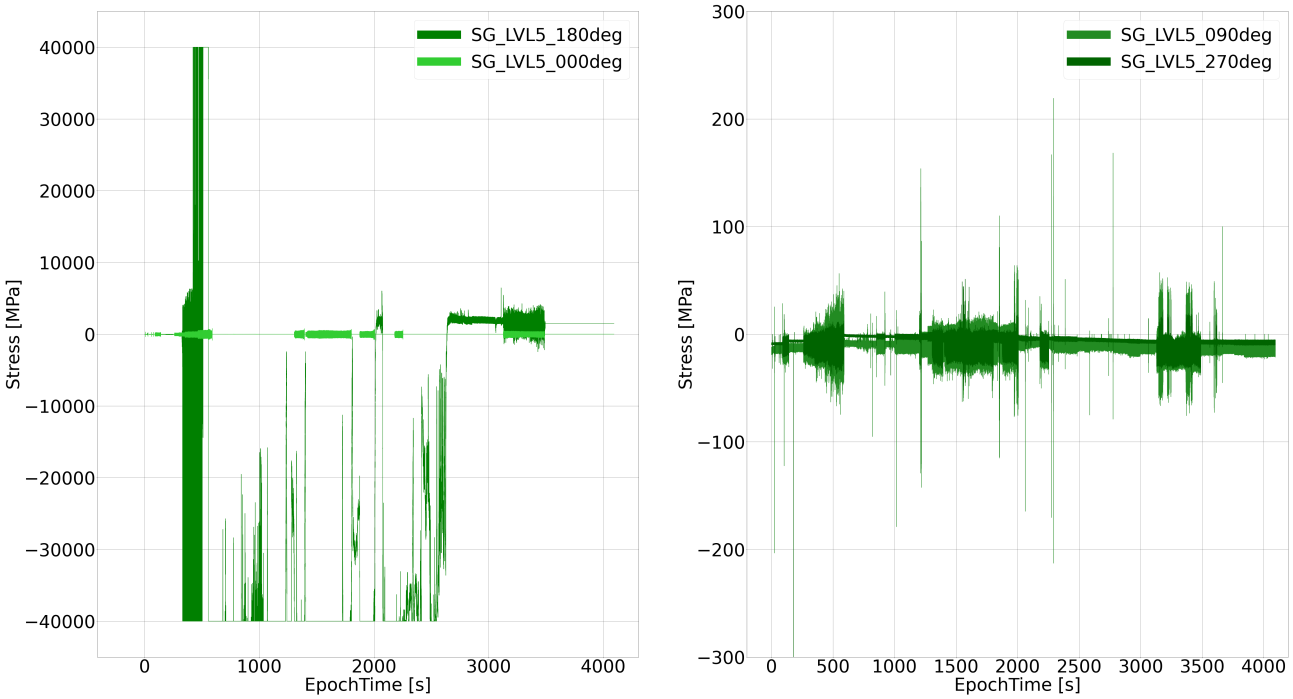

Figure 101: HH3 - LVL 5 - L/D = 0.4 - Strain

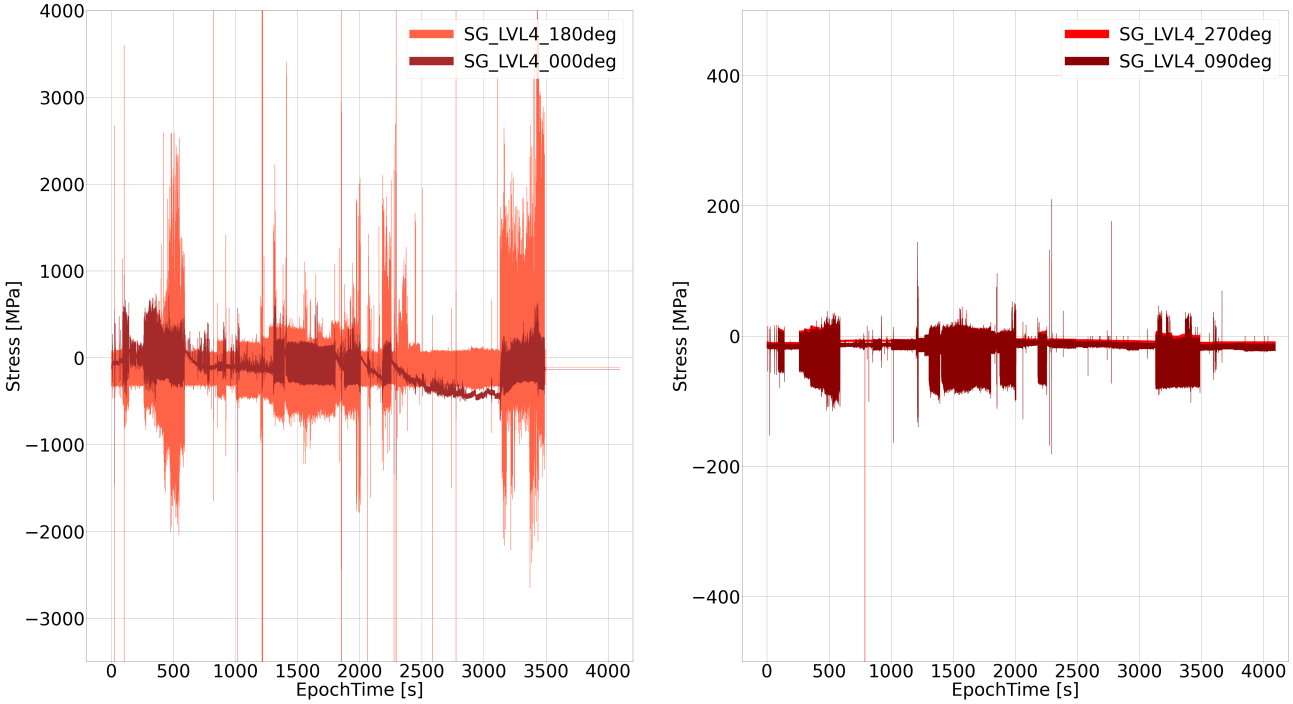

Figure 102: HH3 - LVL 4 - L/D = 2.3 - Strain

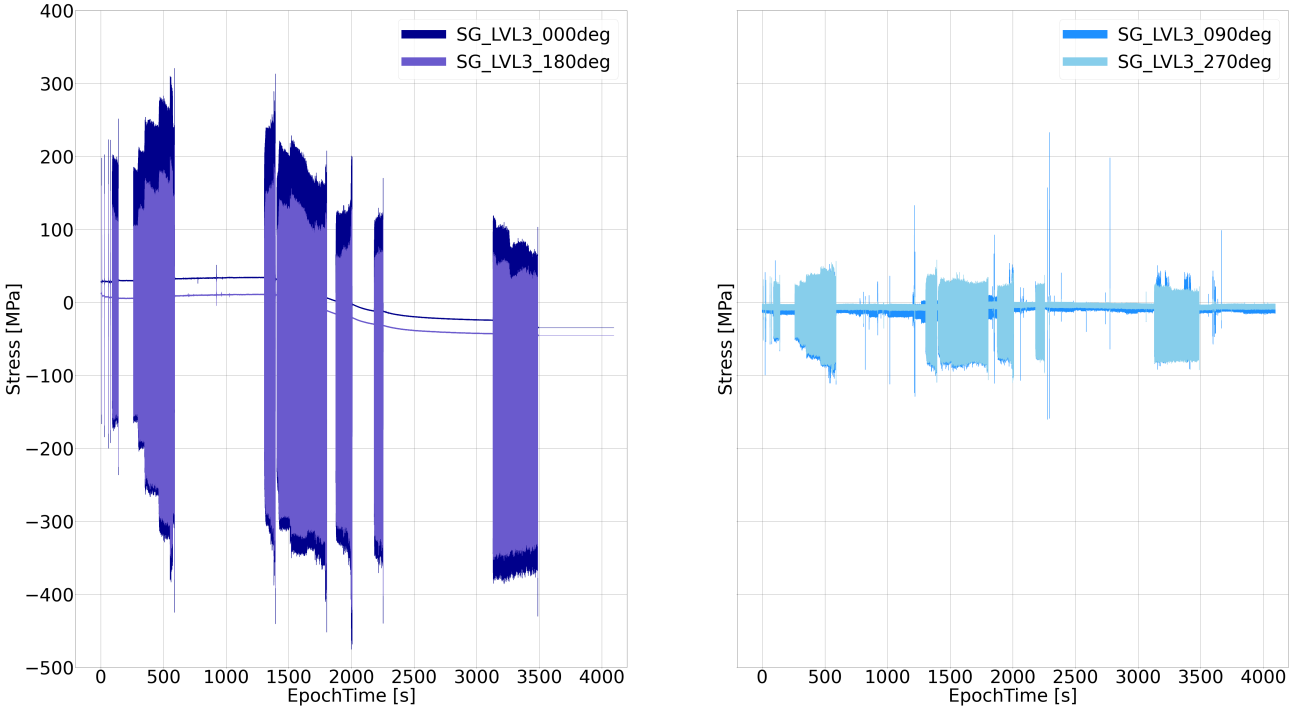

Figure 103: HH3 - LVL 3 - L/D = 4.1 - Strain

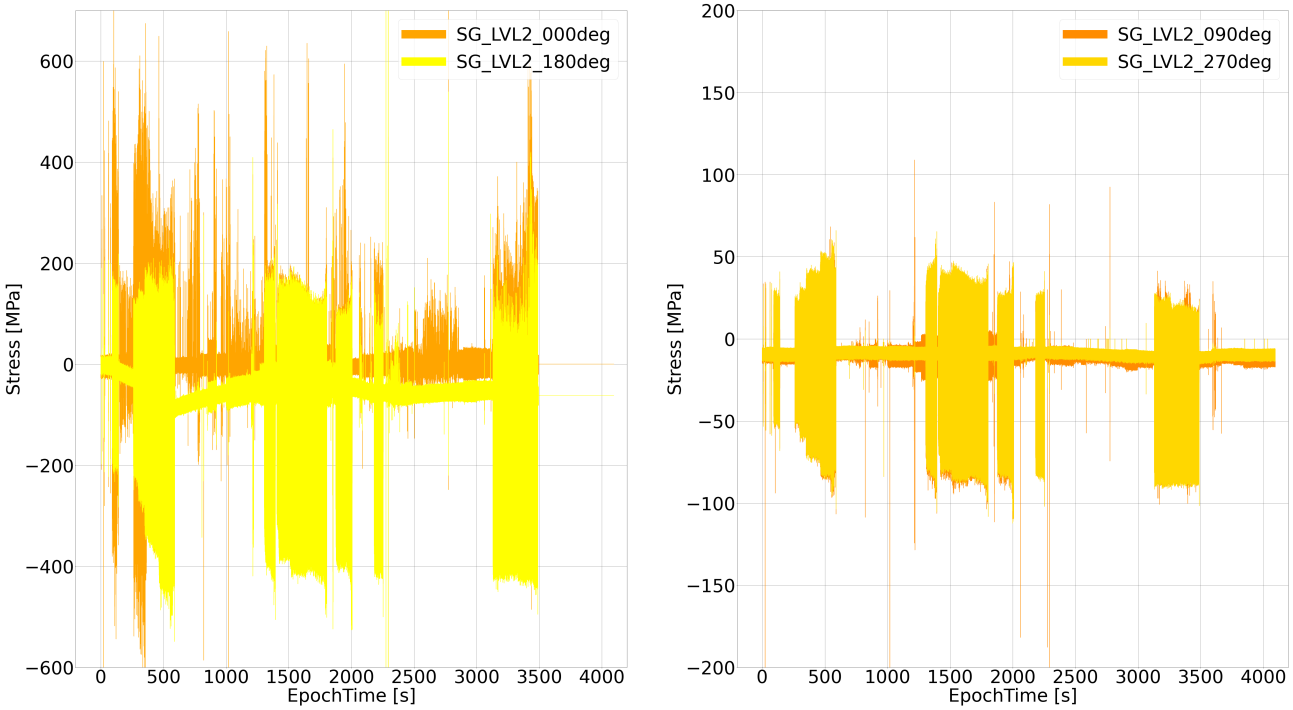

Figure 104: HH3 - LVL 2 - L/D = 5.9 - Strain

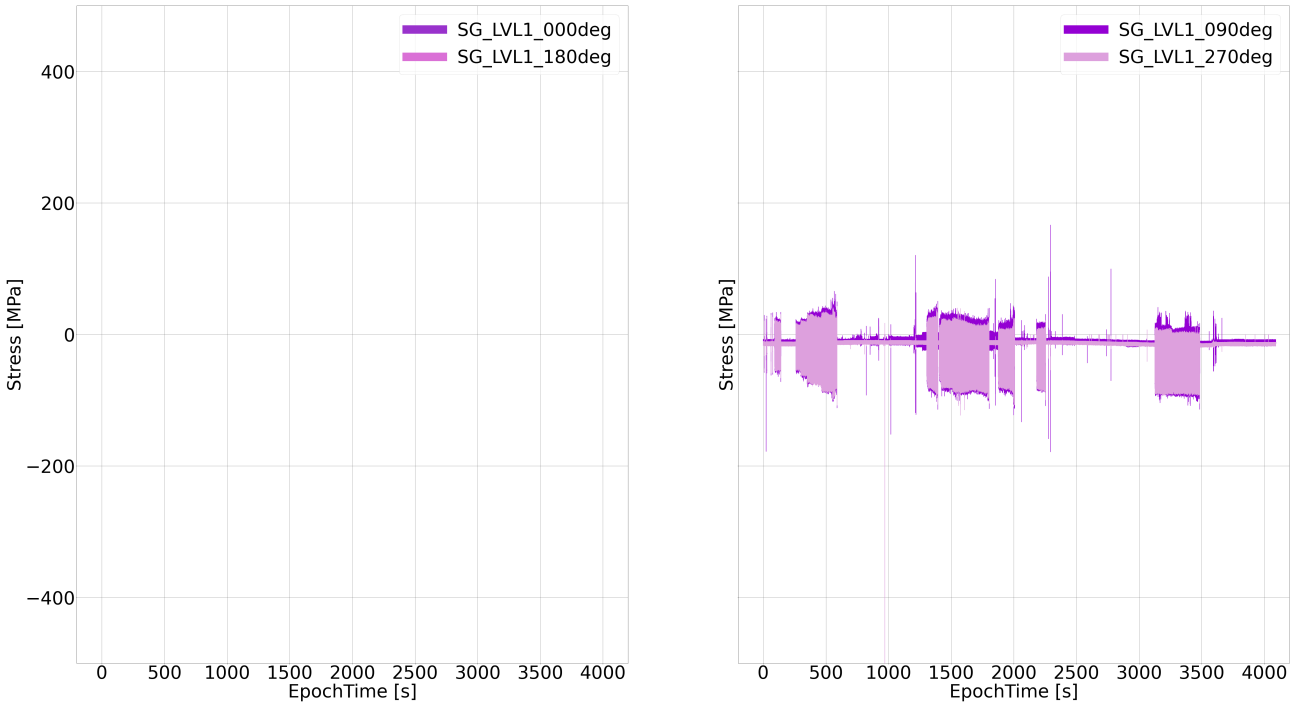

Figure 105: HH3 - LVL 1 - L/D = 7.8 - Strain

F.4.2 Blue Piling Installation

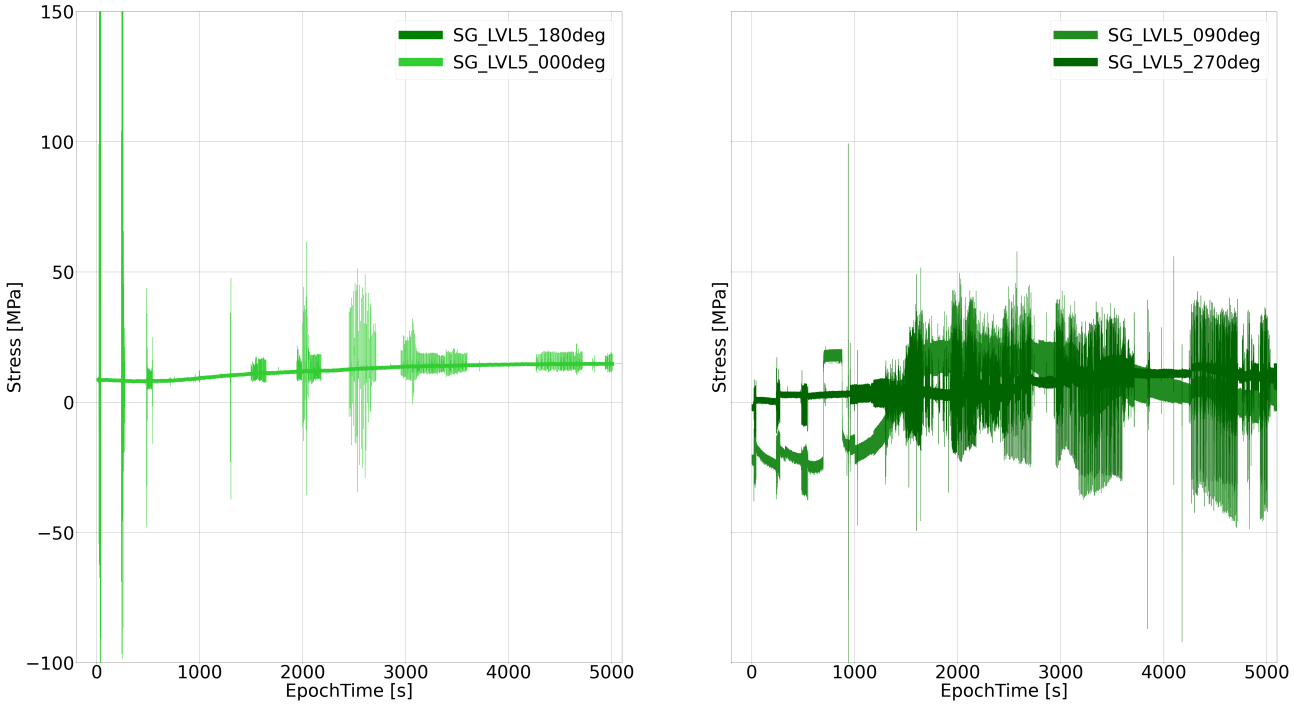

Figure 106: BP4 - LVL 5 - L/D = 0.4 - Strain

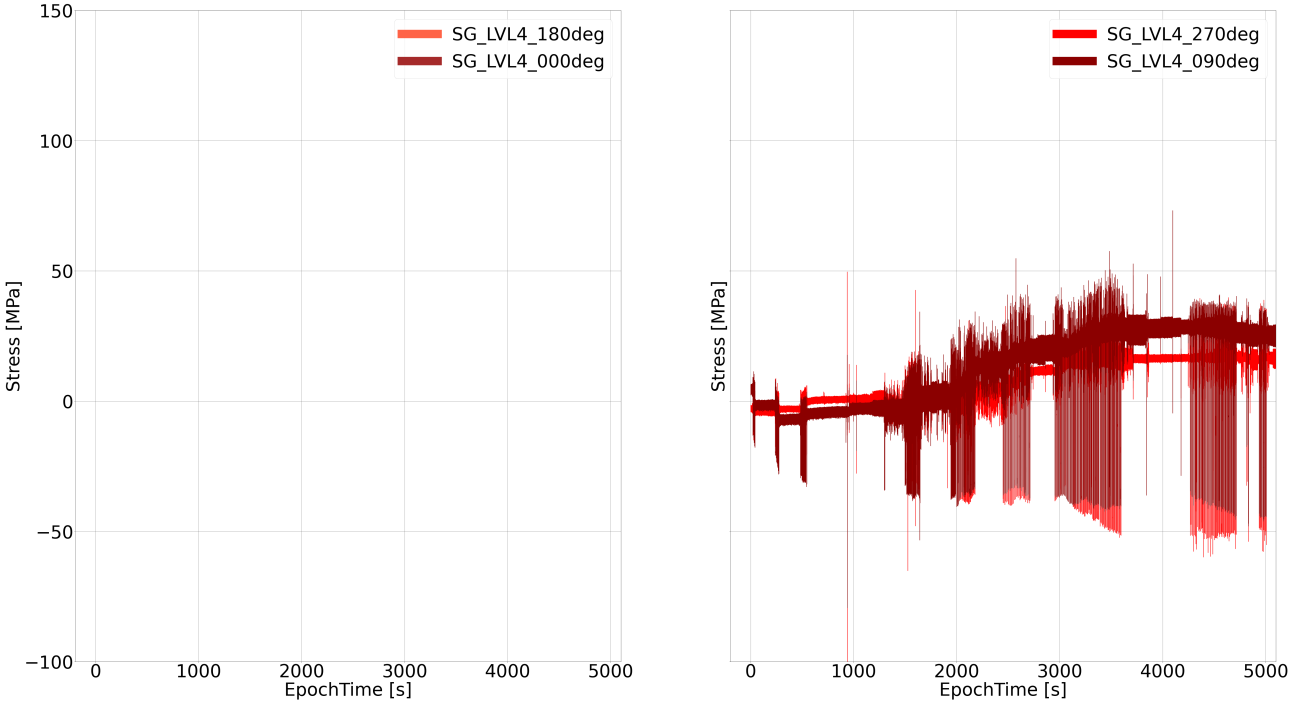

Figure 107: BP4 - LVL 4 - L/D = 2.3 - Strain

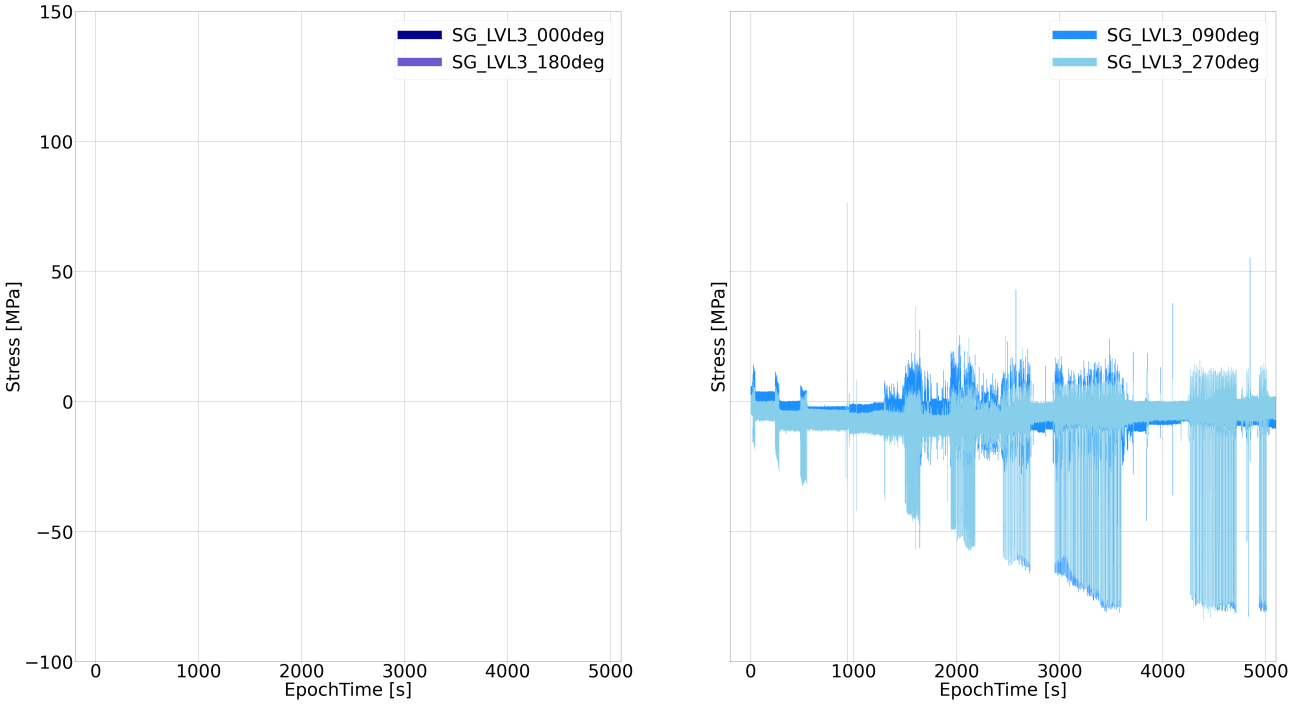

Figure 108: BP4 - LVL 3 - L/D = 4.1 - Strain

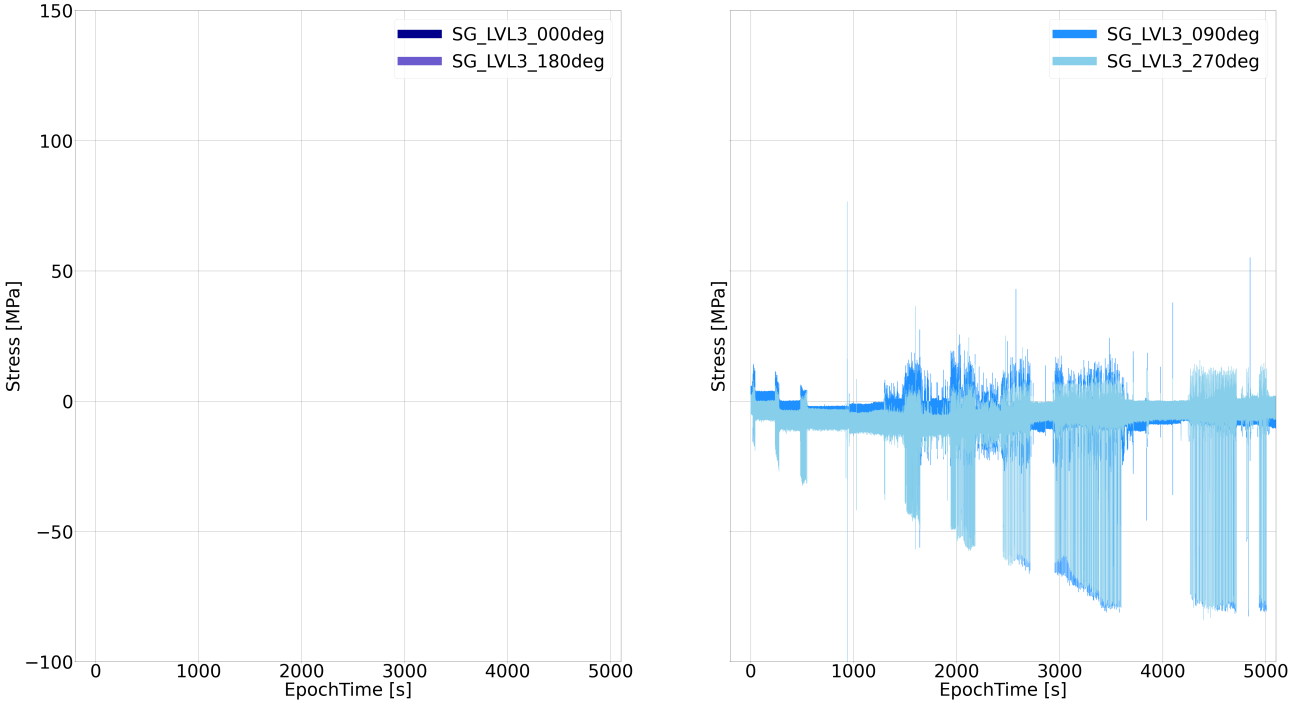

Figure 109: BP4 - LVL 3 - L/D = 4.1 - Strain

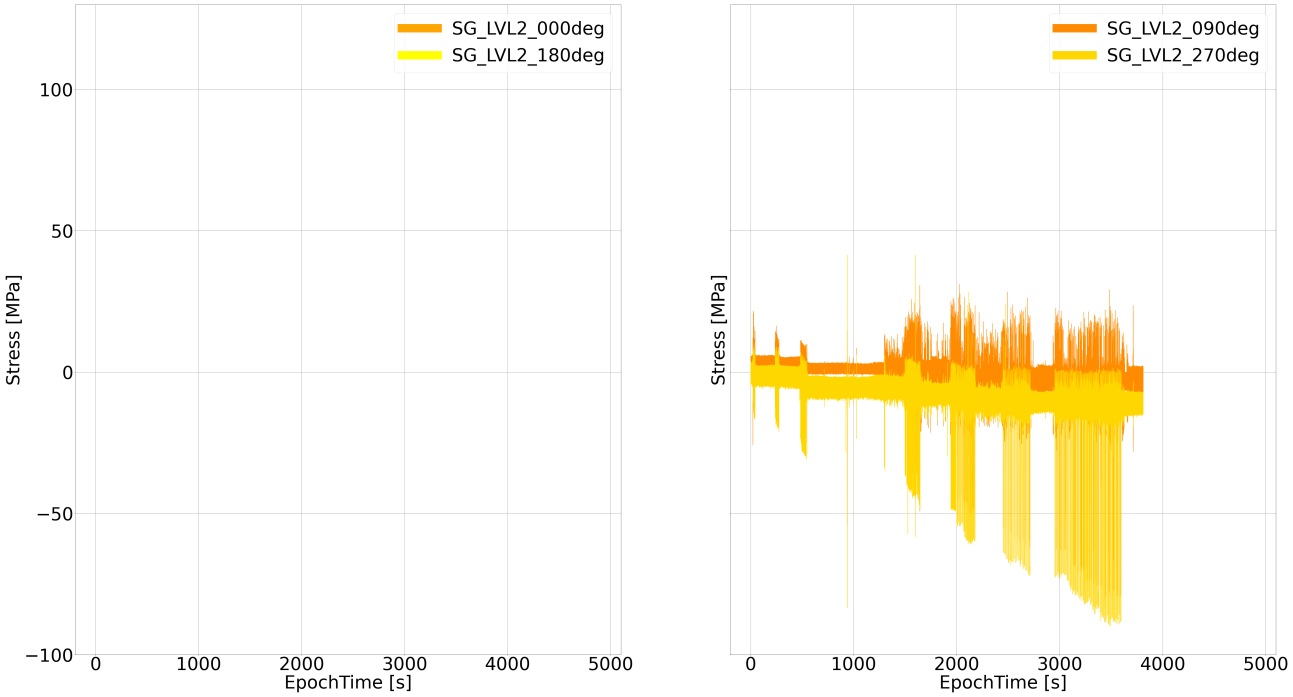

Figure 110: BP4 - LVL 2 - L/D = 5.9 - Strain

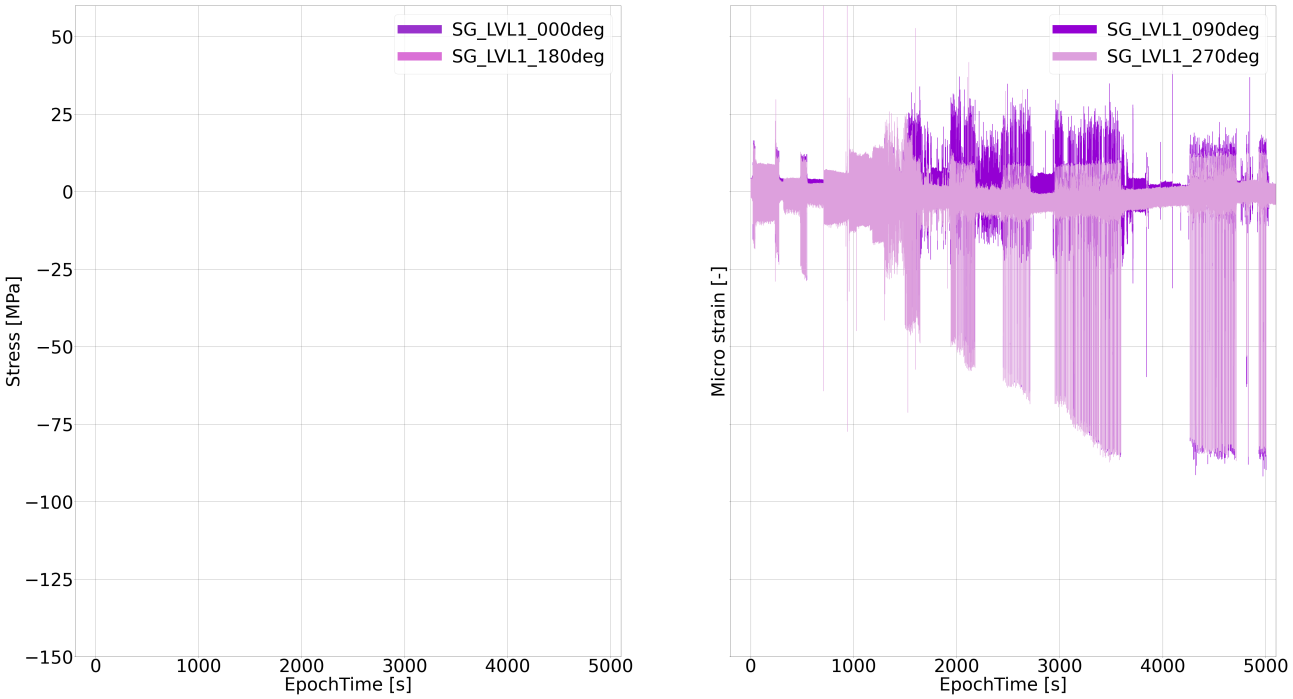

Figure 111: BP4 - LVL 1 - L/D = 7.8 - Strain

Listing 1: Python Code Fourier Transform

```
# -*- coding: utf-8 -*-
"""
Created on Mon Feb 27 15:54:28 2023

@author: csstokman
"""

import numpy as np
import scipy.integrate as spi
import matplotlib.pyplot as plt
from collections import namedtuple
import scipy.sparse as sps
from pandas import read_csv
import pandas as pd
from IPython.display import display
from numpy import fft
from math import trunc
from scipy import signal
from scipy.signal import butter, lfilter, freqz

#%%

soil = pd.read_csv(r'C:\Users\csstokman\OneDrive - IHC Merwede Holding ...
    B.V\documents\Data\HH3_S1_Soil.csv', delimiter=',', parse_dates=[0], index_col=[0])
display(soil.head(5))

#%%

# Find the interval of driving stop.
soil_fourier = []
time_fourier = []

for i in range(len(soil)):
    if soil.index[i] > (1668764635 + 150) and soil.index[i] < (1668764635 + 240):
        soil_fourier.append(soil['SoilPressure_LVL5'].iloc[i])
        time_fourier.append(soil.index[i])

#%%

# Plot of the dataset considered for fourier to find y and translate around this subtracted ...
    average.
y_mid = np.sum(soil_fourier) / len(soil_fourier)
plt.plot(time_fourier, soil_fourier)
plt.axhline(y_mid, color='red')

#%%

Fs = 10000                      # Sampling frequency (10-kHz)
L = len(time_fourier)           # Number of points (number of points in window considered)
t = np.arange(0, L-1)/Fs        # Time vector (tijdsdata uit de dataset)

x1 = soil_fourier-y_mid         # Data centered around y, subtracted average

# n = 1048576                   #High number, Nexpower of 2, in Matlab: 2^nexpow2(L)

y = np.fft.fft(x1)
freq = np.arange(0, Fs/2-Fs/L, Fs/L)

amp = abs(2*y[:trunc(L/2)-1])/L

plt.figure(figsize=(30, 20))
plt.plot(freq, amp, linewidth=3)
plt.xlabel('Frequency [Hz]', fontsize=30)
plt.xticks(fontsize=30)
plt.ylabel('Amplitude [kPa]', fontsize=30)
plt.yticks(fontsize=30)
```

Listing 2: Python Code Displacement measurements

```
# -*- coding: utf-8 -*-
"""
Created on Fri Jan 13 17:50:52 2023

@author:
    cstokman

@project:
    Maasvlakte paaltesten

UNIX time = time since 1970 [s]
BPCont = Bluepiling control
HVR = grote kast
DWT = dewetron
Laser = laser
Alt = Altimeter
Pile PDA = alle rekstroken en versnellingsmeters op de paal
Soil = Soil pressure en water druk
Position = hoogtesensoren van Bob (AAD en WAM)
Noise = geluidsmetingen

"""

#%%

#imports
import numpy as np
import scipy.integrate as spi
import matplotlib.pyplot as plt
from collections import namedtuple
import scipy.sparse as sps
from pandas import read_csv
import pandas as pd
from IPython.display import display

#%%
position = pd.read_csv(r'F:\IQ_048-Engineering_BluePiling\04-R&D\1-Test results\2-In-situ ...
    test\Export\HH3_S1_Position.csv', delimiter=',', index_col=[0])
# Excel_header = [UNIXTime],    [Dimetix DPE-10-500],   [Pile Penetration length],  [Pwater ...
    moving],    [Pwater fixed], [Water hose altimeter height]

#%%

plt.figure(figsize=(20, 10))
plt.plot(position.index-position.index[0], position['Pile Penetration length'])
plt.ylabel('Penetration [m]', fontsize=30)
plt.xlabel('Time [s]', fontsize=30)
plt.title('Displacement of HH3 vs. Time', fontsize=30)
plt.xticks(fontsize=30)
plt.yticks(fontsize=30)

plt.axvline(0, color='black', linewidth=3)
plt.axvline(140, color='black', linewidth=1)
plt.axvline(250, color='black', linewidth=1)
plt.axvline(580, color='black', linewidth=1)
plt.axvline(1300, color='black', linewidth=1)
plt.axvline(1810, color='black', linewidth=1)
plt.axvline(1870, color='black', linewidth=1)
plt.axvline(2010, color='black', linewidth=1)
plt.axvline(2170, color='black', linewidth=1)
plt.axvline(2250, color='black', linewidth=1)
plt.axvline(3120, color='black', linewidth=1)
plt.axvline(3500, color='black', linewidth=3)

plt.axvspan(140, 250, alpha=0.3, color='blue')
plt.axvspan(580, 1300, alpha=0.3, color='blue')
plt.axvspan(1810, 1870, alpha=0.3, color='blue')
plt.axvspan(2010, 2170, alpha=0.3, color='blue')
plt.axvspan(2250, 3120, alpha=0.3, color='blue')

#%%
plt.figure()
```

```
71 plt.plot(position.index-position.index[0], position['Pile Penetration length'])
72 # plt.plot(soil.index-soil.index[0], soil['Pile Penetration length'])
73 plt.ylabel('Penetration [m]')
74 plt.xlabel('Time [s]')
75 plt.title('Displacement of HH3 vs. Time')
76 plt.legend(['Position dataset', 'Soil dataset'])
77 plt.axhline(1.5)
78 plt.axhline(4)
79 plt.axhline(5)
80 plt.axhline(6.5)
81 plt.axhline(8)
82
83 #%%
84
85
86
87 #%%
```

Listing 3: Python Code Data Resampling

```
# -*- coding: utf-8 -*-
"""
Created on Fri Jan 13 17:50:52 2023

@author:
    cstokman

@project:
    Maasvlakte paaltesten

UNIX time = time since 1970 [s]
BPCont = Bluepiling control
HVR = grote kast
DWT = dewetron
Laser = laser
Alt = Altimeter
Pile PDA = alle rekstroken en versnellingsmeters op de paal
Soil = Soil pressure en water druk
Position = hoogtesensoren van Bob (AAD en WAM)
Noise = geluidsmetingen

"""

#%%

#imports
import numpy as np
import scipy.integrate as spi
import matplotlib.pyplot as plt
from collections import namedtuple
import scipy.sparse as sps
from pandas import read_csv
import pandas as pd
from IPython.display import display

#%%

# Load in Soil Pressure
soil = pd.read_csv(r'C:\Users\csstokman\OneDrive - IHC Merwede Holding ...
    B.V\documents\Data\HH3_S1_Soil.csv', delimiter=',', parse_dates=[0])
display(soil.head(5))

#%%

# Transform UNIXTime to date
soil['date'] = pd.to_datetime(soil['EpochTime'], unit='s')
soil['date'].dt.date
soil = soil.set_index(soil['date'])

#%%

# Apply moving average. Parameters are as follows:
# window = size of the window, how man observations we have to take for the calculation of ...
    each window = 100
# min_periods = least number of observations in a window required to have a value [voor de ...
    berekening]
# center = used to set the labels at the center of the window
# win_type = set window type
# on = datetime column of our dataframe on which we have to calculate rolling mean

# Eerste stap is het toepassen van de numpy moving average.
window = 100                # Will in my case be 100 values
freq  = 1/0.03              # Frequency to conform the data to before computing the statistics

# NOTE: Due to the window size, the first 50 and the final 50 values are NaN.

soil2 = soil.rolling(window=window, center=True).mean()


#%%

#Deze voor de hele set
```

```
soil3 = soil2.resample('0.03S', kind='timestamp').last()

#%%

print(soil3.head(5))
soil3.to_csv(r'C:\Users\csstokman\OneDrive - IHC Merwede Holding B.V\documents\Data\HH3_rolling_resample_30Hz_last.csv', sep=',', encoding='utf-8', header='true')

#%%

soil3 = pd.read_csv(r'C:\Users\csstokman\OneDrive - IHC Merwede Holding B.V\documents\Data\HH3_rolling_resample_30Hz_last.csv', delimiter=',', index_col=[0], parse_dates=[])
display(soil3.head(5))

#%%
plt.figure(figsize=(30,20))
plt.title('Soil Pressure LVL5')
plt.xlabel('Time', fontsize=30)
plt.ylabel('Soil Pressure [kPa]', fontsize=30)
plt.xticks(fontsize=30)
plt.yticks(fontsize=30)
plt.ylim((-200, 600))
plt.legend(['Original Soil Pressure', 'Rolling mean', 'Resampled data'], loc='upper right', fontsize=30)

plt.plot(soil.index, soil['SoilPressure_LVL5'], 'b')
plt.plot(soil2['EpochTime'], soil2['SoilPressure_LVL5'], 'r')
plt.plot(soil3.index, soil3['SoilPressure_LVL5'], 'g')


#%%

# Get the values at few different horizons
soil_1_5m_LVL5 = []
pen_1_5m_LVL5 = []
time_1_5m_LVL5 = []

for i in range(len(soil3)):
    if soil3['Pile Penetration length'].iloc[i] > (1.5+0.5-0.2) and soil3['Pile Penetration length'].iloc[i] < (1.5+0.5+0.2): #and soil3['SoilPressure_LVL3'].iloc[i] < 1500 and soil3['SoilPressure_LVL3'].iloc[i] > -250:
        soil_1_5m_LVL5.append(soil3['SoilPressure_LVL5'].iloc[i])
        time_1_5m_LVL5.append(soil3['EpochTime'].iloc[i])
        pen_1_5m_LVL5.append(soil3['Pile Penetration length'].iloc[i]-0.5)

#%%

soil_4m_LVL5 = []
pen_4m_LVL5 = []
time_4m_LVL5 = []

for i in range(len(soil3)):
    if soil3['Pile Penetration length'].iloc[i] > (4+0.5-0.2) and soil3['Pile Penetration length'].iloc[i] < (4+0.5+0.2): #and soil3['SoilPressure_LVL3'].iloc[i] < 1500 and soil3['SoilPressure_LVL3'].iloc[i] > -250:
        soil_4m_LVL5.append(soil3['SoilPressure_LVL5'].iloc[i])
        time_4m_LVL5.append(soil3['EpochTime'].iloc[i])
        pen_4m_LVL5.append(soil3['Pile Penetration length'].iloc[i]-0.5)

#%%

soil_5m_LVL5 = []
pen_5m_LVL5 = []
time_5m_LVL5 = []

for i in range(len(soil3)):
    if soil3['Pile Penetration length'].iloc[i] > (5+0.5-0.2) and soil3['Pile Penetration length'].iloc[i] < (5+0.5+0.2): #and soil3['SoilPressure_LVL3'].iloc[i] < 1500 and soil3['SoilPressure_LVL3'].iloc[i] > -250:
        soil_5m_LVL5.append(soil3['SoilPressure_LVL5'].iloc[i])
        time_5m_LVL5.append(soil3['EpochTime'].iloc[i])
```

```
132         pen_5m_LVL5.append(soil3['Pile Penetration length'].iloc[i]-0.5)
133
134 #%%
135
136 soil_6_5m_LVL5 = []
137 pen_6_5m_LVL5 = []
138 time_6_5m_LVL5 = []
139
140 for i in range(len(soil3)):
141     if soil3['Pile Penetration length'].iloc[i] > (6.5+0.5-0.2) and soil3['Pile Penetration ...
            length'].iloc[i] < (6.5+0.5+0.2): #and soil3['SoilPressure_LVL3'].iloc[i] < 1500 and ...
            soil3['SoilPressure_LVL3'].iloc[i] > -250:
142         soil_6_5m_LVL5.append(soil3['SoilPressure_LVL5'].iloc[i])
143         time_6_5m_LVL5.append(soil3['EpochTime'].iloc[i])
144         pen_6_5m_LVL5.append(soil3['Pile Penetration length'].iloc[i]-0.5)
145
146 #%%
147
148 soil_1_5m_LVL4 =[]
149 pen_1_5m_LVL4 = []
150 time_1_5m_LVL4 = []
151
152 for i in range(len(soil3)):
153     if soil3['Pile Penetration length'].iloc[i] > (1.5+2.75-0.2) and soil3['Pile Penetration ...
            length'].iloc[i] < (1.5+2.75+0.2): #and soil3['SoilPressure_LVL3'].iloc[i] < 1500 and ...
            soil3['SoilPressure_LVL3'].iloc[i] > -250:
154         soil_1_5m_LVL4.append(soil3['SoilPressure_LVL4'].iloc[i])
155         time_1_5m_LVL4.append(soil3['EpochTime'].iloc[i])
156         pen_1_5m_LVL4.append(soil3['Pile Penetration length'].iloc[i]-2.75)
157
158 #%%
159
160 soil_4m_LVL4 =[]
161 pen_4m_LVL4 = []
162 time_4m_LVL4 = []
163
164 for i in range(len(soil3)):
165     if soil3['Pile Penetration length'].iloc[i] > (4+2.75-0.2) and soil3['Pile Penetration ...
            length'].iloc[i] < (4+2.75+0.2): #and soil3['SoilPressure_LVL3'].iloc[i] < 1500 and ...
            soil3['SoilPressure_LVL3'].iloc[i] > -250:
166         soil_4m_LVL4.append(soil3['SoilPressure_LVL4'].iloc[i])
167         time_4m_LVL4.append(soil3['EpochTime'].iloc[i])
168         pen_4m_LVL4.append(soil3['Pile Penetration length'].iloc[i]-2.75)
169
170 #%%
171 soil_5m_LVL4 = []
172 pen_5m_LVL4 = []
173 time_5m_LVL4 = []
174
175 for i in range(len(soil3)):
176     if soil3['Pile Penetration length'].iloc[i] > (5+2.75-0.2) and soil3['Pile Penetration ...
            length'].iloc[i] < (5+2.75+0.2): #and soil3['SoilPressure_LVL3'].iloc[i] < 1500 and ...
            soil3['SoilPressure_LVL3'].iloc[i] > -250:
177         soil_5m_LVL4.append(soil3['SoilPressure_LVL4'].iloc[i])
178         time_5m_LVL4.append(soil3['EpochTime'].iloc[i])
179         pen_5m_LVL4.append(soil3['Pile Penetration length'].iloc[i]-2.75)
180
181 #%%
182
183 soil_6_5m_LVL4 = []
184 pen_6_5m_LVL4 = []
185 time_6_5m_LVL4 = []
186
187 for i in range(len(soil3)):
188     if soil3['Pile Penetration length'].iloc[i] > (6.5+2.75-0.2) and soil3['Pile Penetration ...
            length'].iloc[i] < (6.5+2.75+0.2): #and soil3['SoilPressure_LVL3'].iloc[i] < 1500 and ...
            soil3['SoilPressure_LVL3'].iloc[i] > -250:
189         soil_6_5m_LVL4.append(soil3['SoilPressure_LVL4'].iloc[i])
190         time_6_5m_LVL4.append(soil3['EpochTime'].iloc[i])
191         pen_6_5m_LVL4.append(soil3['Pile Penetration length'].iloc[i]-2.75)
192
193 #%%
194
```

```
195 soil_1_5m_LVL3 = []
196 pen_1_5m_LVL3 = []
197 time_1_5m_LVL3 = []
198
199 for i in range(len(soil3)):
200     if soil3['Pile Penetration length'].iloc[i] > (1.5+5-0.2) and soil3['Pile Penetration ...
            length'].iloc[i] < (1.5+5+0.2): #and soil3['SoilPressure_LVL3'].iloc[i] < 1500 and ...
            soil3['SoilPressure_LVL3'].iloc[i] > -250:
201         soil_1_5m_LVL3.append(soil3['SoilPressure_LVL3'].iloc[i])
202         time_1_5m_LVL3.append(soil3['EpochTime'].iloc[i])
203         pen_1_5m_LVL3.append(soil3['Pile Penetration length'].iloc[i]-5)
204
205 #%%
206
207 soil_4m_LVL3 = []
208 pen_4m_LVL3 = []
209 time_4m_LVL3 = []
210
211 for i in range(len(soil3)):
212     if soil3['Pile Penetration length'].iloc[i] > (4+5-0.2) and soil3['Pile Penetration ...
            length'].iloc[i] < (4+5+0.2): #and soil3['SoilPressure_LVL3'].iloc[i] < 1500 and ...
            soil3['SoilPressure_LVL3'].iloc[i] > -250:
213         soil_4m_LVL3.append(soil3['SoilPressure_LVL3'].iloc[i])
214         time_4m_LVL3.append(soil3['EpochTime'].iloc[i])
215         pen_4m_LVL3.append(soil3['Pile Penetration length'].iloc[i]-5)
216
217 #%%
218
219
220 #%%
221 # Plot soil pressure
222 plt.figure(figsize=(20,30))
223 plt.plot(soil_1_5m_LVL5, pen_1_5m_LVL5, 'ro', markersize = 6, label='Soil Pressure LVL5 - L/D ...
        = 0.4')
224 plt.plot(soil_4m_LVL5, pen_4m_LVL5, 'ro', markersize=6)
225 plt.plot(soil_5m_LVL5, pen_5m_LVL5, 'ro', markersize=6)
226 plt.plot(soil_6_5m_LVL5, pen_6_5m_LVL5, 'ro', markersize=6)
227
228 plt.plot(soil_1_5m_LVL4, pen_1_5m_LVL4, 'bo', markersize=6, label='Soil Pressure LVL4 - L/D = ...
        2.3', alpha=0.5)
229 plt.plot(soil_4m_LVL4, pen_4m_LVL4, 'bo', markersize=6, alpha=0.5)
230 plt.plot(soil_5m_LVL4, pen_5m_LVL4, 'bo', markersize=6, alpha=0.5)
231 plt.plot(soil_6_5m_LVL4, pen_6_5m_LVL4, 'bo', markersize=6, alpha=0.5)
232
233 plt.plot(soil_1_5m_LVL3, pen_1_5m_LVL3, 'go', markersize=6, label='Soil Pressure LVL3 - L/D = ...
        4.1', alpha=0.5)
234 plt.plot(soil_4m_LVL3, pen_4m_LVL3, 'go', markersize=6, alpha=0.5)
235 # plt.plot(soil_5m_LVL3, pen_5m_LVL3, 'go', markersize=6, alpha=0.5) # The sensor does not ...
        reach up to here
236 # plt.ylim(0, -0.2)
237 # plt.xlim(0, 1)
238 plt.xlabel('Soil pressure [kPa]', fontsize=30)
239 plt.ylabel('Depth [m]', fontsize=30)
240 plt.ylim((10, 0))
241 plt.xticks(fontsize=30)
242 plt.yticks(fontsize=30)
243 plt.title('HH3 - Soil Pressures at the 1.5, 4, 5, and 6.5 meter depth soil horizons', ...
        fontsize=30)
244 plt.legend(loc='upper right', fontsize=30)
```